

INVESTIGATION OF FATIGUE CRACK BEHAVIOR ON NEAR THRESHOLD
REGION OF AISI 4340 STEELS FOR DIFFERENT HEAT TREATMENT
CONDITIONS

A THESIS SUBMITTED TO
THE GRADUATE SCHOOL OF NATURAL AND APPLIED SCIENCES
OF
MIDDLE EAST TECHNICAL UNIVERSITY

BY

SALİM ÇALIŞKAN

IN PARTIAL FULFILLMENT OF THE REQUIREMENTS
FOR
THE DEGREE OF DOCTOR OF PHILOSOPHY
IN
METALLURGICAL AND MATERIALS ENGINEERING

JANUARY 2023

Approval of the thesis:

**INVESTIGATION OF FATIGUE CRACK BEHAVIOR ON NEAR
THRESHOLD REGION OF AISI 4340 STEELS FOR DIFFERENT HEAT
TREATMENT CONDITIONS**

submitted by **SALİM ÇALIŞKAN** in partial fulfillment of the requirements for the degree of **Doctor of Philosophy in Metallurgical and Materials Engineering Department, Middle East Technical University** by,

Prof. Dr. Halil Kalıpçılar
Dean, Graduate School of **Natural and Applied Sciences** _____

Prof. Dr. Ali Kalkanlı
Head of Department, **Metallurgical and Materials Eng.** _____

Prof. Dr. Rıza Gürbüz
Supervisor, **Metallurgical and Materials Eng., METU** _____

Examining Committee Members:

Prof. Dr. Bilgehan Ögel
Metallurgical and Materials Eng., METU _____

Prof. Dr. Rıza Gürbüz
Metallurgical and Materials Eng., METU _____

Prof. Dr. Cemil Hakan Gür
Metallurgical and Materials Eng., METU _____

Prof. Dr. Benat Koçkar
Mechanical Eng., Hacettepe University _____

Prof. Dr. Ziya Esen
Dep. of Inter-Cirricular Courses, Çankaya University _____

Date: 27.01.2023

I hereby declare that all information in this document has been obtained and presented in accordance with academic rules and ethical conduct. I also declare that, as required by these rules and conduct, I have fully cited and referenced all material and results that are not original to this work.

Name, Last name: SALİM ÇALIŞKAN

Signature :

ABSTRACT

INVESTIGATION OF FATIGUE CRACK BEHAVIOR ON NEAR THRESHOLD REGION OF AISI 4340 STEELS FOR DIFFERENT HEAT TREATMENT CONDITIONS

Çalışkan, Salim

Ph.D., Department of Metallurgical and Materials Engineering

Supervisor: Prof. Dr. Rıza Gürbüz

January 2023, 189 pages

Damage tolerant approach is an important phenomenon in engineering practice and must be evaluated at the onset of the design stage for components that are subject to cyclic loading during functioning; if not, devastating fatigue failure may occur. Inaccurate assessments in allowable fatigue data can cause substantial variation in fatigue limit evaluation for components with small crack size. Determining long crack threshold value as a design criterion is not a new research topic; even so, some anomalies arising from different test methods in the literature make this subject suitable for investigation. The fatigue crack growth mechanism takes place in the plastic zone region, which is very small in size; the order is thought to be microstructural units, especially at low stress intensities. Hence, differences in microstructure caused by heat treatment methods are often attributed to changes in monotonic and yield strength, which results in variations in plastic zone size. In this thesis, endurance limit of AISI 4340 steel in annealed and tempered conditions was investigated using the most established staircase and curve fitting approaches, additionally the reliability of data set was also questioned. Moreover, the effect of

microstructure around low stress intensities was detailed by crack growth tests. Also, the influence of stress ratio and compression precracking on near-threshold performance were investigated. Eventually, fatigue limit and long crack threshold values were found as 585 MPa and 4.89 MPa√m for tempered specimens, and 481 MPa and 4.01 MPa√m for annealed specimens. Accordingly, endurance limit assessment for components with physically small crack sizes was obtained by correlating the fatigue limit with the threshold data for each microstructure.

Keywords: Fatigue, Threshold, Crack Growth, Steels, Heat Treatment, Reliability

ÖZ

FARKLI ISIL İŞLEM KOŞULLARINDA AISI 4340 ÇELİKLERİN YORGUNLUK ÇATLAK DAVRANIŞININ EŞİĞE YAKIN BÖLGEDE İNCELENMESİ

Çalışkan, Salim

Doktora, Metalurji ve Malzeme Mühendisliği Bölümü

Tez Yöneticisi: Prof. Dr. Rıza Gürbüz

Ocak 2023, 189 sayfa

Hasara dayanım yaklaşımı, mühendislik pratiğinde önemli bir olgudur ve çalışma sırasında döngüsel yüklemeye maruz kalan bileşenler için tasarım aşamasının başlangıcında değerlendirilmelidir; değilse, yıkıcı yorgunluk arızası meydana gelebilir. İzin verilen yorulma verilerindeki yanlış tahminler, küçük çatlak boyutuna sahip parçalar için karşılık gelen dayanıklılık stresinde önemli farklılıklara neden olabilir. Tasarım kriteri olarak uzun çatlak eşiğinin belirlenmesi yeni bir araştırma konusu değildir; ancak literatürdeki farklı test yöntemlerinden kaynaklanan bazı anormallikler bu konuyu incelemeye uygun kılmaktadır. Yorulma çatlağı büyüme mekanizması, boyut olarak oldukça küçük olan plastik bölgesinde meydana gelir; boyut olarak, özellikle düşük gerilme yoğunluklarında, mikroyapısal birimler olarak kabul edilir. Bu nedenle, ısıl işlem yöntemlerinin neden olduğu mikroyapısal farklılıklar, genellikle monoton ve akma mukavemetindeki değişikliklere atfedilir ve bu da plastik bölge boyutunda değişikliklere neden olur. Bu tezde, AISI 4340 çeliğinin tavllanmış ve temperlenmiş koşullardaki yorulma dayanım limiti, en yaygın merdiven ve eğri uydurma yaklaşımları kullanılarak araştırılmış, ayrıca veri setinin güvenilirliği

de sorgulanmıştır. Ayrıca, mikroyapının düşük gerilim yoğunlukları etrafındaki etkisi, çatlak büyüme testleri ile detaylandırılmıştır. Ayrıca, gerilim oranı ve sıkıştırma ön çatlağının eşik değerine yakın performans üzerindeki etkisi de incelenmiştir. Sonuçta yorulma limiti ve uzun çatlak eşik değerleri temperlenmiş numuneler için 585 MPa ve 4.89 MPa \sqrt{m} ve tavlanmış numuneler için 481 MPa ve 4.01 MPa \sqrt{m} olarak bulunmuştur. Buna göre, fiziksel olarak küçük çatlak boyutlarına sahip bileşenler için dayanıklılık sınırı değerlendirmesi, her bir mikro yapı için yorulma sınırının eşik verileriyle ilişkilendirilmesiyle elde edilmiştir.

Anahtar Kelimeler: Yorulma, Eşik, Çatlak İlerleme, Çelikler, Isıl İşlem, Güvenilirlik

To My Parents

ACKNOWLEDGEMENTS

The author is grateful and expresses his deepest gratitude to his supervisor, Prof. Dr. Rıza Gürbüz, for his advice, guidance, criticism, encouragements, tolerance and the opportunity to work under his supervision.

The author also extends his deepest gratitude to Prof. Dr. Benat Koçkar and Prof. Dr. Bilgehan Ögel, who were the jury members of the thesis advisory committee, for their valuable advice and comments throughout the thesis.

The author would like to express his gratitude to his own company, Turkish Aerospace, for providing academic leave during the thesis period, encouraging the employee to the doctoral program, and providing permission to conduct tests specific to the thesis topic in their own facilities.

The author would like to thank Mr. Yusuf Yıldırım for his support in the heat treatment and Mr. Anıl Yıldırım for his support in the SEM analysis. I would like to express my special thanks to Mr. Faruk Türkmen, Mr. Ömer Duman, Mr. Yusuf Ulu, Mr. Kadir Karaman, Mr. Aykut Kibar, Mr. Fatih Melemez, Mr. Şahin Gören and Mr. Furkan Tuncer for their endless support throughout this research.

Finally, I would like to thank my beloved wife, my beloved parents, and my beloved brother for giving me an extraordinary life and endless love.

TABLE OF CONTENTS

ABSTRACT	v
ÖZ	vii
ACKNOWLEDGEMENTS	x
TABLE OF CONTENTS	xi
LIST OF TABLES	xiii
LIST OF FIGURES	xiv
CHAPTERS	
1. INTRODUCTION.....	1
1.1.MOTIVATION	6
1.2.AIM OF THE WORK AND MAIN CONTRIBUTION.....	7
2. BASIC KNOWLEDGE	9
2.1.ENDURANCE LIMIT	9
2.2.PHYSICAL BASIS OF FRACTURE MECHANICS	12
2.2.1.SHORT & LONG CRACKS	15
2.2.2.LINEAR ELASTIC FRACTURE MECHANISM (LEFM) APPROACH	18
2.2.3.CRACK CLOSURE.....	21
2.2.4.COMPRESSION PRECRACKING	25
2.2.5.FATIGUE CRACK GROWTH THRESHOLD	31
2.2.6.COMPLIANCE MEASUREMENT	34
2.2.7.HEAT TREATMENT ASSESMENT.....	38
3. LITERATURE REVIEW.....	47
4. EXPERIMENTAL PROCEDURE	83
4.1.MATERIAL	83
4.2.SAMPLE PREPARATION	83
4.3.FATIGUE TEST PARAMETERS.....	89

4.4.TEST EQUIPMENTS.....	90
5. RESULTS AND DISCUSSIONS.....	95
5.1.MICROSTRUCTURE OF THE SAMPLE	95
5.2.ENDURANCE LIMIT TEST RESULTS	97
5.2.1.STAIRCASE METHODS	97
5.2.1.1.DIXON-MOOD METHOD	98
5.2.1.2.IABG METHOD.....	100
5.2.1.3.BOOTSTRAPPING METHOD.....	102
5.2.1.4.WEIBULL METHOD	104
5.2.1.5.JSME METHOD.....	106
5.2.2.CURVE FITTING ANALYSIS.....	107
5.2.2.1.BASQUIN METHOD.....	107
5.2.2.2.ASTM E739-91 METHOD.....	109
5.2.2.3.KIM AND ZHANG METHOD	110
5.2.2.4.BILINEAR METHOD.....	111
5.2.2.5.STUSSI METHOD	113
5.2.2.6.AGARD-AG-292 METHOD.....	114
5.2.3.FATIGUE RELIABILITY ANALYSIS	115
5.2.4.FATIGUE LIMIT DISCUSSION.....	120
5.2.5.FATIGUE LIMIT CORRELATION	124
5.3.CRACK GROWTH TEST RESULTS	126
5.3.1.COMPLIANCE METHOD	127
5.3.2.COMPRESSION PRECRACKING	135
5.3.3.PRECRACKING EVALUATION	140
5.3.4.THRESHOLD TEST RESULTS	142
5.3.5.THRESHOLD EVALUATION.....	146
5.4.FAILURE ANALYSIS	149
5.5.RESULTS OF FATIGUE TESTS	159
6. CONCLUSIONS.....	165
REFERENCES	169

LIST OF TABLES

TABLES

Table 1 Classification of small fatigue cracks [43].....	17
Table 2 Machining parameters of the AISI 4140 steel samples.....	85
Table 3 Test variables defined for thesis study.....	90
Table 4 (Cont'd) Bootstrapping algorithm (10 out of 200 re-sampling)	103
Table 5 Variation of probability of survival with standard deviation.....	119
Table 6 Different Approaches to determine fatigue limit of material.....	123
Table 7 Near threshold results for all fatigue crack growth tests.....	161

LIST OF FIGURES

FIGURES

Figure 1 Typical SN curves for metallic materials exhibiting endurance limit [24].	10
Figure 2 (a) Illustration of the polycrystal's persistent slip band geometry. (b) PSB interactions with grain boundaries result in ledges and steps, which are static extrusions across the grain boundary [36].	13
Figure 3 Change in behavior from short to long cracks by dislocation models [41].	15
Figure 4 Characteristic variance in fatigue crack growth rates for long and short cracks, along with the nominal cyclic stress intensity factor [45].	18
Figure 5 Regimes during a crack's lifecycle; it will show LEFM behavior after a certain crack size [51].	20
Figure 6 Fatigue crack closure mechanism [56].	23
Figure 7 The formation of several closure mechanisms is depicted [57].	24
Figure 8 Compression-compression precracking method before determining fatigue crack growth threshold [61].	25
Figure 9 Under cyclic compression-compression loading, schematic representation of plastic zones and stresses ahead of the notch (a) first loading cycle; (b) following a small crack formation; (c) non-propagated crack condition [68].	28
Figure 10 Compression precracking micrograph ($\approx 200 \mu\text{m}$ ahead of the notch) [69].	29
Figure 11 Different types of razor blade applications: (a) Razor blade tapping/sawing, (b) Razor blade hammering, and (c) Via tension/compression device [72].	31
Figure 12 Near threshold region [75].	33
Figure 13 Compliance curves for an uncracked specimen (a), a cracked specimen (b), and a cracked specimen with crack closure (c) [85].	35
Figure 14 Using the ASTM compliance offset method, the opening load can be calculated. Compliance curve (a), determination of opening stress (b) [90].	36
Figure 15 Fatigue crack growth behavior of AISI 4340 steel for quenched and tempered conditions at different stress ratios [102].	42
Figure 16 Technical drawing of the round specimens	83
Figure 17 Manufacturing process of fatigue specimens	84
Figure 18 Heat treatment procedure for smooth fatigue specimens	85
Figure 19 Sampling of round fatigue specimens with extracted orientation	86

Figure 20 SEB specimen dimensions with EDM notch on center of the specimen.....	86
Figure 21 Manufacturing process of crack growth specimens.....	87
Figure 22 Heat treatment procedure for annealed crack growth specimens	88
Figure 23 Sampling of crack growth fatigue specimens with extracted orientation.....	88
Figure 24 BUEHLER polishing machine	89
Figure 25 RUMUL Testronic resonant fatigue machine (performed at TAI M&P Lab.)91	
Figure 26 RUMUL Cracktronic resonant fatigue machine (performed at TAI M&P Lab.)	91
Figure 27 Instron 8801 servohydraulic test bench (performed at TAI Structural Test)..	92
Figure 28 Scanning Electron Microscope (examined at TAI M&P Lab.)	93
Figure 29 Micrograph of the tempered fatigue specimens.....	96
Figure 30 Micrograph of the annealed fatigue specimens	96
Figure 31 Staircase based on Dixon-Mood method.....	99
Figure 32 Mean value with 50% probability of failure and standard deviation provided by 95% confidence level	100
Figure 33 IABG method (Δ : fictitious data)	101
Figure 34 Estimation of mean value and standard deviation with given 95% confidence level via IABG method	101
Figure 35 Gauss distribution of staircase data based on Bootstrapping method	102
Figure 36 Mean curve with 50% probability of failure (solid line), including 95% bootstrap t-interval (dash line) and standard lower confidence limit (long dash dot) ..	104
Figure 37 Weibull distribution of staircase data based on Newton Rapson technique	106
Figure 38 SN curve estimation using Basquin method.....	108
Figure 39 SN curve estimation using ASTM E731-91 method.....	110
Figure 40 SN curve estimation using Kim and Zhang method.....	111
Figure 41 SN curve estimation using Bilinear method.....	112
Figure 42 SN curve estimation using Stussi estimation.....	113
Figure 43 SN curve estimation using AGARD-AG-292 method	115
Figure 44 Comparison of standardized residual and studentized residuals	117
Figure 45 Normal probability plot assessment.....	118
Figure 46 SN curve estimation with probability of failure using Bilinear method.....	120
Figure 47 Alteration in the design curve as a result of probabilistic analysis (C.I.: Confidence Interval, P. of S.: Probability of Survival).....	124
Figure 48 Variation of stress amplitude and failure cycle	125
Figure 49 Variation of endurance limit and hardness	126
Figure 50 Normalized crack opening stress varies with stress ratio in case of constraint factor is equal to 1	129

Figure 51 Normalized crack opening stress varies with stress ratio in case of constraint factor is equal to 3.....	129
Figure 52 Normalized crack opening stress varies with stress ratio in case of $S_{max}/\sigma_0=1/3$	130
Figure 53 Evaluation of crack Size by compliance method	131
Figure 54 Unloading part of load-displacement curve	132
Figure 55 Compliance offset method.....	133
Figure 56 Compliance change with increasing crack size during each phase of test	134
Figure 57 Variation of maximum compression precracking force with stress ratio.....	137
Figure 58 Load profiles for different stress ratios under of compression-compression precracking test	138
Figure 59 Non propagating crack formation after compression precracking: a) Razor blade application prior to precracking b) Front side micrograph c) Back side after formation of non-propagating crack	139
Figure 60 Loading sequence to reach threshold region	143
Figure 61 NASGRO curve fitting after crack growth tests.....	145
Figure 62 Micrography of fracture surface of the crack propagation test	150
Figure 63 Multiple crack initiation during precracking loading	151
Figure 64 Crack growth sequence for tempered specimen	152
Figure 65 Compression precracking stage for tempered specimen	153
Figure 66 Crack growth region for tempered specimen in high magnification	154
Figure 66 Fast rupture for tempered specimen	155
Figure 68 Compression precracking stage for annealed specimen	156
Figure 69 Crack growth region for annealed specimen in high magnification.....	157
Figure 70 Transition region for crack growth test of annealed specimen.....	158
Figure 71 Fast fracture region for the annealed specimen	159
Figure 72 Variation of long crack threshold data	160
Figure 73 Variation of long crack threshold data with stress ratio	162
Figure 74 Kitagawa Diagram of AISI 4340 for different microstructures under R of 0.1	163

CHAPTER 1

INTRODUCTION

A damage tolerant design method is used for components with a long cycle working life, such as transmission parts, and inspection intervals are determined based on fatigue crack growth data [1]. Extrinsic and intrinsic processes cause fatigue crack propagation behavior. Monotonic and cyclic strains ahead of the crack tip can control the intrinsic process. Brittle materials display monotonic loading fracture; ductile materials, on the other hand, show cyclic deformation due to crack blunting and re-sharpening towards steady state crack propagation. Over ductile materials, fatigue crack development is caused by cyclic plastic deformation with below fracture toughness loading. The generation of residual stresses as a result of plastic deformation after unloading causes a change in the local stress ratio, and the fatigue crack growth behavior is adversely influenced [2]. Steels undergo strain hardening during deformation, resulting in reduced stress redistribution and a smaller plastic zone size ahead of the crack tip [3]. Fatigue fractures grow through slip planes with the highest resolved shear stress, and shear stress varies from grain to grain, resulting in a rough surface on the crack path.

Because of inhomogeneous plastic deformation and irreversible strain localization, strain energy is stored during cyclic loading. Small crack propagation is caused by the release of elastic energy ahead of the fracture tip, and this stored energy is responsible for the growth process in terms of driving force. Local strain forms at favorably oriented grains due to differences in grain orientation, resulting in the development of persistent slip

bands at the surface, which are responsible for crack initiation on the surface due to the lack of constraint on the surface compared to the interior in terms of amount of local strain. Shear deformation causes peak and valley views on the surface due to persistent slip bands. Crack initiation is caused by the formation of potential crack nuclei as a result of stress concentration. Crack initiation reduces when the stress amplitude increases.

Stress concentration locations, such as notch, hole, and microstructural flaws, are sources of internal stresses. Internal stress asymptotically reduces as one moves away from the source. However, when fracture length increases, applied stress increases, and there is competition in terms of total stress. If the applied stress is less than K_{th} and K_{max} , fracture growth stops because the total stress is insufficient. Fatigue crack growth characteristic of lengthy cracks is due to the removal of internal stress. Because internal stresses occur, the local stress ratio at the fracture tip will be larger than the remote load ratio. In the event of all stresses considered, equal driving forces exist for fatigue crack growth behavior between short and long cracks.

Dislocation-based models, as well as plastic accumulation models, have been presented to explain crack growth behavior. This method may be used to determine the mechanism of fracture types, the involvement of grain boundaries, and irreversible damage caused by the slip mechanism. Taira et al. [4] investigated crack growth retardation due to grain boundaries blocking plastic slip movement, requiring a greater frictional shear stress for slip glide over grains. The transition from a small to a long fracture can also be assessed using a slip model, in which slip activity is subjected to consecutive coaction of grain boundaries, and effective impedance decreases as crack extension increases. Crack propagation eventually reaches the steady state zone. On steady state, crack progression appears zig-zag because the displacement difference at the crack tip during loading and unloading sharpens the crack and activates the parallel slip plane.

Crack closure is an intrinsic characteristic of the growth process that increases as the crack length rises. It is determined by the stress ratio and calculated by determining the crack

depth at which complete crack closure occurred. Intrinsic property, on the other hand, can be expressed as microstructural resistance to fracture formation. The difference between applied stress and closure stress is used to calculate effective stress, which is linked to intrinsic characteristic.

During the propagation phase, the crack plane yields, and residual stresses accumulate, which affect crack propagation beyond the plastic zone. Residual stresses and loading below the threshold stress produce crack arrest. When the pre-crack size is near the plastic zone size, residual stress effects are minimized for further constant amplitude testing. Long cracks must be fully opened in the steady-state zone before load reduction is used to get an appropriate threshold value using fatigue crack growth tests with no residual stresses. Even though compression precracking eliminates residual stresses, crack propagation is necessary to ensure that closure effects are also avoided, and the crack size may be expanded up to 5 mm in steady state in some situations to conform the closure free concept. Consistent threshold values can eventually be attained by doing a constant K test followed by compression precracking.

Compression precracking is a technique for obtaining data on fatigue crack growth with minimal load history effects. Precracking is done under constant amplitude compressive-compressive loading, which allows for tensile yield ahead of the crack tip, which is responsible for straight and natural cracks. The tensile cyclic plastic zone shrinks as the fatigue crack extends due to internal stress relaxation, and the fracture eventually stops when it reaches the monotonic compressive zone. The size of the compressive plastic zone is proportional to the amount of crack growth for precracking. Because there is no accessible driving force, a stalled crack is referred to as a non-propagating crack under compressive loading. As a result, the size of the crack following compression precracking is proportional to the monotonic compressive zone after the first compressive loading.

Threshold stress becomes important, especially for structures with high cycle loading, resulting in a large percentage of initiation and a short time for propagation, hence correct

threshold stress is required for life estimation. Long crack threshold values are commonly employed in design calculations for such structures, yet it is well known that small cracks grow at different rates than long cracks. The crack closure idea must be mastered in order to understand differences in propagation rate. Elber [5] described the phenomena of fracture closure by observing crack flakes contacting each other even under tension-tension loading.

Controlling the microstructure of a material through heat treatment allows for better fatigue characteristics and mechanical qualities. Because of microstructural barrier resistance, microstructurally short cracks (on the order of grain size) withstand crack propagation, and arrest results in the fatigue limit being unaltered until a certain size. These cracks usually form on the surface, and the stress threshold is known as the smooth or plain specimen fatigue limit. Long cracks, on the other hand, have sufficient driving force for growth and fatigue limit lowers as crack size increases [6]. For the growing process of long cracks, the applied K must be greater than the crack closure phenomena threshold value. Small cracks are physically located between microstructural small cracks and long cracks, and crack closure begins to become effective despite their sensitivity to microstructural alterations. For low carbon steels, this range can be defined as 50 μm and 0.5 mm fracture size. Microstructural short cracks predominate below 50 μm , and microstructural barriers have no effect on fatigue limit. However, when crack size increases, the fatigue limit decreases parabolically until it reaches the long crack size area. As a result of the loss of fracture closure effects, the fatigue limit has a linear relationship with increasing crack size and asymptotically decreases for physically short cracks.

Crack initiation is related to fatigue failure induced by surface features; conversely, crack growth is linked to material interior characteristics. As a result, cracks are easily generated at high stress values, resulting in minimal scatter; yet, in the converse case, substantial scatter is found around the fatigue limit due to local circumstances [7]. Despite coupon level testing can provide data concerning scatter, it can be impetus to forecast in real-world scenarios. Grain size and direction, material composition, surface polish after

machining, and heat treatment all affect SN curves [8]. As a result, scatter produced by material and manufacturing-related reasons cannot be exaggerated for operation goods and must be validated by structural testing. It is a standard practice to conduct tests at least two times over the course of a service life to identify significant points in terms of crack susceptibility. The scatter influence is evaluated in the literature by confidence levels and statistical methodologies [9].

If otherwise not stated, all SN curves in the database are introduced as a mean curve with a 50% probability of failure. The 95 percent confidence level is used by designers to ensure that the safe fatigue limit is met [10]. Curve fitting practice based on the log-normal or Weibull distribution are often used to create design curves. Because it does not deal with complexity, SN curve fitting may be evaluated using only two parameters, and it provides well-suited and accurate results [11]. Fatigue life of metallic materials have a log-normal or Weibull distribution based on analytic equations with some discrepancy; thus, all methodologies must be validated through fatigue testing to obtain trustworthy data [12].

Although fatigue strength has a predominantly normal distribution, the coefficient of variation in the fatigue strength has a log-normal distribution, and the scatter is bigger in the fatigue initiation dominant life zone than in the propagation one, which is subjected to high stress loading. The first fits well with the Weibull distribution, while the second fits well with the log-normal distribution. Standard deviation changes as a function of applied stress; as a result, as stress or strain decreases, standard deviation rises. To estimate observed data, the maximum likelihood method uses linear regression to cover run-out data points. Least square estimate is a strategy for reducing experimental data's residuals (sum of squared deviation). Because there is no stress concentration, two million cycles can be chosen for smooth specimen run-out requirements [13]. Barbosa et al. looked at a variety of estimated fatigue models to see which ones had the best fit between test and fitted data [14]. The distinction between these models is that they ensure the best match from low to high cycle regions; yet, the medium and high cycle regions are the

focal for structural design issues. From a statistical standpoint, Schijve et al. explored limitations in analyzed methods and found that the Weibull distribution is preferable suited than the log-normal distribution [7]. Stüssi proposed a different technique, in which a nonlinear equation can be written with stress and life relations, including ultimate and infinite endurance stress [159]. Model parameters can be calculated using linear regression, however Caiza et al. developed a combined Stüssi and Weibull distribution technique, which turns out strong fit in all regions of the SN curve because of preferable model parameter estimates [15].

Burhan et al. also looked at numerous curve fitting methodologies for characterization of fatigue data per SN curve competence, fitting parameter consistency estimation, adaptation to other stress ratios, fatigue damage assessment, and curve form ability including ultimate stress point [16]. Micro-crack density, rather than micro-crack length, grows up logarithmically as fatigue cycles increase, according to Kim et al. [17]. Lipski et al., on the other hand, looked at constructing an SN curve based on thermography analysis, which gives them the advantage of being able to cease testing before catastrophic failure due to temperature change [18]. In a log scale, ASTM E739-91 [19] provides a straightforward linear relationship between stress and life. The model is based on a log-normal distribution and can be handled using linear regression using the maximum likelihood method. Additionally, it clarifies how many specimens you'll need in order to acquire accurate results. As a result, a data set of 12 to 24 specimens is advised. As a rule of thumb, the confidence level for estimating the confidence band that covers observed experimental data should be between 5% and 95%. Because of the model's limitations, very low cycle regions are not taken into account, hence the ASTM E739-91 model is only suited for medium and high cycle fatigue zones.

1.1. MOTIVATION

Nowadays, interest in extending the high-cycle fatigue life of aerospace structures is more important. Therefore, increasing use of damage-sensitive aircraft structures is favored.

Investigation of crack initiation, closure effects, and small crack behavior phenomenon is becoming an increasingly popular research topic. It is known that a long fatigue life depends on keeping cyclic loads close to or below the fatigue threshold, understanding the behavior near the threshold. Correct estimation of fatigue threshold is critical during design phase of the project in terms of fatigue life of components. It is directly affecting design load for crack propagation and evaluation of inspection interval of components. Therefore, reliable test data estimation by following procedures for endurance limit and crack behavior needs to be assessed.

1.2. AIM OF THE WORK AND MAIN CONTRIBUTION

The purpose of this study is to emphasize the crack closure effect and establish a relationship between crack size and endurance limit. It is also to use a statistical approach in the evaluation of threshold values for different stress ratios. Another point is to characterize different heat treated AISI 4340 steel specimens because of being good candidate on aerospace components. In this way, it will help the industry in terms of the fatigue behavior of the specified material, and it would also be useful to present the procedure on how to find the precise and reliable data using statistical approaches after fatigue tests are performed.

CHAPTER 2

BASIC KNOWLEDGE

2.1. ENDURANCE LIMIT

Fatigue limit is defined as a material's resistance to the propagation of nucleated fractures, and the associated threshold stress for fatigue limit must be crossed microstructural obstacles in the growth process. As a result, fatigue limit is directly related to microstructure attributes such as grain diameters at the commencement of fatigue initiation and the early growth phase, and can also be referred to as a microstructural threshold. In the standard safe life design technique, SN curves can be viewed as a function of tiny crack initiation [20]. Wöhler, a German engineer, was the first to employ SN curves, and he constructed the stress-life as a linear equation, in which the logarithm of life is associated with oscillating stress. Basquin later developed a new model based on the natural logarithms of stress and life on either side [21]. The inclusion of a first boundary data point (ultimate stress) to the SN curve, on the other hand, resulted in inaccurate estimation. Strohmeyer presented a non-linear model by smoothing earlier models [169]. Researchers continued to propose new models to improve the best fit of the SN curve, essentially using the same strategy as before, by including parameters or altering the complicity of the relationship. Some of these are commonly used in the construction of SN curves. Many techniques have been provided in the literature that best suit data with a large number of specimens, nevertheless inconsistency occurs when data sets with less specimens are used [22]. Despite the fact that new technologies now allow

for ultra-high-test frequency fatigue tests on resonant test systems, SN curve methods must be compatible with few data sets because of UHCF time constraints [23].

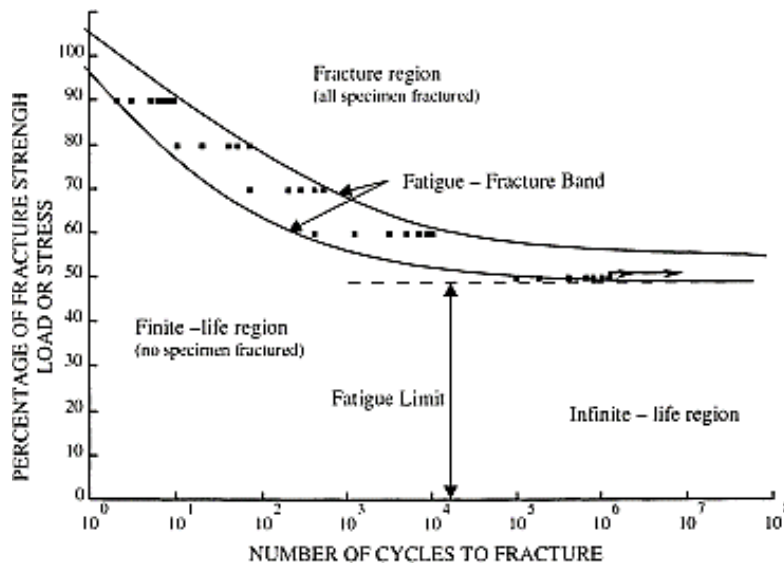


Figure 1 Typical SN curves for metallic materials exhibiting endurance limit [24].

According to Dixon [25], the goal of the staircase method is to concentrate data points around the mean value. As a result, the data size needs to be large enough. Dixon advised at least 40 specimens for a thorough meaningful data review. The increment range should be between 0.5 and 2 if standard deviation is known; otherwise, short intervals waste time if the starting point is not close to the mean value. Dixon revised his method, proposing that the increment step be approximated as and a maximum standard deviation error of 50 percent be accepted. As a result, the increment step for a credible prediction may be $2/3$ or $3/2$, because a small gap before gives lower covariance; nevertheless, a large step size reduces the number of trials around the mean value [26]. Despite the fact that the staircase approach recommends analyzing 15 specimens, the test data is often controlled by 6 samples, and various discussions are accessible to assess the fatigue limit of a material with fewer specimens while maintaining data reliability [27]. The usual distribution of material fatigue limits is often followed. It also has a log-normal distribution in engineering applications. The primary criteria of the staircase approach are to estimate

using a normal distribution; however, to avoid oversizing, the safety factor must be evaluated using a log-normal distribution.

The medium and high cycle fatigue regions of the SN curve, according to Zheng's research, pursue normal and log-normal distributions, respectively [114]. Rabb investigated whether or not the starting position has an impact on the staircase method and found that it has a minor impact [9]. To improve the accuracy of the analysis, the most common strategy is to start with an estimated fatigue limit.

The log-normal and Weibull distributions can be utilized to analyze the staircase approach if logarithmic stress levels are evenly spaced. Choosing an increment level between $2/3$ and $3/2$ to determine the mean data and confidence level of fatigue data gives a well-established methodology [28]. Fundamentally, it can be pretended that there is a threshold above the fatigue limit that enables fracture formation when a higher force is applied than the endurance limit [29].

The knowledge of mean data and standard error is required to reduce the fatigue limit. While fatigue limit is unaffected by increment size, standard deviation is significantly altered. Because low values of CoV produce practically identical results but not worthy for high values, Dixon-Mood is preferable method in this situation [30]. Lin et al. found that the method used to estimate endurance limit can be taken based on data covariance; for small covariance, the ray projected method (extrapolating through low cycles data) provides a better result, but for large covariance, the Dixon-Mood method (based on Maximum Likelihood Estimate) is recommended [27]. However, below 10^4 cycles, the projection approach is unreliable, therefore the stress level is crucial for faster assessments. Even though the most prevalent methodology for the staircase method is Maximum Likelihood Estimation, Wallin justified this approach since the scatter has a Weibull distribution rather than a normal distribution, which is the underlying hypothesis for MLE [117].

Iterating data points in terms of arithmetical operations is offered as a Monte Carlo approach [31]. Pollak et al. employed the bootstrapping approach to reduce standard error for data sets with small sample as a substitute to the Dixon-Mood method, which yields

accurate results for big specimens (at least 40 specimens) but underestimates result for small data sets [23]. The Bootstrap technique counts the standard deviation and confidence level throughout the mean data as an alternate method. The advantage is that it does not require the use of a distribution hypothesis, as in traditional approaches, but it still produces the same findings and data points evolve when data points are replaced by replication [32]. The fatigue life of a material is regulated by the inhomogeneous distribution of various sorts of flaws, according to various approaches. It has been established that non-propagating cracks in front of micro-notches occur beneath the endurance limit's stress level. Elicited from Murakami and Endo's assumptions [170], fatigue limit study yielded comparable results for annealed condition steel; however, due to the effect of non-metallic impurities, it will differ for hardened steel. Beretta et al. investigated fatigue qualities via statistical methods and the smallest number of defects interior part of the microstructure, concluding that maximum likelihood is the best estimator due to the lower standard deviation of excessive flaws [33].

2.2. PHYSICAL BASIS OF FRACTURE MECHANICS

Fatigue fracture behaviour is mainly characterized after cyclic damage, which causes cyclic hardening or softening, microcrack initiation from flaws, microcrack coalescence, macroscopic propagation, and catastrophic failure [34]. Local strain forms at favorably oriented grains as a result of the difference in grain orientation, resulting in the development of persistent slip bands at the surface, which are responsible for crack initiation on the surface due to the lack of constraint on the surface compared to the interior in terms of local strain amount. The shear deformation mechanism causes persistent slip bands to generate peak and valley views on the surface. Crack initiation is caused by potential crack nuclei caused by stress concentration. According to a research paper released by Tokaji et al. [35], ferrite areas are fracture start sites for low carbon alloys. Due to inhomogeneous plastic deformation and irreversible strain localization, strain energy is stored during cyclic loading. In terms of driving force, this stored energy

is responsible for growth, and minor crack propagation is caused by the release of elastic energy ahead of the crack tip.

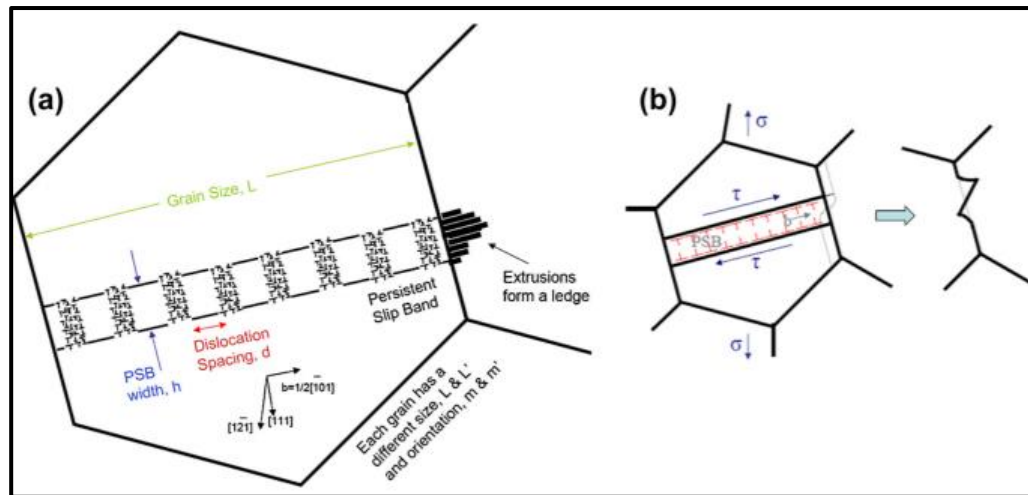


Figure 2 (a) Illustration of the polycrystal's persistent slip band geometry. (b) PSB interactions with grain boundaries result in ledges and steps, which are static extrusions across the grain boundary [36].

Under fatigue loading, crack initiation is influenced by stress amplitude, whereas crack propagation is influenced by strain amplitude. Surface crack initiation occurs most frequently in the early stages of the smooth specimen's life, but the change from microstructural to mechanical small crack takes time, depending on the material. This transition is defined by Lankford [37] as reaching a crack size where the plastic zone size ahead of the crack tip is bigger than the grain diameter. In essence, it is determined by the applied stress and the material's microstructure. As a generalization, the mechanical crack size for low alloy steels can be assumed to be 200 μm [38].

Cracks are high-energy flaws, and crack initiation and propagation need a lot of energy. External and internal strains provide the driving force for fracture development and progression. Dislocation plasticity causes internal stress during inhomogeneous deformation. External stress is related to crack size and inversely proportional to crack size; hence, larger stresses must be applied in the case of small cracks. Fatigue cracks start at the greatest surface grain because it has the best slip deformation orientation. As a result

of dislocation pile-up on microstructural impediments, persistent slip bands form. Extrinsic mechanisms or the amount of cycles applied to generate fatigue damage that increases internal stresses for the development of dislocation arrays can be used to continue fatigue crack propagation. Dislocation release occurs at the fracture tip as a result of fatigue crack propagation. K_{max} influences the size of the monotonic plastic zone, while K value influences the size of the reverse or cyclic plastic zone around 1/4 monotonic from the crack tip. When applied stress is insufficient to overcome monotonic plastic zone size, a threshold is defined [39].

Because of material behavior differences, fatigue crack initiation and propagation models started with Basquin equations (SN curves) and Paris equations (da/dN versus K) respectively. Irreversible slip bands are linked to the initiation of cracks in the form of persistent slip bands. Slip localization near the fracture tip, on the other hand, is responsible for crack growth till material failure.

Under cyclic loading, crack initiation occurs due to strain localization and accessible flaws acting as stress concentration to create a natural fracture. In the latter situation, persistent slip bands protrude from the surface, resulting in the construction of peak and valley topography. Then, crack nuclei form on the vertices because of the existing pushing force for fracture nucleation. As a generalization, fracture initiation occurs most frequently as crack nuclei in persistent slip bands, although their ability for damage accumulation for propagation are limited. The goal of persistent slip bands is to start cracks and expand them along a crack path. Grain boundaries are good places for fractures to start, and the number of grain boundary cracks increases as the stress amplitude decreases. Increased stress amplitude leads to a reduction in defect initiation [40].

The following criteria must be met for crack development to occur: Applied loading yields values greater than $K_{max,th}$, and K_{th} . The value of the long crack threshold is a material attribute that is unaffected by crack size or specimen shape. Slip bands, dislocation pile-up, or existing faults can cause small fractures to advance on locations with in-situ or pre-

existing stress concentration. Cyclic deformation causes fatigue damage by causing dislocation pile-up and forming a persistent slip band, which creates an ideal environment for crack initiation. Short crack behavior can be described as crack length dependence, greater crack growth rates, progression even below long crack threshold values, and crack size variance.

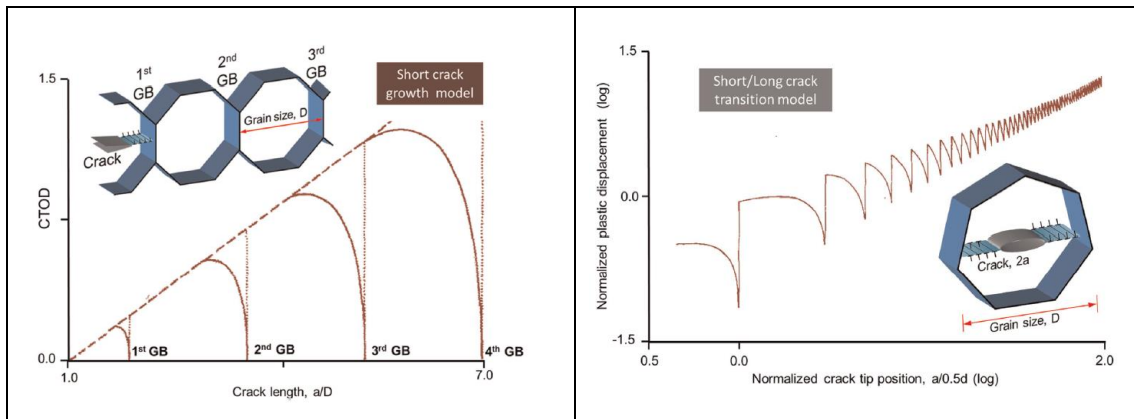


Figure 3 Change in behavior from short to long cracks by dislocation models [41]

Strain localization causes crack extension due to irreversible slide at the crack tip. Under cyclic loading, strain accumulates on stress concentration zones due to a sliding mechanism. Irreversible slip is the cause of a sharpening crack caused by a variation in displacement on the slip. Because the plastic zone's slip activity is limited, the slip system is engaged on a more favorable oriented slip plane, and crack extension occurs as a result of slip irreversibility [42].

2.2.1. SHORT & LONG CRACKS

Fatigue limit can be expressed as material resistance in terms of nucleated crack propagation and corresponding threshold stress for fatigue limit needs to overcome microstructural barriers for growth process. As a result, fatigue limit is directly related to microstructure properties such as grain dimensions at the onset of fatigue initiation, initial growth phase, and can also be referred the microstructural threshold. Controlling the microstructure of a material through heat treatment allows for superior fatigue properties as well as excellent mechanical properties. Because of microstructural barrier resistance,

microstructurally short cracks (on the order of grain size) endure crack propagation, and arrest results in the fatigue limit remaining unchanged until a certain size. These cracks typically form on the surface, and the threshold stress is referred to as the smooth or plain specimen fatigue limit. Long cracks, on the other hand, have sufficient driving force for growth, and the fatigue limit decreases as crack size increases.

For long cracks, the applied K must be greater than a threshold value associated with the crack closure phenomenon. Physically small cracks exist between microstructural small cracks and long cracks, and crack closure begins to become effective, despite the fact that they are sensitive to microstructural changes. For low carbon steels, this range corresponds to 50 μm and 0.5 mm crack size. Below 50 μm , microstructural shot crack predominates, and microstructural barriers have no effect on fatigue limit. However, as crack size increases, the fatigue limit begins to decrease parabolically until it reaches the long crack size region. The fatigue limit then has a linear relationship with increasing crack size due to the loss of crack closure effects, which is responsible for the asymptotically decreasing for physically short cracks. For most short cracks, the majority of the fatigue life is spent during the propagation phase.

In terms of crack closure, microstructural sensitivity, and relative plastic zone size based on crack length, short crack behavior differs from long crack behavior. Short cracks are known to propagate at a faster rate than long cracks. Small fractures can be divided into four categories in general. A microstructural small crack is one that is smaller than the grain size. Mechanically small crack: it is smaller than the plastic zone size. Physically small crack: less than one-hundredth of a unity crack is fully developed (considered as 1 mm). Chemically small crack: it can be up to 10 mm in size, depending on the crack tip environment.

Table 1 Classification of small fatigue cracks [43]

<i>Type of small crack</i>	<i>Dimension</i>	<i>Responsible mechanism</i>	<i>Potential solution</i>
Mechanically small	$a \lesssim r_y^a$	Excessive (active) plasticity	Use of ΔJ , ΔS or crack-tip-opening displacement
Microstructurally small	$a \lesssim d_g^b$	Crack tip shielding, enhanced $\Delta \epsilon_p$	Probabilistic approach
Physically small	$2c \lesssim (5-10)d_g$ $a \lesssim 1 \text{ mm}$	Crack shape Crack tip shielding (crack closure)	Use of ΔK_{eff}
Chemically small	Up to about 10 mm ^c	Local crack tip environment	

^a r_y is the plastic zone size or plastic field of notch.

^b d_g is the critical microstructural dimension, e.g. grain size, a is the crack depth and $2c$ the surface length.

^c Critical size is a function of frequency and reaction kinetics.

Microstructural changes influence small crack growth, while large scale yielding at the crack tip and crack closure act as driving forces for propagation. Crack propagation rate decreases in the pearlite phase due to thin ferrite lamellar on the microstructure; however, cementite part is responsible for rapid propagation LEFMs. Cracks begin on the ferrite phase and propagate through the ferrite across retained austenitic regions in a microstructure containing ferrite and bainite phases.

Because of the lack of closure effects, fatigue growth in small cracks requires higher internal and applied stress. Internal stresses due to dislocation pile-up to sustain crack growth decrease as crack length increases, which is inversely proportional to R curve change. Specimens with short cracks require a higher stress amplitude and a greater number of cycles to develop fatigue damage near the crack tip, which is required for crack growth.

When compared to long cracks, short cracks grow at a much slower rate due to their high propagation rates. The threshold of stress intensity range for small cracks increases until it reaches an asymptote to long crack threshold value as crack length increases, and this phenomenon is known as the R -curve or resistance curve to fatigue crack propagation. This curve is useful for determining the fatigue limit of materials with small size defects [44].

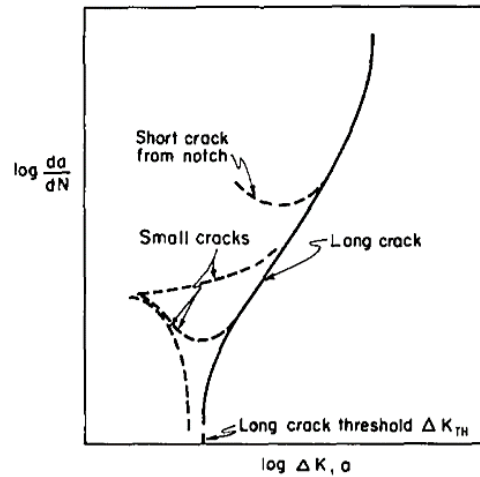


Figure 4 Characteristic variance in fatigue crack growth rates for long and short cracks, along with the nominal cyclic stress intensity factor [45]

In the standard safe life design technique, SN curves can be viewed as a function of tiny crack initiation. Compressive residual stresses cause the material to be unusually stiff, requiring larger driving pressures for fracture formation. As a result, compressive residual stresses enable cracks close faster. The stopping of minor cracks could be due to a shift in grain boundary direction that causes strain concentration [46].

Small fractures have a distinct curve form than long cracks when it comes to fatigue crack propagation. To predict crack growth rate, a variety of analytical models are introduced. Short cracks are known to expand their crack size even when the applied stress is less than the matching long crack threshold value. As a result, changing the threshold value has a significant impact on the residual life of a component. A change of $1 \text{ MPa}\sqrt{\text{m}}$ on the threshold value changes the residual properties of a component by around 18% [47].

2.2.2. LINEAR ELASTIC FRACTURE MECHANISM (LEFM) APPROACH

By combining crack propagation at the threshold with crack closure effects, the LEFM model can successfully estimate crack propagation near the threshold [48]. Even though LEFM is a popular method for crack propagation, it has some drawbacks, such as small-

scale yielding near the crack tip. The LEFM model was found to underestimate fatigue fracture development rates for small cracks, which had higher propagation rates in reality [49]. Based on two-dimensional stress singularity, the LEFM model claims that the stress field surrounding the fracture tip is expressed as a stress intensity factor. When compared to plain stress situations, where additional surface singularity complicates the stress field, square root singularity allows for faster crack formation in plain strain settings. For plain strain and plain stress, the stress singularity exponent is 0.5 and less than 0.5, respectively. Slow fatigue crack propagation on the surface region and concave markings on the fracture zone are the outcome [50].

If the crack tip plasticity needs to be small in relation to the crack size, LEFM is available. When the crack size is very small, stress becomes infinite by Irwin tip radius mode I; nonetheless, local crack tip yielding occurs, and the corresponding size is called the plastic zone ahead of the crack tip. For reverse loading conditions, a monotonic plastic zone forms during loading and a cyclic plastic zone forms after unloading that is one quarter the size of the monotonic zone. If the size of the plastic zone ahead of the crack tip is comparable to the crack length, the stress intensity range used to define the stress field for the existing fracture tip is insufficient. J-integral characterizes strain hardening based on elastic-plastic conditions, and small-scale yielding is connected with strain energy release rate. For elastic-plastic circumstances, another way is to use crack tip opening displacement to establish effective stress ahead of crack. In comparison to the LEFM method, the elastic-plastic approach is better for small cracks to normalize disparities between short and long cracks.

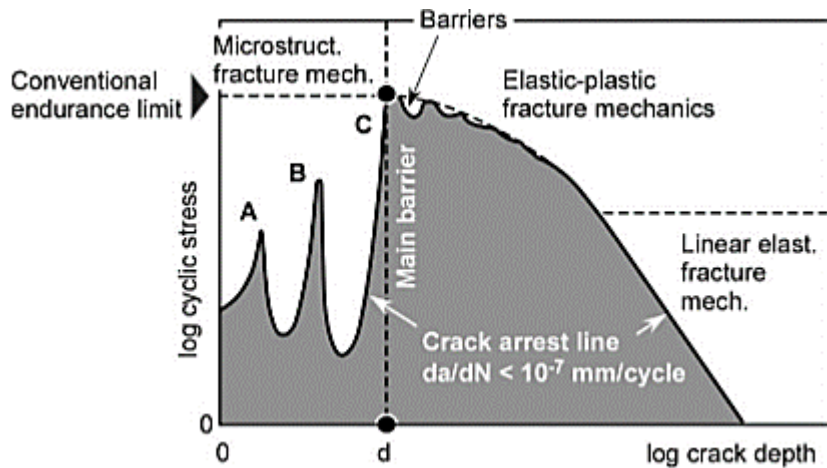


Figure 5 Regimes during a crack's lifecycle; it will show LEFM behavior after a certain crack size [51]

The rate at which fatigue cracks propagate (da/dN) is determined by continuum characteristics such as stress range, fracture length, and stress ratio. The advantage of the LEFM model is that it can assess damage trends in real time. Many scholars attempted to develop the fatigue crack growth rate (da/dN) vs K relationship and provided the rationale for the constant value of the first region asymptotes. Elber [5], for example, linked fatigue crack development behavior to the presence of plastic wake on crack flanks. Extra material distorted plastically flows and accumulates on fracture sides during crack extension, resulting in crack closure even under tensile loading due to contact of crack surfaces.

Newman [52] proposed that triaxial stress state conditions provide reduced degree of crack closure because out of plane flow is not possible; on the other hand, plain stress state conditions provide necking-like plastic deformation while propagating crack because flow of plastically deformed material is allowed, and the crack wake acts as a wedge for crack growth.

Short cracks have much more scatter than long cracks, therefore using the LEFM technique with the similitude concept isn't a good idea. The fracture propagation rate near

the threshold is less than 10^{-9} m/cycles. The fracture growth rate in the threshold region is 10^{-11} m/cycles. Because of the lack of plasticity in the near-threshold area, LEFM can be employed. Crack closure, microstructural effects, and relative plastic zone size dependent on crack size all contribute to differences in threshold values between small and long cracks. Crack closure based on oxide production due to fretting limits the effective stress intensity range and crack propagation rate at low intensities. As a result, it can be stated that environmental influences are more prominent at the near-threshold zone. For non-ferrous materials, higher yield strength results in a lower threshold value, and reverse relationship is possible. The amount of hydrogen in the material increases as the yield strength increases, resulting in a faster propagation rate. Higher yield strength, on the other hand, enhances the material's fatigue limit due to lower plastic strain per loading cycle. As a result, hard materials have a higher fatigue strength but a faster crack propagation rate. Because of the Hall-Petch equation, grain size effects are mostly determined by the material's yield strength. As a result, smaller grains have a greater fatigue limit, and smaller grains allow slip bands to reach grain boundaries under low applied loads, enhancing fatigue crack propagation and lowering threshold values. Due to high flaws on the microstructure, decreased shear deformation causes cleavage surface [53].

2.2.3. CRACK CLOSURE

Crack closure is an extrinsic characteristic of the growth process that increases as the crack length grows. It is determined by the stress ratio and calculated by determining the crack depth at which complete crack closure occurred. Intrinsic property, on the other hand, can be expressed as fracture growth microstructural resistance. Effective stress is defined as the difference between applied and closure stress. Crack closure stresses are computed using the compliance approach, which yields good results when tested at constant amplitude. Remote closure is detected at low stress intensities near the biaxial stress threshold; thus, opening stress increases near the plain stress region and is not observed under plain strain conditions. In case of plain strain conditions and the near-

threshold region, the remote closure and threshold processes cannot be expected as plain stress conditions. After observing fatigue crack growth rate asymptotes to constant value, Paris [54] suggested a method to determine threshold stress. Then, following the guidance of Saxena et al. [55], ASTM produced a standard test procedure for determining crack propagation rate near the threshold. The threshold value is significantly affected by crack closure.

Higher roughness and oxide induced closure are possible with larger grain sizes, resulting in lower fatigue fracture development rates. Long crack fatigue propagation rate is significantly more susceptible to environment, stress ratio, and microstructure when the stress intensity factor is low. Because stress intensity range and stress ratio have an impact on crack closing, each effect must be evaluated in tandem. Because out of plane material movement causes plasticity induced fracture closure, the plain stress state demonstrates plasticity closure when contrasted to the interior component. By storing plasticity ahead of the crack tip zone, overloading causes compressive residual stresses and slows crack development. Because of increasing asperities around the threshold zone, oxidation also improves roughness. Plasticity-induced crack closure is not crucial for small cracks at positive load ratios, but it becomes more critical as the load ratio approaches negative. Plasticity-induced crack closure is caused by out-of-plane elongation of extra metal, resulting in a reduction in thickness, and it is only applicable under plain stress situations. By cyclic plastic deformation, plastic wake influences crack growth rate. Plastic wake is delayed by contact with tension loading phase as a crack propagates through the plastic zone. The effect of cyclic deformation is reduced as a result of the crack wedge, and fatigue propagation is retarded. Triaxial stress state condition and plastic wake are not observed in plain strain conditions because there is no out of plane flow accessible. If there is disproportional loading, the crack tip will increase with misalignment and rough crack flakes will appear. Roughness-induced crack closure increases as the distance from the fracture tip grows longer, eventually becoming constant at a distance greater than the plastic zone size. Furthermore, roughness-induced crack closure is triggered by the difference in displacement between crack flakes, and coarser grains have a rougher

surface than small grains, resulting in slower fatigue crack growth rates. Roughness-induced crack closure, for example, does not occur in ultra-fine grains. The production of oxide or corrosion debris on fracture surfaces causes crack closure and serves as a crack propagation barrier. Continuous forming and breaking during crack contact and fretting causes oxide production. Around the threshold zone, an open atmosphere allows for the bonding of oxide layers on the crack surface at very low stresses.

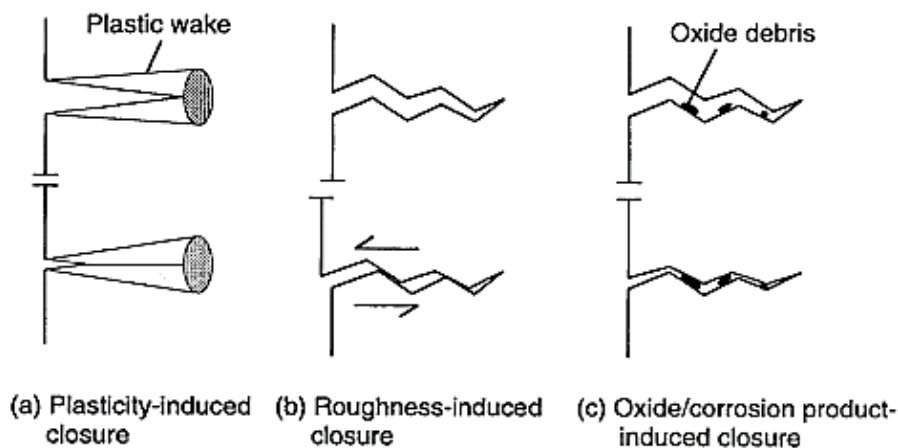


Figure 6 Fatigue crack closure mechanism [56]

Because crack development rate is independent of load ratio and remote closure under low stress intensity loading, the driving mechanism for small crack extension can only be cyclic plastic deformation, and the influence of monotonic loading can be ignored. This is due to a lack of crack closure for small cracks, which leads to rapid propagation rates. For long cracks under small scale yielding conditions, the tensile component of loading causes crack closure. Crack closure and crack opening stress are different in the low cycle fatigue regime than in the high cycle fatigue regime, which exhibits small scale yielding. Plasticity, roughness, and oxide-induced crack closure all contribute to crack closure in small scale yielding. Because fracture closure is caused by compressive-load induced crack closure at low cycle fatigue regions, its influence increases as strain amplitude decreases. Plasticity-induced crack closure does not occur under plain strain conditions because a local wedge forms near the crack tip due to plastic shear deformation in the

wake of the crack. The crack closure stabilizes as it grows from a small to a long crack, and it increases as the crack length increases until it reaches a stable state. Closure in terms of fracture wake plasticity is maximum in this location, but its effectiveness is reduced as effective stress increases. The presence of crack closure allows crack flakes to come into contact with each other during unloading, resulting in a change in compliance curve slope. When the stress ratio for long fractures is increased, the crack closing effects decrease and the R of 0.7 condition is reached. Crack closure for small cracks gradually increases as crack size increases, implying that the threshold stress for small cracks increases until a specific value is reached, at which point the little crack approaches the length of a long crack. The R curve, also known as the resistance curve, specifies the corresponding threshold value for each crack length. Plastic-induced crack closure is responsible for the R curve behavior. When the R curve reaches its limit, increasing the crack size has no effect on the threshold value.

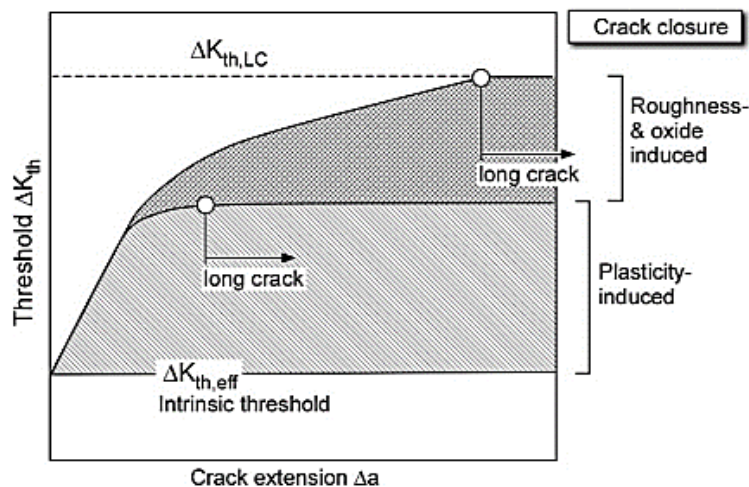


Figure 7 The formation of several closure mechanisms is depicted [57].

After at least 1 mm crack size advancement, roughness induced crack closure builds up in the steady state region and increases by increasing crack size. Oxide-induced closure, on the other hand, takes at least 80 hours to attain steady-state conditions. To create steady state conditions in terms of roughness and environmental driven crack closure, at least one million fatigue cycles are required [58]. Because of slip dissolving and oxidation in

the aqueous environment, the rate of fatigue crack formation in water decreases at lower stress intensities.

2.2.4. COMPRESSION PRECRACKING

Compression precracking has been recommended in the past for materials with low fracture toughness and the potential to fail under tensile precracking conditions. Hubbard proposed compression precracking to minimize load history effects and obtain correct crack growth rates at the threshold [59]. To establish steady state crack development conditions, non-propagating cracks must advance at least three monotonic compressive zone sizes after compression precracking. For investigating threshold behavior of long fractures at low stress amplitudes, compression precracking is followed by constant amplitude loading is regarded a desirable approach [60].

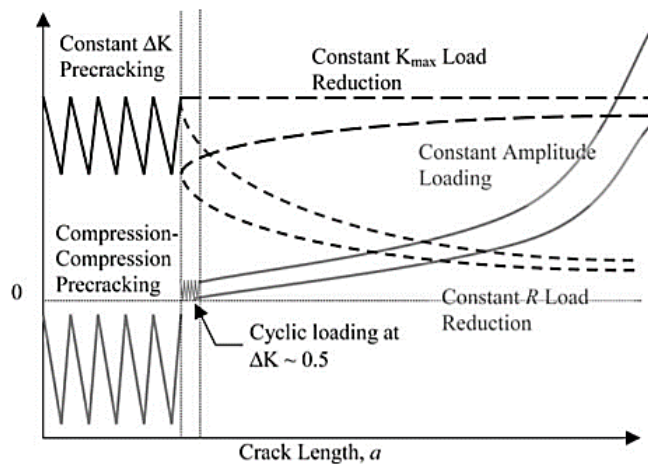


Figure 8 Compression-compression precracking method before determining fatigue crack growth threshold [61].

Compression precracking is an effective technique for obtaining data on the propagation of fatigue cracks with minimum load history effects. Load history effects coming from test process, specimen size, and test setup are the most common causes of misleading threshold values. Remote closure occurs when there is a larger applied precracking

loading, which reduces driving force and resulting in a higher threshold value. The benefit of compression precracking is that stress intensity is below zero while the crack is closing during the pre-cracking period, therefore the crack will open directly without being influenced by load history in a constant amplitude fatigue crack growth test.

Small cracks propagated below long crack threshold stress intensities established by test standards, according to Pearson [62]. Then, under constant amplitude loading, Newman investigated the behavior of short and long cracks around the near-threshold on remote crack closure effects effective on long cracks [63]. Because there is no crack closure, small cracks that are less than a specific length propagate faster than large fractures. Elber [5] identified a fracture closure concept that impacts residual stress distribution and plastic wake around crack sides under alternating loading. This phenomenon is known as load history effects on crack propagation. The effects of compression precracking as tensile residual stress on the threshold value were investigated by James et al. [64]. Load history effects can occur as a result of specimen configuration and test procedure used. Even if residual strains in the plastic zone are minimized due to stress release, the scale of yielding during precracking cannot be overlooked and has an impact on crack growth rates. Load history and environmental variables produce near-threshold fanning, culminating in remote closure. By combining crack closure effects and the Modified NASGRO equation, Maierhofer et al. created a crack growth rate model for small cracks with small scale yielding [65]. After a specific amount of fracture extension, each closure mechanism takes effect. Because of the rising plastic zone size, plasticity-induced crack closure increases until it reaches a definite crack size and then becomes constant. For all three sections of the da/dN curve, some equations were added to connect crack growth rate with K . The steady state and unstable crack growth zones are often adequately matched, but the near-threshold region, especially for lower stress ratios, is troublesome.

Because of their inability to develop fatigue cracks ahead of notch at low stress intensities, load reduction procedures have been used for a long period. As a result of producing high closure loading and remote crack closure, as described by ASTM E-647 [66], load

reduction results in a high threshold value, which slows crack propagation. Load reduction is defined in this process as 10% increments by 0.5 mm crack extension under a -0.08 mm^{-1} gradient. Because of out-of-plane distortion during crack propagation, residual stress allows for the creation of a crack wedge on the surface. For ductile materials, an ASTM E647 load reduction process can be performed.

To propagate the crack, constant amplitude loading is applied after compression precracking is commenced at low stress intensities. In the event that crack propagation is not noticed after five hundred thousand cycles, the load increment is increased by 10%. After achieving around 4 times of tensile cyclic plastic zone, load reduction is applied in 3 to 10 percent increments. This sequence is repeated until the rate of crack propagation has stabilized, at which point a threshold can be set. Because of the roughness and oxide induced crack closure that causes the rough crack flank, the ASTM E-647 load reduction process has a low crack propagation rate and high threshold values. To reduce residual stress effects ahead of the crack tip, the precracking stress value should be as low as possible. Effective K is accepted as $2.5 \text{ MPa}\sqrt{\text{m}}$ for ferritic steels and defined as the minimal stress intensity with no crack extension. Crack arrest is defined as a crack growth rate of less than $6 * 10^{-11} \text{ m/cycles}$. Wang et al. discovered that the long crack threshold value for the K decreasing approach is lower than the K increasing method [67].

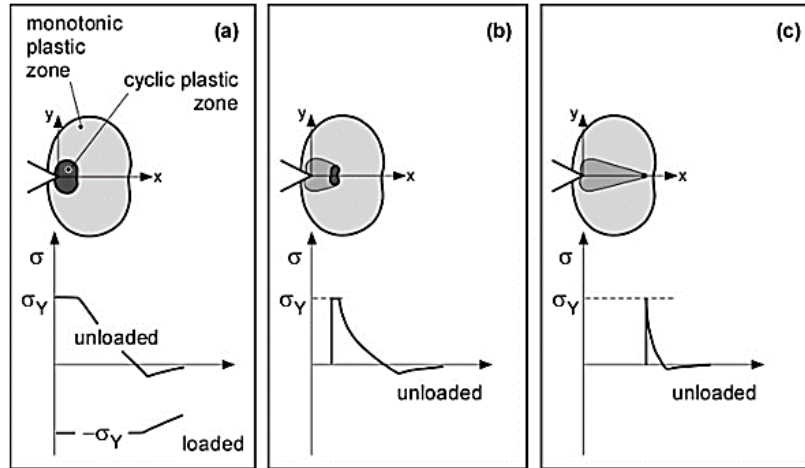


Figure 9 Under cyclic compression-compression loading, schematic representation of plastic zones and stresses ahead of the notch (a) first loading cycle; (b) following a small crack formation; (c) non-propagated crack condition [68].

When compared to load reduction, compression precracking before crack growth testing results in faster crack growth rates and a lower threshold value. Under the load decrease scenario, initial K has an impact on threshold values. After compression precracking, cracks will be fully open and will attain steady state under continuous amplitude loading. As a result, before load reduction approaches crack growth to effective stress intensity, a stabilized crack is provided, and variation around the threshold is minimized. Constant amplitude loading is applied just below the threshold value until crack propagation rate is marginally raised. The most difficult element at this point is estimating the initial K value since the initial data is influenced by tensile residual stresses from precracking. If the rate of crack formation continues to slow, loading will be raised by about 5% to 10%. When a positive rate of crack propagation is seen, the load is maintained constant. Before starting the load reduction operation, constant amplitude loading is continued until numerous compressive zones have been stabilized to minimize any tensile residual stresses induced by compressive loading. The upper bound of the threshold area can be regarded the load reduction approach; on the other hand, constant amplitude loading after precracking allows for a lower bound in terms of near threshold behavior. The load is reduced under

the condition that the crack growth rate is less than 10^{-8} m/cycles. Because more residual stress is induced, this rate might sometimes be higher, resulting in a slower crack propagation rate. If a crack does not grow under constant amplitude loading based on the first estimate, K is increased by trial and error.

Compression precracking is preferred over tensile-tensile precracking due to issues such as controlling crack propagation and maintaining an appropriate crack length. In terms of aligned and elongated grains, precracking productivity is determined by grain boundary orientation. To reduce tensile residual stresses, small K should be used for precracking. Under cyclic compression, small scale yielding occurs ahead of the crack tip front after precracking. Precracking size is less than cyclic tensile zone consisting of after unloading, and non-propagating crack size is roughly 0.2 mm or higher. Precracking size must be outside of the monotonic compressive zone by assuring small scale yielding ahead of the crack tip in order to produce meaningful fatigue crack growth data. This is accomplished by applying tensile fatigue loading following compression precracking to remove residual stresses.

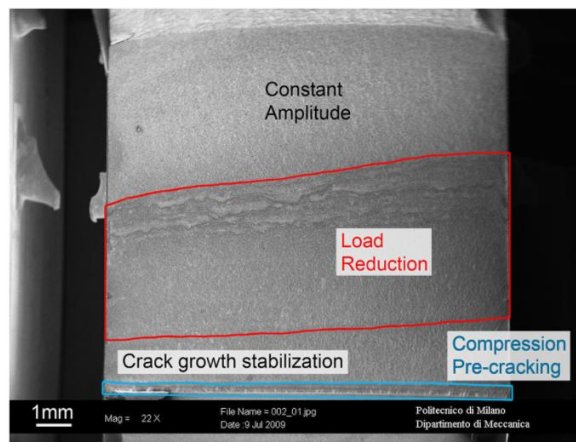


Figure 10 Compression precracking micrograph ($\approx 200 \mu\text{m}$ ahead of the notch) [69].

Elongated grain boundaries perpendicular to the crack propagation direction stop fatigue fracture growth. As a result, microstructural anisotropy, such as grain boundary blockage,

has a significant impact on residual stress. Stress reduction can be used to relieve residual strains created by compression precracking, although it is not recommended due to changes in microstructural characteristics caused by heating steels to roughly 600°C. Residual stresses from machining can be reduced before precracking by using local compression, a high R -ratio, and reverse bending [70]. Local compression caused by 1% local strain across thickness reduced residual stress and led in a uniform fatigue crack. Taguchi et al. looked at the effect of three-point bending fatigue loading after compression precracking to see if it may reduce the tensile residual stresses caused by fatigue precracking [71].

After the first loading case, a monotonic compressive zone forms, and tensile yielding ahead of the notch occurs after unloading, and a tensile plastic zone forms inside the compressive zone. As testing progresses, a cyclic plastic zone develops, resulting in small-scale yielding and crack development. Residual stress relaxes as the crack propagates, and the size of the cyclic plastic zone shrinks. It continues until the fracture reaches a monotonic compressive zone size, at which point the crack is stopped due to a decrease in the driving force for crack growth. Compression precracking has the advantage of providing a fully open crack, which minimizes the possibility of crack closure effects, resulting in lower crack propagation rates at low stress intensities. Crack growth rate approaching the threshold is influenced by increased stress intensity caused by crack growth and ascension of the threshold due to crack closure effects. Building crack closure becomes slower and stress intensity becomes dominant for crack extension after a specific length propagation approaching the threshold value.

Because of the small plastic deformation for precracking, razor blades are considered to be a useful approach for creating acute cracks approximately 20 μm . After the EDM notch has been prepared, the notch is sharpened with a razor blade and 1 μm diamond paste. Wires with a diameter of 30 μm are used to machine the EDM notch for accurate measurements. The zigzag appearance on the surface after fractography examination is a symptom of shear type fracture propagation produced by a change in slip system.

Increased environmental temperature resulted in a smoother crack surface, which provides less crack closure effects at higher temperatures. Dark patches on the surface during fractography investigation represent fretting debris as the crack propagates.

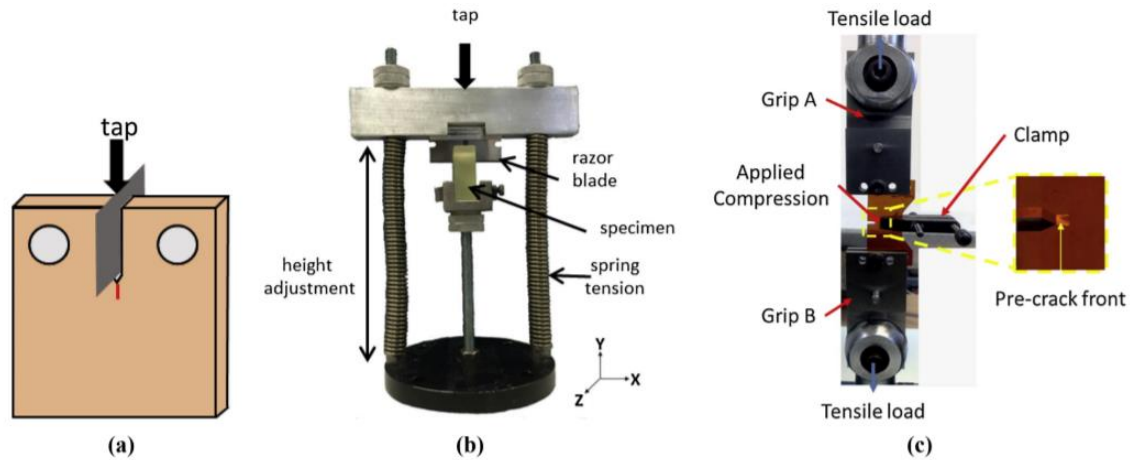


Figure 11 Different types of razor blade applications: (a) Razor blade tapping/sawing, (b) Razor blade hammering, and (c) Via tension/compression device [72].

Cracks may not originate at maximum permitted rates for AISI 4340 steels during load reduction in some instances; however, precracking allows cracks to initiate around K_{th} by eliminating load history effects [73]. Despite the fact that compression precracking is thought to provide more accurate fatigue crack growth data with fewer load history effects than traditional methods, new research has found that load history effects exist in the form of residual stresses after compression precracking, which affect fatigue crack propagation rates.

2.2.5. FATIGUE CRACK GROWTH THRESHOLD

Initiation, shear growth, tensile growth, and unstable growth are the four stages of a material's fatigue characteristic. The ability of a material to resist strain localization and plastic deformation can be described as its fatigue limit. Plasticity can be seen on the J-integral through stress-stain curves or load versus displacement curves that measure crack

tip opening displacement. The threshold stress for short cracks can be calculated using Kitagawa diagrams using long crack threshold values and smooth specimen endurance limits. Because of the lack of closure for short cracks, the fatigue threshold drops. The compliance curve is calculated using the derivative of the load and displacement curves generated by the crack opening displacement gage, and it is used to assess completely open and closed crack behavior. After performing tests in this manner, the spacing between striations is also utilized to define the opening stress range.

Crack growth is influenced by crack size and stress ratio. In general, as the load ratio increases, the threshold value decreases. The scatter is often less than 10% for long crack threshold value. The fatigue crack growth rate and threshold value can be determined using polynomial fit to the entire region. Mixed mode (tension and shear) fatigue growth near the threshold region results in an irregular crack surface, which is attributed to the cause of roughness-induced crack closure. By observing crack surface displacement under loading and unloading cases, Newman [74] demonstrated that crack closure is more effective for low constraint conditions. As a result, even in the maximum loading for biaxial stress state, crack surfaces make contact with each other, resulting in a lower crack propagation rate due to increased closure stress. Under low stress intensity conditions, an increase in crack opening stress causes residual plastic deformation. In general, residual plastic deformations will be greatest under high constraint conditions and near the threshold region with low crack growth rates. It is approximately 50 times greater than the crack tip opening displacement.

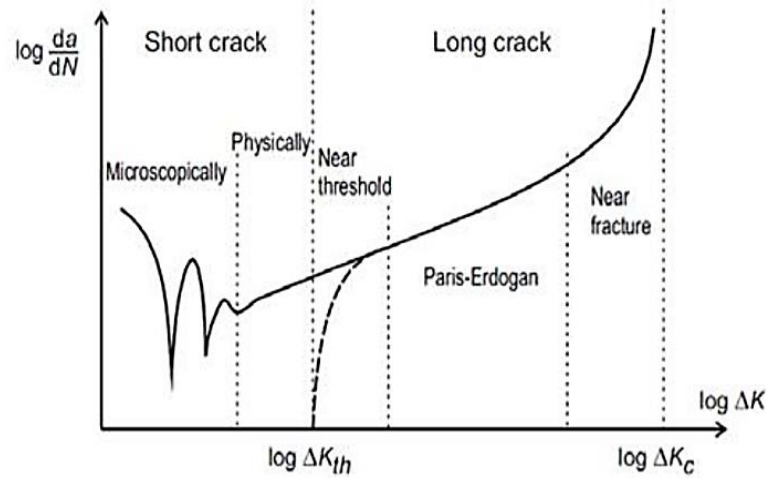


Figure 12 Near threshold region [75]

Load shedding or reduction techniques allow for the determination of a threshold value that ensures no more than a 10% reduction in K . The replication method is commonly used to track the initiation and propagation of minor flaws. Fatigue tests are interrupted at regular intervals to determine whether or not the size of the crack has changed by sticking 0.1 mm cellulose tape softened with acetone to replicate the crack surface. Surface cracks can be identified using optical inspection. Fatigue crack growth is determined by crack size in terms of grain size and grain boundaries, which are known as preferential crack path and localized inclusions on these sites result in smaller grain size and higher fatigue propagation rates. The grain boundary, on the other hand, is an impediment for microstructural small cracks, and smaller grain size has a lower fatigue crack growth rate. For small cracks, the minimum crack growth rate occurs when the crack size equals the grain diameter. Changes in grain orientation improve growth rate at the boundary. Kitagawa et al. [76] discovered that the threshold for small cracks decreases with crack length in cases where the critical crack size is found by a long crack threshold value. To characterize short crack growth behavior, El-Haddad defined stress intensity in terms of actual crack size plus fictitious or intrinsic crack size [77].

2.2.6. COMPLIANCE MEASUREMENT

The compliance method represents the elastic and plastic parts of the load-displacement curve as a function of tricenary crack length. In other words, it is inverse stiffness, and plastic work provides crack size determination by evaluating the compliance curve [78]. For isotropic and linear elastic materials like metals, the compliance method yields consistent results. The concept of compliance is based on the fact that crack propagation reduces the stiffness of the specimen. The calibration curve is used to link crack length to compliance. Compliance will increase as the stress ratio decreases, and a shorter crack length will result in higher compliance [79]. When performing fatigue crack growth tests in non-isothermal conditions, exact crack length measurement can be difficult. Through the compliance method, changes in stiffness can be correlated. Because stiffness is assessed on the elastic region of the unloading part, a calibration curve for crack length measurements is not required for each test because stiffness is normalized via stiffness of non-cracked geometry [80].

To estimate crack length, the following numerical methods are proposed: laser interferometry, potential drop, ultrasonic isoscanning, and crack tip opening displacement [81]. The compliance curve can be useful in determining opening stress through visual investigation, the replica method, or other techniques. However, because of its simplicity, the crack opening displacement gage is the most commonly used [82]. The normalized ASTM method is advantageous when there is a small change in the compliance curve, whereas the general method can result in a large scatter on the opening value. As a result, the 2 percent offset method yields lower crack opening values for the aforementioned compliance curve. The relative offset method, on the other hand, reduces data scatter. Song et al. investigated a relative offset method that outperformed the ASTM method in terms of opening load estimation by 8% [83]. Among other methods, the compliance curve remains the most advantageous technique for determining crack closure. It can be carried out via remote or local compliance methods. The difficulty in adjusting effective

stress is due to the non-linear behavior of the compliance curve caused by hysteresis and measurement noise. In general, second order polynomial curve fit is used for the lower part of the curve and linear fit is used for the upper part of the curve. Nonetheless, when comparing curve fitting to noise, noise is the most problematic cause for analysis. The scatter in opening stress results corresponds to the reliability of the method [84].

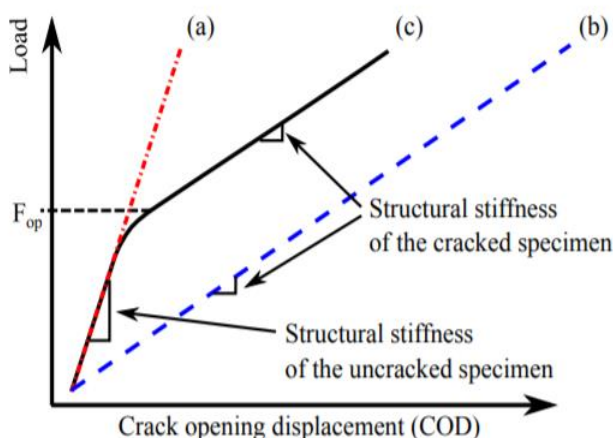


Figure 13 Compliance curves for an uncracked specimen (a), a cracked specimen (b), and a cracked specimen with crack closure (c) [85]

To represent an appropriate calibration result, the compliance curve is restricted to the $0.25 < a/w < 0.8$ region. Saxena et al. investigated an extrapolation method to predict compliance expression by confirming experimental results [86]. Compliance does not exist at high stress intensities where the crack has been stabilized. Heine described opening stress as being more than 3% higher than closure load. Heine investigated the effect of thickness on compliance; as a result, crack closure is reduced for the thinnest geometries [87]. Opening stress was calculated using the unloading portion of the load-displacement curve. The compliance value is attributed to the upper part slope using least square regression and focusing on 25% of the data. Local slopes can be calculated using 10% of the data, and opening stress can be calculated using the compliance-offset technique at 1, 5, and 15% deviations. A higher sampling rate allows for less data scatter,

so at least a 50 Hz sampling rate is required [88]. Compliance can be calculated by omitting 10% of the upper and lower parts of the curve to minimize non-linear effects and applying least square fits on the unloading part of the curve three times for each crack length. Polynomial regression can be used to correlate normalized crack length [89].

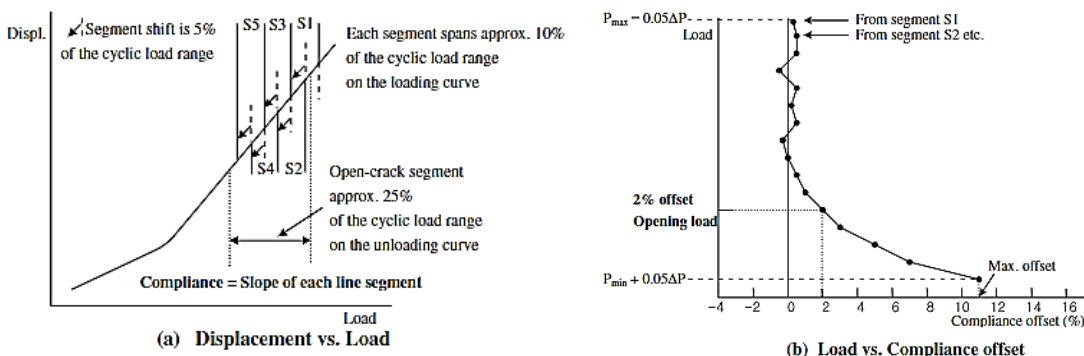


Figure 14 Using the ASTM compliance offset method, the opening load can be calculated. Compliance curve (a), determination of opening stress (b) [90]

Patriarca investigated various methods for determining opening stress and discovered that 1.5 percent offset is a good candidate for the compliance offset method, while other methods resulted in a 20 percent deviation from each other [91]. Because of the inaccuracy of naked-eye observation, compliance evaluation is dependent on the operator's experience. As optimum results, the ASTM method presents least square fitting around percent 25 of the upper part of the unloading curve and a 2% offset. However, this method has some drawbacks, such as a problem with discontinuity when calculating compliance offset. Decreased segment size leads to incorrect compliance estimation, so it is not recommended. The inconsistency problem caused by changing the opening value with the compliance offset can be solved using the normalized ASTM method.

Song et al. concluded that the normalized ASTM method is appropriate for random and constant amplitude loading [92]. Plasticity-induced crack closure can be considered the most dominant of the closure effects, particularly for metallic materials. The yield strip model makes it possible to evaluate crack closure in an analytical manner. To estimate

opening stress, the model concentrates on a small number of constraints during yielding at the crack tip under alternating loading. Local compliance measurements may be used to precisely measure crack closure at this point. Larger plastic zone sizes ahead of the crack tip result in greater hysteresis on the load-displacement curve [93]. Even though plasticity-induced crack closure under plain stress and plain stress conditions is anticipated, roughness and oxide-induced crack closure are difficult to predict.

Crack propagation can be influenced by both intrinsic and extrinsic mechanisms. The former, which is controlled by monotonic and cyclic strains, results in the formation of fracture surfaces ahead of the crack tip. Crack propagation is aided by cyclic deformation. The latter influences the rate of crack propagation by influencing monotonic and cyclic deformation at the crack front. The formation of an extrinsic mechanism is caused by the plasticity and contact of crack flakes. As a result, compliance quantifies the variation of contact force in terms of mechanical response. Since plasticity, oxide, and roughness induced crack closure all contribute to changes in compliance, fatigue cracks alternately close and open from the crack tip. Furthermore, cyclic deformation and surface fretting cause a change in the load-displacement curve due to small hysteresis. The damage tolerant approach imposes stringent design requirements in terms of accurately predicting crack growth rate. K_{eff} eliminates the stress ratio's dependence on crack growth rate. The concept of plasticity-induced crack closure is related to the stress ratio effect on crack growth.

Local compliance varies throughout the cycle, even when the crack is completely open. The stress ratio effect can be eliminated by employing an effective stress intensity factor, which results in crack growth rates that lie on a single curve. Compliance methods presented in the literature can be used to obtain opening stress. The compliance offsets method can reduce scatter in the compliance curve caused by fluctuation in displacement data. As a result, the connection between load versus offset data at a range of opening parts and load versus compliance offset data determines opening stress. The length of the crack and the size of the plastic zone affect compliance. Skorupa investigated the change

in compliance of an open crack during a load cycle for structural steels, finding that the compliance value for a totally open fracture does not remain constant [94].

2.2.7. HEAT TREATMENT ASSESMENT

Fatigue propagation around the threshold has drawn relatively little attention in the research field and, as a result, there is insufficient information and not enough accurate fatigue data on growth mechanisms at very low propagation rates. Such insight, especially a stress density information below which cracks do not propagate, can be considered critical in the analysis of problems such as cracking in turbine rotor shafts. The stress intensity around near threshold and corresponding crack propagation rates were found to be affected by stress ratio, yield strength of material, particle size distribution, and impurity segregation when the microstructure is modified through isothermal transformations. The crack growth threshold ΔK_0 is found to be inversely associated to steel strength, and a relationship between ΔK_0 and cyclic yield stress is stated. It was demonstrated how cyclic softening, coarsening the preexisting austenite grain size, and stabilizing impurity segregation to grain boundaries can increase near-threshold crack growth resistance. These influences are characterized with the behavior of crack growth at higher growth rates.

Based on limited studies, material strength and microstructure complexity are the key factors for evaluating fatigue crack growth rate near the threshold. Accordingly, lower crack growth rates have been indicated in lower-strength steels by reducing yield strength, and higher threshold values have been revealed in the steels and titanium alloys by maximizing grain size. Fatigue crack growth rates become sensitive to microstructure and stress ratio at high stress intensities, in keeping with the formation of static failure modes during striation growth. Change in microstructure and stress ratio have no effect on crack growth rate in the mid-range of crack growth rates. Apart from these, major impact of load ratio and microstructure on crack growth rates are noticed at low crack growth rates;

the highest sensitivity to stress ratio occurs in lower-strength steels and the maximum sensitivity to microstructure exists at low stress ratios.

Ritchie et al. provided an overview of the effects of microstructure on near-threshold fatigue-crack propagation in an ultra-high strength steel [95]. The research aimed to investigate the effects of strength, grain size, and impurity separation. Microstructure and stress ratio have the greatest impact at low stress intensities, where crack growth rates are around 10^{-6} mm/cycle. It has shown a common trend of ΔK_0 's inverse dependence on material strength. Indeed, UTS, rather than yield stress, produces a far better correlation with ΔK_0 . This implies that strain hardening is meaningful in terms of crack growth evaluation. Nonlinear variation in da/dN curve that changes crack growth rate with ΔK can be explained by various primary fracture modes. For the middle range of the curve, failure in steels is primarily caused by a transgranular ductile striation mechanism, with little involvement from microstructure and stress ratio. When K_{max} approaches K_{IC} , crack growth rates become highly sensitive to both microstructure and stress ratio because of a shift away from striation growth and toward static fracture modes like cleavage and intergranular fracture. At low crack growth rates near threshold, microstructure and stress ratio have a comparable significant impact on growth rates, as well as an extreme sensitivity to crack closure and environmental impacts.

According to a review of the literature, increasing ΔK_0 with decreasing ultimate strength can be assessed for steels. The threshold for fatigue-crack growth decreases as cyclic strength increases, either due to high initial monotonic strength or through cyclic hardening. On the other hand, after cyclic softening, the softest condition arranged via tempering temperature results in the largest threshold. Tempering temperature obviously has a significant influence on threshold levels and implicitly near-threshold crack growth rates. The threshold ΔK_0 increases as the tempering temperature rises, accompanied by a decrease in tensile strength. The same trend of increasing ΔK_0 with decreasing strength is still visible at higher stress ratios, but the influence is considerably

decreased for the same loss of strength. Cyclic softening, which is defined as the decrease in dislocation density with cyclic loading, can be considered as favorable in terms of enhancing near-threshold crack growth resistance. Although there was no change in the threshold stress intensity, coarsening the prior austenite grain size was observed to increase near-threshold crack growth resistance as well. With larger grain sizes, the crack growth results showed a decrease in crack-growth rate as well as an increase in M_o in low-strength steels [96]. The interpretation of lower crack growth rates in coarser-grained steel can be explained in terms of hydrogen atom accumulations to grain boundaries. The accumulation of residual impurities in grain boundaries after heat treatment has been seen to significantly deteriorate crack growth resistance at near-threshold rates, while having slight influence at intermediate growth rates. Because of the attractive interaction between impurity and hydrogen atoms, the existence of an impurity atom in a grain boundary could increase the local hydrogen concentration [97]. Near-threshold fractography analysis consisted of a flat, ductile transgranular mode with separated parts of intergranular separation. The fraction of intergranular facets is expected to be low near the threshold around 1 %. The coarser microstructure exhibited much rougher near-threshold fracture surfaces, indicating a faceted, ductile transgranular mode with intergranular fracture portions that resulted in higher threshold values with lower crack growth rates at low stress intensities. The clear distinction in residual stress between martensite and ferrite can result in the formation of intergranular cracks at the martensite-ferrite interfaces.

The microstructure plays an important role in the near-threshold fatigue crack propagation region. Although there are numerous studies in the literature for the crack growth phenomenon, there is still no comprehensive understanding of this problem in terms of the mechanism behind it. The fatigue crack growth mechanism takes place in the plastic zone region which is quite small size; the order is considered as microstructural units particularly at low stress intensities. Microstructural differences because of heat treatment methods are frequently attributed to changes in monotonic strength and yield

strength, resulting in differences in plastic zone size. Driving force required for crack growth under alternating loading is directly related with plastic zone size ahead of crack tip.

Washida et al. investigated the effect of grain size on fatigue crack growth at low stress intensities for low carbon steel. It was stated that crack closure due to roughness induced increased the long crack threshold value in particular the coarser microstructure [98]. Putatunda investigated the effect of material strength on crack growth rate and crack closure mechanism in medium carbon alloy steel. Even though the yield strength values differed more than twice, the change in long crack threshold values was relatively small. The variance was greatest in the Paris region of the crack growth curve. In fact, the effect of microstructure and the direct effect of material strength were investigated by comparing martensitic-bainitic and pearlitic-ferritic microstructure [99].

Keum et al. investigated the influence of microstructural characteristics on fatigue crack propagation rate at low stress intensities in steel specimens by applying K decreasing method. In the pearlitic lamellar structure, cyclic softening existed at low stress intensities, while a cyclic hardening emerged at a higher strain amplitude. Nevertheless, cyclic hardening was the only process that existed in the spheroidized structure. Because of surface roughness, the crack propagation rate in the near-threshold region decreased with increasing pertaining austenite grain size. Crack growth resistance for spheroidized microstructure has higher than pearlitic microstructure therefore, the latter one has a lower ΔK_{th} . Indeed, the crack propagation takes place selectively through the ferrite phase [100]. Shin et al. investigated effect of microstructure on near threshold fatigue crack growth rate. Accordingly, the long crack threshold value increased with increasing tempering temperature, but the effective threshold stress intensity range was relatively constant. As the tempering temperature increased, the grain size increased [101].

A pretty notable influence of microstructure has been noticed in mild steel, where the formation of duplex ferritic and martensitic microstructures can result in increased crack

growth resistance at low stress intensities and material strength on the contrary to industrially heat-treated steel. Indeed, dual phases microstructures with a prolonged martensitic phase that completely enclosed the ferritic phase were observed to have greater strength and a considerably higher threshold than similar structures with the ferritic phase enclosing the martensite after appropriate heat-treatment procedures. The conclusion is unexpected for the relationship between strength and near-threshold behavior; however, it brings a very favorable way of increasing the fatigue-crack growth resistance in terms of microstructure dependance as shown in Figure 15. Even though isothermally-transformed structures stay cyclically unchanged; cyclic softening occurs in quenched and tempered structures. Therefore, it is expected higher near threshold resistance for tempered compared to annealed condition.

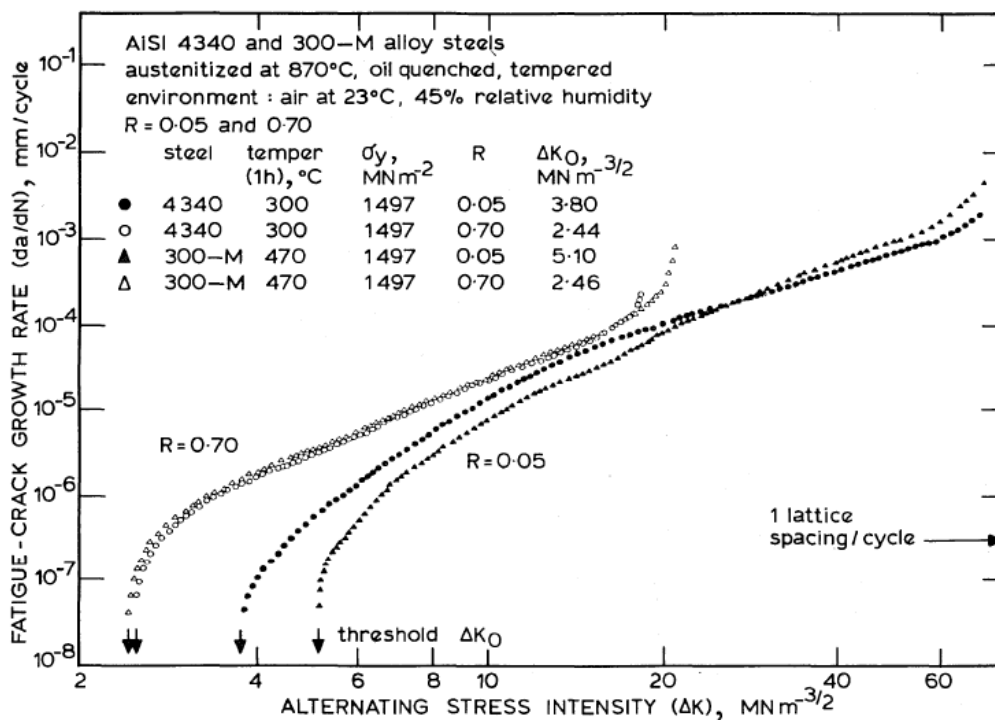


Figure 15 Fatigue crack growth behavior of AISI 4340 steel for quenched and tempered conditions at different stress ratios [102]

In near-threshold regions, the material with the ferritic-pearlitic structure has a higher roughness than the material with the martensitic structure. In contrast to the pearlitic phase, where no striation was observed, the ferritic phase exhibited a striation pathway. In the martensitic material, a different mechanism was involved: lacking striation, however it has fine secondary cracks present at the near threshold, whereas sharp cracks occur at high stress densities. The pearlite has a higher strength than the ferritic phase and directly restricts ferrite deformation in the plastic zone during crack propagation period. The pearlite structures unable to maintain its strength upon cyclic hardening through certain periods of plastic deformation, and the strength and plastic deformation are distributed to the neighboring ferritic colonies. This sharp rise in deformation provokes the image of micro crack increments in the ferrite colonies with each cycle, eventually leading to their breakage. Another factor influencing crack growth characteristics is the higher roughness of the fracture surface of the pearlitic - ferritic microstructure compared to the martensitic one. The striations are prevailing on crack growth region in the pearlitic-ferritic microstructure. On the other hand, there are several secondary microcracks, not striation, on fracture surface of the martensitic microstructure. The annealed material had considerably higher threshold levels than the martensitic microstructure. Similarly, bainitic and pearlitic-ferritic microstructure had a similar characteristic to the martensitic one. On the other hand, the effect of microstructure on crack growth rate has not observed at high stress intensities [103].

Fatigue crack propagation rate is primarily controlled by following crack closure mechanism for heat treated alloys: plasticity-induced or roughness-induced [104]. The crack growth rates of numerous aluminum alloys were tested and the results were found to fluctuate by a factor of about 20 at corresponding ΔK values in a study conducted by Bergner et al. [105]. They suggested that the inconsistencies can be explained by a combination of the crack closure caused by microstructural variabilities and the environment. The crack growth rate of an alloy is primarily determined by plasticity

induced crack closure alone or other hindering mechanisms like roughness induced crack closure.

The hardness of material is a quite significant effect on crack growth, and crack propagation increases with the hardness of material under variable stress ratios [106]. Lv et al. indicated that as temper temperature increases, fatigue crack propagation behavior of nickel-based alloy decreases and the main cracks of the heat-treated samples propagate toward ferrite phase because of the higher hardness of the martensite phase [107]. Accordingly, as the specimen is tempered at lower temperatures, it was observed that large secondary cracks form; on the other hand, the secondary cracks decrease as the temper temperature is high. Secondary cracks decrease because of the release of stored energy as tempering temperature is increased in terms of comparison of fatigue crack propagation rate of different heat-treated conditions. Secondary cracks are mainly accountable for slowing crack growth by consuming the energy of the crack tip [108]. A great percentage of facets were observed on the fracture surfaces of tempered samples, indicating that the fatigue propagation of the alloy is operated by cleavage fracture at low stress intensities around threshold region. As the stress intensity increases, the crack tip plastic region increases in size, and when the crack tip plastic region reaches a critical value, the fatigue striation mechanism becomes the primary fracture mechanism. As a result, the crack deflection effect caused by the microstructure has little effect on the fatigue crack propagation resistance, resulting in crack growth curves exhibit similar fatigue crack growth rate at high stress intensities regardless of microstructure.

The crack front and implicitly crack growth direction alter during crack growth process since the crack front is likely to be tortuous rather than straight propagation due to competing mechanisms. The comprehension of crack closure is a topic of debate in the fatigue society. This is primarily due to the difficulty in measuring it and the ambiguity of the crack closure mechanics [109]. Carvalho et al. demonstrated that COD output decreases as the length of the flat regions increases near threshold region, indicating that the crack closure effect is more evident [110]. Roughness induced crack closure is

affected by microstructural features like grain size. As a result, tortuous crack path arises because of effect on fracture surface roughness.

The crack growth is influenced by a combination of shearable and non-shearable precipitates. Accordingly, slip bands caused by subsequent dislocations cutting through shearable precipitates, where softening takes place if the effective size of the particles is small; on the other hand, strong precipitates that cannot be cut when their size reaches a critical limit and are relatively large compared to shearable ones, and the inter-particle spacing of non-shearable precipitates dominate the effective crack length. There were two major mechanisms preventing the crack from extending entirely. Primarily, the crack front was wedged by primary precipitates that block crack propagation. Additionally, primary precipitates are less capable of forming leading barriers to crack advancement with increasing stress ratio. The second mechanism was emphasized shear-controlled crack propagation of long cracks, which can be visible as hilly shapes on the crack lips especially at high stress ratios and this effect is unaffected by microstructure or rolling texture [111].

When the plastic zone size is nearly equivalent to the microstructural feature size in case of being at near threshold, a transition in the mechanism of fatigue crack growth occurs. The maximum and cyclic plastic zone sizes near the threshold under plane strain conditions are evaluated within the continuum mechanics framework. Therefore, a significant improvement for fatigue crack growth resistance can be observed around near threshold compared to Paris and unstable crack growth regions. Distinctly; the size of the cyclic plastic zone is on the order of tens of microns or greater quite well in the Paris regime, where ΔK is sufficiently high, and thus exceeds grain size. As a result, cracks form across the grain boundaries, making their growth rate insensitive to microstructural features [112].

The fracture attributes of the longitudinal and transverse specimens were identified to be quite identical [113]. The amount of low angle grain boundaries in materials decreases

significantly after heat treatment, while the amount of high angle grain boundaries increased significantly. It was previously established that high angle grain boundaries have a high grain boundary energy, which can highly affect fatigue crack propagation resistance. Materials with high local dislocation density have higher residual strain and dislocation density. The high residual stress in martensite and the large number of sub-grain boundaries are attributed to enhanced fatigue crack growth resistance.

CHAPTER 3

LITERATURE REVIEW

This part of literature review covers statistical approaches to determine endurance limit of materials under alternating loading: staircase and curve fitting methods, respectively.

Dixon et al. (1948) investigated a method in terms of collecting and analysis sensitivity data and it is also called as up & down method to estimate mean value of a data set. If the evaluation to be described is to be applied size, the sample size must be large. The quantitative study relied on large sample theory, so if one utilizes the evaluation on a forty-specimen size. They also concluded that a small interval may result in a waste of occurrences unless a good preference for the initial level is produced. If an inadequate choice comes, many findings must be made to move from that stage to the region of the mean. The basic advantage of this approach is that it naturally centers evaluating near the mean. On the other hand, this method has one evident disadvantage in certain types of experiments since it involves that each sample be evaluated independently [25].

Metropolis et al. (1949) investigated the Monte Carlo method involving only a few specimens by iterating samples. The normal method for finding a specific solution consists in iterating an algebraical step. This can be done with as few or as many faults as preferred. Furthermore, it is not essential to maintain a group of such quantities in the system; rather, by iterating a well-defined numeric process, the computer system can be configured to generate values that simulate the above features. Their assessment might be

quite useful in practice since it would enable us to adjust the sample size to the desired precision [31].

Dixon (1965) elaborated staircase study for small number of data sets around six specimens. The method describes test levels and data sets that are determined successively. The assumptions exhibited a mean square error that is roughly distinct of the test sequence's starting level and the spacing between test levels. For reasonably well-chosen starting levels, the exact sample size barely reaches the nominal sample size by more than two. He concluded that good estimates can be obtained by selecting an interval size between $2/3$ and $3/2$ of standard deviation. If the mean value is identified very clearly in beforehand, a lesser spacing will result in estimates with a lower mean square error. In case of the greater interval; on the other hand, the number of trials will be conducted that are far from the mean value [26].

Little (1972) examined the precision of the assumptions about fatigue data to key assertion options like minimum chi square analysis versus maximum likelihood analysis, or an implicit extreme value (smallest) response distribution versus a normal response distribution. Engineering evaluation of the estimated median fatigue limit's "accuracy" necessitates serious analysis of both its statistical variance and quantitative sensitivity. Using large sample statistical formulas, it is not possible to obtain reliable median fatigue-limit assessments for sample sizes. Small sample assessments, on the other hand, must be carefully examined in terms of both their variance under sampled data and their "sensitivity" to diverse analytical methods and assertions. He concluded that staircase strategy is inadequate. As a result, standard deviation estimate can only be used in the lack of reliable previous knowledge [28].

Zheng et al. (1995) demonstrated that upon the fatigue life regards the log-normal distribution, the fatigue strength coefficient, theoretical endurance limit, and fatigue strength at a specified life obey the log-normal distribution; however, the theoretical endurance limit and fatigue strength follow the normal distribution for infinite part of SN curve. In the case where the fatigue life test data comply the log-normal distribution, reliable expressions of SN curves can be acquired from the variances of the fatigue

strength coefficient and the theoretical endurance limit. In addition to this, they discussed the distribution of fatigue life and fatigue strength. Based on the findings presented in this paper, it may be postulated that fatigue strength has a log-normal distribution in engineering applications. It is, nevertheless, uncertain to presume that the standard deviation of fatigue strength is constant. Eventually, it should be noted that the procedures proposed in this research were relevant in the infinite region of SN curve, in which the dispersion of fatigue life cannot be actually considered in terms of performing experiments [114].

Beretta et al. (1998) suggested that evaluating the maximum existing flaw size can accurately predict the lower limit of fatigue properties. The purpose of this paper was basically to address the two issues and examine the quantitative properties and characteristics separate estimation methods: least squares, moment, and Maximum Likelihood. The research, which was carried out using the Monte Carlo method, enabled the authors to recommend the optimal approach via statistical evaluation and the least number of defects required accurate analysis for highest number of existing flaws. Eventually, the results revealed that the Maximum Likelihood method is the most effective approach for fatigue data analysis, with the lowest standard error estimates of the excessive flaws [33].

Bathias (1999) demonstrated that investigating the life range between one million and one billion cycles will provide a more secure framework for modeling since SN curves are generally constructed until ten million cycles region. He investigated experimentally that fatigue fracture can still take place in a large variety of alloys after ten million cycles. In certain situations, the variation in fatigue life between one million and one billion cycles to failure can be as much as 100, even 200 MPa. His observations indicated that the idea of an infinite fatigue life on an approximation SN is incorrect. In such circumstances, a fatigue limit identified by statistical methods between one million and ten million cycles cannot ensure an infinite fatigue life [24].

Lin et al. (2001) evaluated different staircase methods and curve fitting methods by extrapolation of finite data on endurance region to determine statistical properties of

fatigue data. Even though the fatigue life of components is hard to obtain they simulated results via four different methods since the fatigue life of a smooth and polished ferrous specimens is clarified by a knee in the SN curve, but it disappears under conditions with high temperature, overloads, interfacial pits and nicks, and under humidity conditions. They came to conclusion that curve fitting method is sensible for small number of coefficients of variance. For this condition, Dixon-Mood method also produced successful estimate of fatigue data. In case of large number of coefficients of variance, Dixon-Mood method is advised for fatigue limit determination [27].

Loren (2002) investigated endurance limit criteria for finite lives. He compared two methods in his article. One method focusses on estimation of the fatigue limit, while another practices to determine the endurance limit. The latter that estimates the endurance limit is one that only considers failed specimen at a given stress level and runout specimen as well. The former method that estimates the fatigue limit also makes use of information about when the specimen fails, i.e., how many cycles the specimen endures until failure. On both real and simulated staircase tests, the two models were compared. He demonstrated that the distribution of the fatigue limit can be estimated even though the fatigue limit itself cannot be identified. When the two models produce distinctively different results, it can be concluded that the run-out level chosen is excessively low [29]. Loren (2004) investigated a method for determining the fatigue limit distribution depending on the inclusion size correlation. The corresponding stress for components under alternating loading was assumed to be inhomogeneous. Obtained test data during study was derived from two types of fatigue tests: rotating bending and uniaxial testing. For these two experiments and two separate components, the fatigue limit behavior was examined. The fatigue limit distribution, size and intensity of inclusions were all given with confidence intervals. He concluded that the method may be used to estimate the probability that the component might fail for various test techniques and different form of components [115].

Rabb (2003) studied stair case evaluation for fatigue data in terms of confidence and reliability aspect. Because of the characteristics of the staircase test, obtaining a correct

sample standard deviation estimate is quite challenging. Monte Carlo simulations of the staircase data can be used to derive the proper amplitude and variability distributions. The sampling distribution that is analyzed is usually significantly closer to the correct value. As a result, a credible assessment of the sample standard deviation may be calculated using the statistical size effect noticed in two staircase tests with varied specimen sizes. Although the normal distribution is commonly used to examine a staircase test, he interpreted that using it to compute the reduction factor can result in unwanted oversizing. As a result, the log normal distribution was suggested for this reduction [9].

Carlos et al. (2005) was examined the adoption of the Maximum Likelihood Estimate (MLE) to determine the fatigue behavior in terms of staircase tests and Life-Regression Models. A modified Basquin model and the Random Fatigue Limit (RFL) technique were both examined as life-regression methods. MLE was determined to be the optimum method for analyzing fatigue data since it was statistically accurate and extremely adaptable. In fatigue, life-regression analysis can be used to calculate the probability - based SN curve, which enables the fatigue life distribution to be estimated for any number of cycles. For the metal studied, the Random Fatigue Limit model provided better regression than the Modified Basquin model. Nevertheless, they advised that MLE is sensible for fatigue data analysis [116].

Pollak et al. (2006) were investigated the impacts of test parameters (specifically, step size and sample size) by mathematical models to evaluate the reliability of fatigue life standard deviation measurements using traditional staircase statistics, generating an estimate of standard deviation bias as a function of step size and sample size. To compensate for the standard deviation bias common in small-sample testing, a non-linear adjustment was developed. Furthermore, the model was utilized to test how well a bootstrapping approach performed on standard deviation estimates. In small-sample testing, the bootstrapping approach was found to considerably reduce the risk of significant standard deviation errors. The employment of the non-linear correction factor in conjunction with the bootstrapping process may result in a more accurate approach of

estimating the statistic behavior of fatigue life distribution compared to staircase methods [23].

Minak (2006) quantitatively tested a number of different methods using Monte Carlo simulation for determination of fatigue limit for metallic materials. He also conducted uniaxial fatigue testing on steel specimens with nonmetallic inclusions in two different heat treatment states, annealed and hardened, and even on cast products, eventually he determined the fatigue limit using the approaches regarded. The acquired results showed that in the case of materials containing inclusions or voids, the approaches evaluated could produce inconsistent data. In the case of annealed steel, all methods yield similar fatigue limit values, whereas in the case of hardened steel containing nonmetallic inclusions or aluminum alloy containing internal voids, the results by using staircase and curve fitting methods were different. In case of having low cycle fatigue tests of less than ten thousand cycles, the stress level may have a substantial effect on the results of curve fitting methods and extrapolated results can be evaluated as nonreliable. In the case of high coefficient of variance, such as hard metals containing impurities or cast products containing voids, all methods produced consistently poor outcomes. For such as cases; the Dixon-Mood method can be evaluated as the most robust [30].

Wallin (2011) investigated the reliability of the maximum likelihood estimate thoroughly. It was demonstrated that the maximum likelihood method is ineffective for estimating the scatter of fatigue data via a staircase evaluation [117]. Depending on binomial probability, an alternative analysis method was unlikely proposed that allows for a better estimate of confidence limits. This new analysis approach was same inconsistency in terms of scatter of data compared to maximum likelihood estimate. Nevertheless, the final decision was that the staircase test cannot be evaluated to estimate scatter of fatigue data. Monte Carlo simulation was used to investigate the statistical uncertainty in staircase data for fatigue limit assessment. Uncertainty on maximum likelihood analysis was assessed, and eventually an adjustment offered for conservative or accurate scatter estimation. For this, a modified testing method was suggested. Better estimates of the scatter and the implicit distribution were achieved by combining modified test method with binomial probability

assessment. It was concluded that staircase test method cannot result in accurate scatter data or implicit distribution.

Müller et al. (2017) studied estimation of fatigue limit via different staircase methods by artificial fatigue test data and their accuracy were compared. All of the evaluated analysis methods exhibited favorable behaviors at a comparable scale, delivered strong sample mean estimators, and were resistant to undesirable staircase variables like estimation of sample mean and logarithmic standard deviation. In case of small data sets; staircase estimators' quality is low, and high safety factors are required to achieve reliable results. For the assessment, they were suggested that the advanced IABG method or the maximum-likelihood method with bias correction can be preferable. Among the staircase methods; Deubelbeiss method should not be used to calculate the logarithmic standard deviation. If the logarithmic standard deviation is needed, values from experience or the literature are acceptable if the sample size is small, like less than twenty. This study revealed the use of different statistical approaches to compare experimental data for qualified standards [118].

Molina (2020) studied a Weibull method approach for evaluation of the probabilistic percentiles for the SN curve for steel specimens. The desired Weibull/SN correlation is based on the true stress and true strain data, both of which are obtained via the stress-strain curve. The Weibull parameters were calculated directly from the maximum and minimum corresponding stresses values for the evaluation. The parameters of the SN curve are attained for one thousand and one million cycles. The application parameters obtained from previous published experimental data for the same steel specimens in order to calculate the true stress and true strain parameters. Furthermore, the SN curve construction, its probabilistic percentiles, and the Weibull parameters that represent these percentiles were determined through adopted procedure in the article [119].

Pascual et al. (1997) studied a random fatigue-limit concept which is used in their article to characterize the variation of fatigue behavior based on stress level, the scatter in fatigue life, and the component variability in the fatigue limit. They used maximum likelihood techniques to validate the fatigue data with existing fatigue data points and investigated

the best fit under various distributions. Analyzers are frequently interested in small quantiles of the life distribution. Therefore, lower confidence limits relying on likelihood ratio approaches can be acquired for such distributions. Fixed fatigue-limit concepts do not account for the possibility of fatigue limit variability. This difference could be attributed to the endurance limit's influence on structural features, which may differ from test piece to test piece. Eventually, they established analytic graphs and operated curve fitting tests and residual assessments to evaluate the model's fits [8].

Kim et al. (2001) investigated fatigue damage concept and life assessments for composites. For the fatigue life estimation, empirical damage data were collected and analyzed. SN data and curves were generated, and fatigue mechanisms in terms of stiffness loss/fatigue modulus and empirical damage were described at various stress levels. Microcracking and debonding have been identified as main contributors to damage. The damage rate was examined, and it was discovered that it follows a power law; in other words, the concentration of micro-cracks accelerated logarithmically with the number of loading cycles. To estimate an SN curve using experiential variables, a model based on fatigue modulus drop was evolved. The predicted life values were found to be in accordance with the test results [17].

Schijve (2005) studied statistical interpretation of fatigue data especially for low probability of failure cases. Different kinds of scatter on fatigue data were discussed. Various practical concerns were identified for which statistics were useful. The drawbacks of statistical assumptions were briefly explained. In his article, three statistical distribution functions were compared: the log-normal distribution, Weibull distribution by three parameters, and the log-normal distribution including minimum fatigue life parameter. Basically, the last function has received little attention in the literature. The second and third functions both cover a statistical minimum of the fatigue life parameter, but in different ways. Both features provided a good curve fitting of the results for 30 close tests, but it was noted that the distribution function is essentially unknown since low probability of failure conditions is estimated by extrapolation of fatigue data because of

not supporting experimental data. Therefore, the physical interpretation of the estimated minimum fatigue life parameter is unknown [7].

Pollak et al. (2008) investigated different maximum likelihood methods for fatigue strength analyses for titanium alloys showing fatigue limit. Some statistical models were taken into account to determine fatigue strength in the ultra-high-cycle regime which is around one hundred million cycles for a titanium alloy commonly used in aerospace applications. Maximum likelihood estimation techniques were used to construct SN curves by curve fitting to experimental data via the Pascual and Meeker random fatigue limit approach and two simplified approaches which are bilinear and hyperbolic. The bilinear and hyperbolic models well fitted large-sample experimental data for another phase of titanium alloy, and they were then practiced to a small-sample data set for a beta annealed variant of the alloy by assessment of fatigue strength in the gigacycle regime. For evaluating probabilistic fatigue strength, the bilinear and hyperbolic methods were advised [120].

Boylan et al. (2011) presented an outline of distributional attributes in the context of the 4 different moments and examined how deviations in these moments significantly alter probability plot, with a special focus on the existence of skewness and kurtosis, including the influence of variability in their manuscript. They then provided a detailed examination of how different analytical attributes within a sample group can affect the shape and resulting features of a normal probability plot, proving how deviations in the data's characteristics can indicate or cover up the extent of concavity, convexity, or the S shape in the plot, and the expanded of the data around the mean and in the tails. This enables having a clear grasp of how data evaluation through the normal probability plot and provides a better framework for basic assumptions and enabling more precise estimation and enhancement results [121].

Najim et al. (2012) estimated the shape and scale parameters for Birnbaum-Saunders distribution in their article. The parameters were determined using the Maximum likelihood, Modified moment, Bayesian approximation technique, and Shrinkage Bayesian methods, and corresponding parameters were calculated for each technique.

They considered Bayesian estimators for the uncertain variables of the Birnbaum-Saunders distribution. Analytical representations of Bayesian estimators are not available. To acquire the Bayesian estimators, an approximate Bayesian approach based on Lindley's idea was introduced. Then all variables were estimated using numerical indicators and mean square percentage error was calculated among the four estimation methods. When the results of calculations were compared, it was found that the Shrinkage method provided the best estimation technique [122].

Li et al. (2016) introduced a computational method regarding the maximum entropy principle for defining the statistical distribution of fatigue life to decrease biased uncertainties and achieve sensible likelihood function. In the maximum entropy principal optimization process, the first four statistical moments of fatigue life were used to construct constraints. A precise method for finding the Lagrange multipliers in the maximum entropy distribution was also introduced, which can prevent arithmetical singularity when solving a set of equations. They suggested curve fitting methods which are evaluated using two fit variables. Two sets of fatigue data were adopted in the literature and the rationality and effectiveness of the proposed method were demonstrated based on these fatigue data [11].

Davide et al. (2017) was studied curve fitting methods with frequentist and Bayesian inference to model and estimate unknown variables in the fatigue life of welded samples under alternating loading. A new SN curve is suggested and fitted to fatigue experimental data by using the Maximum Likelihood Method approach. The results were assessed using the Random Fatigue Limit Model and the Bilinear Random Fatigue Limit Model. The proposed SN curve seems to be more appropriate to describe the SN correlation in high-cycle fatigue region: it introduces a smooth transition from finite to infinite-life regions and, apart from preceding non-linear S-N relations with fatigue limit, this conversion was operated by a separate model parameter. As a result, numerical adjustment resulted more versatility for curve fitting. Furthermore, a Bayesian approach with informative and non-informative statistical models was described to fit the recommended correlation [22].

Burhan et al. (2018) were deeply evaluated for competence using the following requirements: curve fitting abilities and reliability, practicability to data sets at different load ratios, representability of fatigue damage at failure, and fulfillment of the initial boundary condition [16]. The SN curve methods were categorized: those intended to classify fatigue data separately of stress ratio and those intended to estimate the effect of stress ratio. The method developed by Weibull, Sendeckyj, Kim and Zhang, and Kawai and Itoh for fatigue data analysis were investigated. The Kim and Zhang method outperformed the Weibull and Sendeckyj approaches in terms of indicating fatigue damage at failure. The Kohout and Vechet method was also considered to have excellent curve fitting ability, but with an inherent limitation for influencing the SN curve at certain stress ratios. SN curve methods for estimating the effect of stress ratio was considered to be comparatively inadequate in data fitting abilities to those formed effectively for fatigue data analysis [16].

Khameneh et al. (2018) tried to establish a method that predicts the probabilistic behavior of cast iron. The numerical analysis of the most widely used statistical probabilities was conducted and compared to achieve this goal. Reliability requirements for the fatigue data were investigated and calculated using probabilistic analysis based on the best fitted probability density on experimental data. Furthermore, the SN diagram with its scatter-band was performed at different confidence intervals. According to another research, the criterion for designing the crankshaft is the infinite cycle, or, in more realistic terms, the structure with considered acceptable stress levels below the fatigue limit. Fatigue endurance limit analysis were carried using the staircase test approach. The Dixon-Mood method, based on maximum likelihood estimation, was then used to assess fatigue limit via statistical approaches [123].

Barbosa et al. (2019) was carried out a review study in terms of the effectiveness of the methods used to establish probabilistic SN areas and indicated the techniques used to fit the SN fields that are best fit to estimate fatigue life of the various materials. The test data demonstrated that the probabilistic Stussi and Sendeckyj methods were the best choice for composite materials, as only the probabilistic Stussi model fitted the experimental results

well for all fatigue regimes for metals. In most circumstances, the most meaningful fatigue regions for metallic alloys are that of high and medium cycle region with a clearly delineated fatigue limit outlined by Basquin law. In this respect, probability-based fatigue approaches such as Castillo and Fernandez-Canteli, the ASTM standard, and Stussi appeared to be the most appropriate [14].

Wang et al. (2020) studied fatigue reliability assessment and the introduction of a new fatigue life model of reliability and crack propagation methods for particular stainless steels in the very-high cycle fatigue regime, which has recently become voguish. Initially, a fatigue test was conducted to determine the mechanism of failure in the very-high cycle regime. The fatigue life distribution and SN curves were characterized using test results and fatigue reliability concept. According to fracture mechanics and the conventional life assessment method, a novel fatigue life evaluation method for steel was envisioned. A new hypothesis of an SN curve was validated with the comprehensive application of SN curves and a recently developed fatigue life analysis methodology which statistically articulates the correlation between fatigue life, reliability, and fatigue cracking [124].

Murakami et al. (2021) clarified the basic model of the SN curve based on the estimation technique for fatigue life and limit of materials having defects on their microstructure from the point of view of small crack mechanics. The suggested technique's extensive implementation to constant amplitude cyclic loading and variable amplitude loading was addressed. The suitability of Miner's rule was also described in terms of the decreasing trend in fatigue limit with the number of cyclic stress and crack propagation. This article's evaluation solution for S-N curves can be mainly utilized to fatigue under constant amplitude cyclic loading and variable amplitude loadings. The explanation for the breakdown of Miner's rule application was specified in terms of a consistently decreased fatigue limit under fatigue loading [21].

This part of literature review covers small and long crack behavior, crack closure phenomenon, compression precracking, fatigue crack growth threshold, compliance measurements and failure analysis, respectively.

McEvily (1970) examined small crack growth behavior which represents the recent developments in analytical and experimental studies of this field. He clarified that short fatigue cracks act differently than long cracks because of their greater sensitivity to microstructure, a larger plastic region size compared to crack length, and a smaller extent of crack closure. Interpretation of the fatigue crack propagation concept of short cracks has sophisticated, and this comprehension has been used in the application of computational treatments for short fatigue crack propagation. This improvement was reviewed in this article, and the importance of small fatigue crack behavior was investigated for technically important fields. He emphasized that when damage-tolerant approach is implemented, the behavior of small cracks will be more concern [40].

Leis et al. (1983) was studied to determine the importance of the short-crack concept in relation to a damage tolerant assessment of jet turbine constituents. To define the crack tip variables that influence fatigue crack propagation rates for small cracks, a comprehensive system of experimental research and analysis was conducted. The research started with a detailed critical analysis of the existing literature. The results of the literature review were highlighted in this paper. According to this review, circumstances represented as short crack concerns can be attributed to a variety of factors. Stress ratio effects; violation of LEFM constraints; improper, inaccurate, or incomplete execution of LEFM; and transients because of crack initiation were examined distinctly [49].

Suresh et al. (1984) investigated small fatigue crack growth behavior. The physics and micromechanics of small fatigue cracks' subcritical propagation were addressed in their paper, and features of their growth behavior were compared to that of long cracks in terms of fracture mechanics, microstructure, and environmental factors. Short cracks were described as having a short length in comparison to significant microstructural measures, having a short length in comparison to the extent of local plasticity, or being physically small. Because all three forms of small cracks propagate faster than corresponding long fatigue cracks applied to the same theoretical driving force, existing defect tolerant fatigue design processes that rely on long crack data can lead to lifetime overestimation. The

effects of local plasticity, microstructure, crack tip environment, mechanism of propagation, crack driving force, and premature crack closure were systematically evaluated in light of the aspects of the small crack phenomenon [34].

Sadananda et al. (1997) was demonstrated that the short crack propagation behavior does not contain any abnormalities. The apparent abnormality results from neglecting the second variable affiliated with the threshold, and the presence of internal stresses in the crack tip region, at which short cracks initiate and propagate. Internal stresses in small cracks originating from notches can be pre-existing or developed in situ only when cracks develop at a free surface. In the latter circumstance, intrusions and extrusions at persistent slip bands serve as nucleating regions for crack nucleation initiation in case of having sufficient internal stresses. As a result, author concluded that small cracks propagate under a combined force that includes both internal and applied stresses, fulfilling the similar two thresholds as in long cracks. Based on the results, they rephrased the similarity principle as follows: for the same crack propagation process, identical crack tip forces result in similar crack propagation rates, assuming all relevant forces are considered [46].

Sangid (2012) focused the relationship between fatigue crack initiation and material microstructure. Many studies have been conducted on this hypothesis over the decades, and the purpose of this article was to insert this study in context and enhance potential research on fatigue in polycrystals based on the material's microstructure. To identify fatigue phenomenon, it is crucial to first investigate the methods that promote crack initiation. In a material, slip irreversibility's arise and pile up during cyclic loading condition. Irreversibility's occur at the imperfection level as a result of dislocation motion. Such irreversibility's in slip are the first indicator of damage throughout fatigue loading. As a result of accommodating the irreversible slip operations and raising dislocation density throughout continuous alternating loading, the dislocations try to establish low-energy state in order to become stable structures. Subsequently, strain is concentrated in a small zone of the materials, resulting in persistent slip bands and dislocation packs. Crack initiation is preceded by strain clustering. The experimental studies of strain

clustering, as well as the principle and quantitative simulation of slip irreversibility's and low energy configuration defect systems, were the target of this review article. The better comprehension is required to investigate persistent slip bands in metals, as well as the essential characterization, principle, and simulation. Both micromechanical and crystal plasticity concepts, which were also discussed, can be used to assess crack initiation based on this fundamental knowledge [36].

Pokorný et al. (2015) concerned with determining the residual fatigue life span of a railway axle with an existing crack. The research studied standard steel EA4T, which is popularly used in the manufacture of railway axles. The scatter of fatigue data in the measured between fatigue crack propagation rate and the stress intensity factor (da/dN versus K) curve is caused primarily by the steel's intrinsic material properties. The da/dN versus K curve was described using the Paris-Erdogan equation. Two material parameters were used to identify the scatter of the entire da/dN versus K curve. The scatter of the material constant C was the first criterion to be considered. The scatter of the stress intensity factor threshold value K_{th} was the second criterion. Both scatters were defined by a normal distribution, and certain probability curve fitting of measured data were performed. This demonstrated that the sensitivity of the residual fatigue lifetime estimations of the railway axle on da/dN versus K curve scatter is greater for shorter initial crack lengths. The conclusions drawn can be used to ensure the safe execution of railway axles in service [127].

Hutař et al. (2016) introduced an approach for assessing residual fatigue lifetime relying on the fracture mechanics methodology, taking into consideration the real spectrum of cyclic loading, the presence of press-fitted wheels, and surface residual stresses formed after train axle's heat treatment operation. It is revealed that the impact of residual stresses is substantial and should not be overlooked when calculating the axle's residual fatigue life span. The effect of residual stresses on fatigue life decreases with longer fatigue crack, but it's vital. The research shows that taking residual stresses into account can explain the discrepancy between conservative fatigue life assessment without residual stresses and

experimental tests. The residual stresses decrease the fatigue crack's total stress intensity factor and make a contribution to the axle surface's resistance to crack growth. The absence of residual stress from fatigue life assessment results in a significant underestimation of axle fatigue life [128].

Chowdhury et al. (2016) provided a review of the major kinetics and perceptive concepts underlying fatigue crack propagation mechanisms. The proposed modeling efforts are classified based on their basic principles, with an emphasis on identifying them. Contributions and constraints are carefully evaluated in the light of the most recent experimental findings. The goal is to give different perspective to engineers and researchers. In the modern sense, this comprehensive and still critical narrative would primarily enable to formulate even more advanced microstructure–damage interactions. The optimized design objective in manufacturing metals and alloys is to optimize the microstructural parameters for improved resistance to both crack initiation and crack growth in order to improve overall fatigue behavior. Eventually, they provided a brief overview of what is known experimentally about the character of the fatigue crack growth mechanism [41].

Yakura et al. (2017) studied effect of inclusion size on fatigue properties and regarding that the research was carried out to understand the fatigue behavior of a low-alloy steel used for an engine's crankshaft, including the properties in a high cycle fatigue region. Fatigue tests were performed on samples taken from a crankshaft and others from a round forged bar. The fracture mechanics were used to investigate the relationship between inclusion size at crack initiation locations and fatigue behavior. For crack initiated from the surface and internal inclusions, the research employed a relationship formula between the fatigue life and inclusion size, as well as a relationship equation between the threshold stress intensity range and inclusion size. These results demonstrated that reducing inclusion size enhances not only surface fracture fatigue strength but also internal fracture fatigue strength [129].

Maierhofer et al. (2018) presented a review of determination R curve and its applications. Aside from an introduction to the fundamental principles, the discussion

focused on experimental determination on the one hand and application issues on the other. A brief review of the state-of-the-art in determining and applying the cyclic R-curve defining the crack size reliance of the fatigue crack growth threshold in the mechanically small crack regime has been provided. The following issues have been discussed: fundamental questions about the cyclic R-curve; its experimental dedication, including essential and uninvestigated points; and its relationship to the Kitagawa-Takahashi diagram, including an estimation technique based on a modified Kitagawa-Takahashi approach on the one hand and a method for constructing Kitagawa-Takahashi diagrams for notched specimens on the other. Finally, aspects of its application in component evaluation and material development were discussed [57].

Li et al. (2018) studied how a single tensile overload affects fatigue crack growth behavior in dual phase steel specimens. Under constant amplitude loading and overload conditions, the compact tension specimens were examined. The findings revealed that all material conditions responded positively to single tensile overloads; the amplitude and scope of crack retardation was magnified leading to an increase in overload ratio and a longer crack length at overload implementation. The Wheeler model was modified with a plastic zone size factor to measure the fatigue crack growth rate during the retardation period after an overload; the projected results coincided well with the empirical observations. During the implementation of an overload, a half - moon shaped fracture zone with cleavage surfaces, tearing ridges, dimples, and voids founded in front of the crack tip [3].

Elber (1971) investigated fatigue crack closure by performing experiments on aluminum alloy under alternating loading conditions. According to the test results, a fatigue crack can be closed at the tip of the crack for nearly fifty per cent of the loading amplitude, rendering this component of the cycle inefficient in terms of crack growth. Rather classical assumption, it was recommended to express the crack growth rate in terms of effective stress amplitude. This interpretation was fitted to tested aluminum alloy for constant amplitude fatigue crack growth data. The variables were investigated to provide a superior fit to the data than some other previous experimental expressions. On the other hand, the crack closure concept could contribute for acceleration and retardation impacts

in crack growth, according to the results of empirical studies with variable amplitude loading. As a result, the author described for the first time the presence of crack closure even under tensile loading [5].

Correia et al. (2016) investigated crack closure effects on fatigue crack growth rate. To evaluate the effect of crack closure, a theoretical approach that relies on the same presumptions as the analytical models proposed by Hudak, Davidson, and Ellyin was asserted. This application was applied to the steel specimens using an inverse evaluation of experimental fatigue crack growth results, which was relied on Walker's propagation law. The crack opening stress intensity factor, the crack length, and the load ratio were all approximated using the proposed model. This involved assessment of the effect of crack closure on fatigue crack growth rates for different stress ratio levels. They interpreted the crack closure and opening effects without resorting to long and complex computation times due to complicated methodologies. Finally, authors were commented that clear correlation between the conceptual model and the analytical results [130].

Rabbolini et al. (2016) monitored crack closure stages throughout low cycle fatigue propagation using an innovative approach that relies on digital image correlation. The influences of crack closure on the growth of small cracks were explored in depth. An experimental campaign was carried out on samples manufactured with notches in the low cycle fatigue region, taking into account two separate load ratios: previously, tests were carried out under fully reversed deformation, while the impact of an applied mean stress was studied using a load ratio of 0.5. An ingenious method based on digital image correlation was used to describe crack closure: crack opening and closing parts were measured commencing from the experimental crack tip displacement areas. Eventually, experimental data were determined using Newman's mathematical framework [131].

Pippan et al. (2017) published a review about crack closures caused by plasticity, roughness, and oxide. The physical origin, the outcomes for methods for determination, and the estimation of the effective crack driving force for crack growth are all taken into account. Plasticity-induced crack closure under plane strain and plane strain conditions

necessitates a different interpretation in concept; however, both characteristics are predictable. This is true even in the transition region from the plane strain to the plane stress condition, as well as under all types of load levels, such as constant and variable amplitude loading and the transition from small to large scale yielding. Roughness-induced and oxide-induced closures, on the other hand, are more difficult to estimate. The causes of plasticity-induced, roughness-induced, and oxide-induced crack closures, as well as the consequences were discussed in terms of assessment and experimental results [2].

Bohác et al. (1995) studied fatigue precracking methods and their influences. The goal of their study was to highlight three fatigue precracking techniques for single edge bending specimens having residual stresses. Local compression, the use of a high stress ratio in the fatigue cycling loading, and reverse bending were the examples of these techniques. The potential impacts of these methods on fracture toughness values were evaluated. The overall conclusion was that local compression diminishes measured fracture toughness by up to 50%, and different materials are sensitive to 1% plastic strain. Local compression resulted in greater value scatter. Although reverse bending has no effect on fracture toughness, more experiments are required. The use of a high stress ratio had some drawbacks of necessitating a rise in overall precracking time. Eventually, all three methods yielded consistent fatigue crack front advancement [70].

James et al. (2005) described the load history problems caused by compression precracking using 3D finite element results and empirical studies for compact tension samples. The results revealed that for low tensile loading rates near the threshold region, residual stresses resulted the calculated crack tip driving force to be 25 percent or little greater than the implemented driving force. Furthermore, substantial crack advancement of approximately twice the approximated plastic zone size is required to propagate away from the residual stress distribution and decrease the determined crack tip driving force to be within 5 percent of the implemented driving force. For the materials and loading examined, test results revealed that development of two to three times the anticipated plastic zone size is required to achieve consistent propagation rates under continuous K

loading. During compression precracking, constant K evaluation might show if residual stress effects are no more substantial and assure stable growth rates [1].

Newman et al. (2010) highlighted most of the fatigue crack-growth rate evaluating data obtained in the threshold and near-threshold regions for two aluminum alloys, a titanium alloy, a high-strength steel, and a nickel-based superalloy. They employed tests by following methods: compression precracking under constant-amplitude loading, compression precracking load-reduction, and the ASTM E-647 load-reduction testing procedures. By using compact tension specimens, tests were carried out over three different stress ratios. One of the aluminum alloys and steel showed such little discrepancy between the approaches; however, the other three materials varied significantly, with the compression precracking testing methods providing lesser thresholds and accelerated crack propagation rates than the load-reduction testing method. Materials exhibited substantial differences either rough crack-surface profiles or fretting particles along the crack surfaces in the threshold and near-threshold regions [73].

Yamada et al. (2010) investigated crack closure behavior under high stress ratio and maximum stress intensity scenarios. They performed fatigue crack growth rate tests on compact tension specimens for a variety of materials at different stress ratios and maximum stress intensity test conditions. In the threshold region, test data was collected employing compression pre-cracking with constant-amplitude or compression pre-cracking load reduction test procedures; and constant-amplitude loading at higher crack growth rates. Crack propagation moment was monitored using remote back-face strain gages. Crack-opening stresses were assessed using both back face strain gage and local strain gages positioned along the crack path. Earlier researches had shown that high stress ratio and maximum stress intensity tests resulted in closure free conditions. Even so, under high stress ratios and maximum stress intensity test conditions, crack-closure behavior was related to residual plastic deformations, crack-surface roughness, and fretting particles. They concluded that the effective stress intensity factor range after calculating opening stress emerged to be particularly related to crack-growth rate from compliance measurements from threshold to higher crack growth rate conditions [132].

Garcia et al. (2015) focused on determining an equation for the crack length of single edge bending fatigue specimens using the back face strain gage method for a large extension and accuracy. Their work had a relatively small crack length with a substantial stage of inaccuracy. It is worth noting that the high percentage of fatigue tests involve crack monitoring via direct current potential drop, but its use in corrosive media is still debatable and unaffordable. Two methods were used in their work: simulation by finite element model and fatigue testing, with crack tracking on single edge bending steel specimens. In terms of testing, a method for using the back face strain gage technique was presented here in a specimen dipped in the corrosive medium in this article. Eventually, the fatigue curves were evaluated by comparing curves obtained from British standards [133].

Stein et al. (2017) investigated the near-threshold behavior of long cracks in different heat treatment conditions using precracked specimens of an aluminum alloy. Regarding the initiation of the crack tip under compression precracking, the crack propagated roughly with the constant range of the stress intensity factor at values just close to respective threshold levels. It was discovered that there were two significant mechanisms preventing the crack from continuously extending. First, principal precipitates stuck the crack zone. This influence was quite strong, resulting in considerable kinking in the crack front and ductile ridges on the fracture surface. The second mechanism associated shear-controlled crack propagation of long cracks having plastic zones in front of the crack tip, which was very close to opening mode of short cracks. The engagement with main precipitates repelled the shear-controlled cracks however they did not change crack propagation mode [60].

Taguchi et al. (2018) investigated fatigue pre-cracking behavior and fracture toughness in polycrystalline tungsten and molybdenum that have been analyzed with respect to grain boundary configuration in relation to crack extension path. Single edge bending fatigue specimens with three distinct orientations were taken as test parameter and specimens were precracked in two phases: entirely uniaxial compression cyclic loading to initiate the natural crack and its stable propagation from the notch region, followed by three-point bend fatigue loading to propagate the crack. By shifting the crack tip away

from the plastic region, the other phase aimed to reduce the impact of residual tensile stresses produced throughout compression fatigue loading. The specimen orientation has been shown to have a substantial impact on fatigue precracking results [71].

Wang et al. (2019) investigated the impacts of important fatigue testing variables such as loading techniques, crack initiator surface characteristics, and precracking methodologies on the near threshold fatigue crack propagation behaviors of a titanium alloy at room and elevated temperature. The findings revealed that the evaluated fatigue threshold values in titanium alloys are highly sensitive to the test procedure used. The staircase load-increasing procedure, for instance, produced lower threshold values. In case of such a load-increasing procedure was executed, the threshold measurements were determined either from an EDM notch or a precracked formed by compression–compression alternating loading. Furthermore, some variations in the morphologies of the crack initiator were observed depending on closure effects. The most of the above effects are related to the brittle nature of the microstructure and closure effects [67].

Ritchie (1979) evaluated the influences of different physical, microstructural, and environmental factors on fatigue crack growth in steels at growth rates less than 10^{-6} mm/cycle, where the alternating stress intensity reaches of sorts threshold stress intensity factor below which crack development cannot be experimentally observed. The significant effects of stress ratio, material strength, and microstructure on such near-threshold growth were fully examined and focused in terms of potential environmental effects and crack closure mechanism. These influences were compared with fatigue crack growth behavior for different materials with higher crack growth rates. For which materials are exposed to a low amplitude cyclic loading, defects presented during production or formed in service become possible causes of catastrophic failure from subcritical crack initiation at apparently unquantifiable growth rates [102].

Wu et al. (1993) studied a transgranular fatigue crack propagation approach established on a constrained slip reversal phase, in which the transgranular crack propagation rate is proportional to the cyclic plastic strain range in front of the crack tip. A mechanism behind of fundamental law for fatigue crack propagation rate is generated using deformation and

fracture kinetics concepts. In the lack of any environmental effects to crack growth, the theory states the Paris formula with a power law exponent of three at positive stress ratio values. The crack propagation rate is clearly expressed in terms of material characteristics like yield stress, work-hardening coefficient, microstructural factors such as enthalpy change, activation volume, along with test limitations. For experiments where the surrounding has no impact on the crack growth and the material microstructure remains unchanged, the absence of a fatigue threshold is postulated [42].

Lenets' (1995) presented a review of the near-threshold crack propagation behavior of metallic alloys. Established theories and models were evaluated and contextualized. The physical features of near-threshold fatigue crack propagation were evaluated, acceptable testing procedures were assessed and near-threshold crack-tip shielding because of crack lips inserting and crack-tip blunting, and kinetic oscillation of near-threshold fatigue-crack propagation were queried. The author point of view was that near threshold crack growth can be successfully defined within the guideline of linear fracture mechanics by accepting shielding aspects associated to crack wedging into account. They resulted that this method, however, falls short of ensuring an appropriate definition of crack non-propagation, necessitating extra research into the effect of geometric shielding attributes [48].

Garr et al. (1998) investigated the influence of specimen size on the fatigue threshold value. At room temperature, fatigue crack growth rate tests were performed on a nickel-based superalloy that had been heat treated as annealed and aged condition. The fatigue threshold was determined utilizing K -decreasing method under constant stress ratio in each test. The preliminary test was carried at two different locations, one of which used compact tension specimens with width of 127 mm. Earlier test data had been obtained at another laboratory with test samples having width of 50.8 mm. According to the test results; the 127 mm specimen's threshold was significantly higher than that of the 50.8 mm specimen at stress ratio of 0.1. A thorough examination revealed that the difference was not because of heat treatment or laboratory variation. Supplementary tests were carried out on test samples with width of 25.4 mm and at different R values. They

concluded that fatigue threshold changed with specimen width, especially at stress ratio of 0.1, with the widest samples generally resulted in the largest threshold value [125].

Lawson et al. (1999) examined the fatigue threshold concept and the relationship between threshold and endurance limit. The fatigue threshold for crack growth does not exist as a specific value. It is represented as ΔK_{th} in crack growth calculations and commonly associated with crack closure. To investigate mechanism behind of crack closure, they examined complied studies on near-threshold fatigue crack growth propagation with a focus on recent developments. Linear elastic fracture mechanics was used to correlate fatigue threshold, but certain influences like effect of overload on threshold are not easy to clarify using an elastic model approach. A stress intensity threshold range is insufficient to assess the stress ratio effects. The crack closure types, shielding and closure-induced shielding were presented, and eventually resulting in the formation of threshold concepts including closure parameter [53].

Newman (1999) investigated fatigue crack propagation and crack closure in aluminum alloy under constant stress ratio and constant maximum stress intensity threshold test scenarios by considering a plasticity-induced crack-closure concept. Two crack opening stress calculation methods were presented. The first approach relied on contact- K assessments, while the second relied on contact crack-opening displacement evaluations. Under constant amplitude loading, these techniques produced remarkably similar results; however, under load-reduction experiments, the contact- K analyses produced lower crack-opening stresses than the contact COD method. Crack opening stresses calculated using the compliance-offset method concurred with COD analysis results. Crack propagation estimations, on the other hand, appeared to favor the use of contact- K analyses. Crack propagation simulations revealed that remote closure can induce a sharp increase in opening stresses in the near-threshold regime for plane-stress conditions and high applied stress levels for all ranges of stress ratios [74].

Tabernig et al. (2002) studied effect of crack length variation on determination of fatigue threshold. An increasing stress amplitude crack propagation test on compression

precracked specimens under alternating loading was described as a method for defining the crack length variation of the fatigue threshold described by the resistance (R) curve for the ΔK . The test results indicated that the residual stress field in front of the pre-crack can have a considerable effect on the resistance curve. It is critical to use the smallest stress amplitude possible while measuring the specimen R -curve that is unaffected by the pre-cracking situation. A quite small notch root radius is required to obtain this objective. It was demonstrated that at notches operated with a razor blade sharpening procedure, the stress amplitude for pre-cracking can be decreased to values at which load history has no effect on the R -curve for fatigue threshold range [44].

Chapetti (2002) studied assessment of fatigue propagation for steels under high cycle conditions. He proposed a technique for evaluating the high cycle fatigue growth life of steel samples under constant loading amplitude. This procedure is based on scientific data that the fatigue limit signifies the threshold stress for existing crack propagation, so that both the fatigue limit and the fatigue resistance are dependent on the effective resistance of the microstructural obstacles that the cracks must confront. It was also recommended that in circumstances in which the number of cycles required for crack initiation can be ignored, the fatigue crack growth life can be used to calculate total fatigue life. Eventually, a structural steel's high cycle fatigue growth period was calculated [6].

Forth et al. (2004) investigated the performance of D6AC steel using classic and non-standard test procedures to identify steady-state conditions near the threshold region. As it is known, steady-state cracking is classified as a crack that has progressed steadily enough that the volume of the crack-tip plastic region and the sharpness of the crack-tip stay constant with additional crack growth. The full development of plasticity-induced, roughness-induced, and environment-induced crack closure dictate the progress of the steady-state condition. However, the crack growth threshold concept specifies the stress intensity level below which a crack not able to propagate. According to initial results, steady-state cracking does not take place over 80 hours at a specific near-threshold making most conventional test procedures inconsistent of steady-state condition [58].

Meggiolaro et al. (2007) studied threshold estimates for short cracks via assessing notch sensitivity factors under fatigue loading. To assess the attitude of cracks arising from circular and elliptical holes, a generalization form of El Haddad equation was used. The smallest stress range required to form and grow a crack was calculated for several combinations of notch dimensions, yielding expressions for fatigue stress concentration factor and implicitly notch sensitivity factor. The notch sensitivity factor values calculated via aforementioned equation were found to better consistency with experimental crack initiation data. It is also possible to get an expression for the maximum allowable flaw sizes at a notch root region. Eventually, new estimates of the notch sensitivity factor were obtained and compared to previous reported results. The notch sensitivity factor values obtained from corresponding equation were found to be pretty much correlated with crack initiation data [20].

Stanzl-Tschegg et al. (2010) investigated fatigue crack growth and internal cracks around near threshold region. Near-threshold test results on chromium steels were made using an ultrasound test method at varying mean loads in ambient air and vacuum over a large number of cycles. SEM system was used to examine microstructural characteristics and fracture surfaces. The aspect of fractures after cycling loading in the near threshold region was compared to fine granular and smooth areas of internal "fish-eyes" in vacuum environment. In the near threshold region, SEM examination of fracture surfaces revealed primary crystalline fracturing with a relatively smooth surface. The fracture appearance changed to a coarser and more ductile fracture mode at increased stress intensities. The fracture surfaces were usually coarser in humid air, and some interstitial and crystallographic fracture characteristics become noticeable as well [126].

Grasso et al. (2017) investigated a quantitative method for identifying the stress intensity factor range threshold for crack propagation. An analytical method for crack growth data interpolation has been established. The stress intensity factor threshold range has been determined for various materials and specimen geometries. The new method was exhibited to fit to a variety of experimental data obtained at different specimen configurations, materials, and loading conditions with the desired precision. Furthermore,

it was demonstrated that the mentioned model can distinguish the value of the threshold stress intensity factor range with such an error of less than 6%. The model's estimation of the relationship among K_{th} and R ratio concurs well with the previous studies. As a result, the suggested method can be useful in determining the stress intensity factor range threshold for crack propagation [47].

Patriarca et al. (2018) investigated the influence of residual stresses generated by shot-peening in a high-strength steel with the goal of developing a reliable fatigue model that integrates the results of fatigue crack propagation studies in the threshold regime for different stress ratios, as well as the influence of short cracks using a modified El-Haddad approach. The recommended method was verified against constant amplitude loading condition conducted in the fatigue limit region with EDM notch samples in the vicinity of residual stresses caused by shot peening, considering the effects of crack closure and assessing the circumstances for fatigue crack growth of small cracks partially incorporated in the shot-peened surface layer. The envisaged approach was verified further by comparing the results of fatigue crack growth simulations with fatigue crack growth tests performed under variable amplitude loading [69].

Saxena et al. (1978) investigated compliance measurement for different type of crack growth specimens. Elastic compliance expressions for compact tension and wedge opening loading specimens were developed for a broad range of normalized crack lengths using Newman's modified boundary sampling methods and Wilson's intense crack evaluation. The position of the axis of rotation on specimen at different crack lengths has been calculated and used in a suggested curve fitting method to estimate compliance at any position of the specimen suitable for assessing displacement throughout a crack propagation test. For the two specimen types studied, foreseen compliances were discovered to be in consistent with the experimental values. For the central crack tension specimen types, compliance expressions are also covered. Eventually, they proposed an effective curve fitting method for developing compliance curves for any suitable point of measurement [86].

Allison et al. (1988) studied different compliance methods to determine opening stress in the scope of crack growth behavior of material. The purpose of test results was to measure the location of crack closure via different compliance techniques. A titanium alloy, was selected for this investigation because its microstructure can be controlled to generate high variability in the scale of asperity-induced crack closure, making it an ideal material for recognizing this critical crack closure methodology. Two known compliance techniques were compared: back face strain and crack tip opening displacement, as well as a replica method based on surface examination. In test results at low stress intensities, all three techniques generated practically identical crack closure measurements. Various numerical methods were used to decide the turning point in the load versus displacement curve for the two compliance methods. The magnitude and differences in crack closure decided by these compliance techniques were revealed to be highly reliant on the numerical method used [88].

Oh et al. (1997) investigated real time crack measurement and implicitly opening load identification via compliance method. Using an unloading elastic compliance technique, a model has been proposed to automatically measure crack length and crack opening load in real time without adjusting any testing procedure. The crack opening stress was calculated using a new method that makes use of variable deflection test data. The established system's performance was validated using constant-amplitude crack propagation testing. Their system consisted of a computer, an analog electrical subtraction device, a stepping engine, a stepping motor controller, a PIO panel, and software applications. This model was intended to be used for detecting crack length and crack opening load measurements under random loading, as well as small crack propagation studies and determination of effective stress intensity factor range by knowing opening stress [81].

Skorupa et al. (2002) introduced a quantitative method for assessing fatigue crack closure using load and local deformation data. The local compliance is presumed to change over the course of the loading cycle, including the period when the crack is completely open. Evaluations of open crack compliance differences during loading and unloading were

used to identify the closure mechanism-related attribute stress levels. The proper flatness of the measured data was required for this type of compliance assessment. As a result, the method for stabilizing the measured data must be chosen and optimized. As a result, their paper extensively addressed the selection and improvement of the procedure for stabilizing the recorded data. The algorithm's quality was assessed by comparing the calculated closure parameters to their reference values, which have earlier studied to associate with observed crack propagation rate behavior [94].

Carboni et al. (2004) studied crack closure models and local compliance measurements. Experimental tests are typically performed to measure the physical phenomenon, however some elements of the explanation of measured data are still unclear. They used strip yield approach that appears to be the most flexible and effective method for estimating crack closure levels from an analytical standpoint, but its implementation to steels is not yet simple. Their article attempted to contribute some fresh concepts on the explanation of local compliance experimental data in crack closure assessment by modeling experimental load-strain offset loops using an optimized Strip Yield model application enriched by a new and recently described model relied on Westergaard's elastic complex potentials. Eventually, calculations enabled the investigation of some of the various variables that control local compliance measurements [134].

Song et al. (2005) proposed normalized ASTM offset method to determine crack closure level. It was presented and quantitatively assessed in order to enhance the ASTM offset method. The comparative compliance offset is normalized by the maximum offset acquired by the ASTM offset method in this technique. In this research, a corresponding offset criterion of 8% was taken. The normalized ASTM offset method was also analyzed using effective stress intensity estimation method based on the partial crack closure approach. The normalized ASTM method was more accurate and had the same precision as the ASTM method. Verification and validation results also revealed that the normalized ASTM method using the load–displacement curve, when combined with effective stress intensity estimation method, performed better the visual evaluation by a well-trained viewer using the load–displacement curve. To summarize, the normalized

ASTM offset method is very appealing as an accurate, easy, and useful alternative to the ASTM method for opening stress determination, and it was strongly advised to use the method with effective stress intensity estimation method [83].

Skorupa et al. (2007) studied feasibility of ASTM compliance offset method in terms of evaluation of crack closure levels. The effectiveness of the method that is recommended for compliance offset method to estimate crack closure in steels was investigated. The local and remote compliance data produced in crack growth tests on steel specimens were obtained under a wide range of loading scenarios enabled them to select the best strain gauge location and offset criterion values for the standard compliance offset method and its normalized version. The reliability of the closure measurements was determined by examining the ability of the generated effective stress intensity factors to account for the noticed impacts of applied loads on fatigue crack propagation rates. A deeper examination on the compliance data obtained in their experiments revealed that compliance was usually varying across the entire loading condition, in contrast to the fundamental premise used in the ASTM procedure while assessing crack closure [84].

Carroll et al. (2009) investigated fatigue crack levels via digital image correlation method. For this, two full-field physical models for evaluating fatigue crack closure scales based on digital image correlation displacement measurements were asserted. The first of the two full-field methods attempted to measure effective stress intensity factors using the displacement field. This approach showed crack closure levels comparable to crack closure levels far from the crack tip. The second full-field approach employed a compliance offset monitoring based on displacements captured near the crack tip. These methods produced similar values crack tip opening levels obtained directly behind of crack tip. The starting point was tested at low and intermediate stress intensity levels. It was demonstrated that the second full-field macroscale method yields crack opening levels comparable to surface crack tip opening levels. Eventually, they suggested that effective stress intensity factors calculated from full-field displacements could be used to estimate crack closure levels [82].

Creel et al. (2009) studied crack closure levels for biomaterials through compliance assessments. Two approaches for evaluating compliance measurements were characterized in their article. Those are the standard ASTM method and a new model developed by the authors particularly for anisotropic materials. An explanation of how data from equine cortical bone can be interpreted was clarified. Closure measurements were carried out thirty-six 3PB specimens extracted from metacarpal bones in this study. Cracks propagated in three dimensional relative to the longitudinal axis of the bone. Load-displacement data was used to calculate specimen compliance and crack closure was evaluated for a normalized crack size of 0.30 to 0.65 times the specimen width. Test results indicated that the ASTM method was inapplicable to anisotropic biomaterials such as bone [89].

Song et al. studied crack closure measurements via the normalized-extended ASTM procedure. It was improved to solve the optimization problem of the standard ASTM method, and widely employed to random loading conditions for aluminum specimens, utilizing an approach applicable to random loading for assessing open stress via compliance curve and the predictable maximum compliance offset. The effective stress intensity factor range premised on the crack opening stress that is calculated by the normalized-extended ASTM method can easily be estimated under random loading. This clearly showed that the normalized-extended ASTM method is very effective for both random and constant amplitude loading condition. The crack opening stress of the specimens under random loading was below the results obtained under constant amplitude loading, reflecting that estimating the crack opening stress under random loading explicitly was non-conservative estimations compared to constant amplitude loading results. This tendency varies dramatically from the trend of crack opening stress for a different aluminum alloy tested [92].

Kanters et al. (2015) practiced compliance measurements on non-linear materials such as polymers. They compared compliance results obtained via optical monitoring method to examine its possible use in non-linear, time-dependent materials like polymers. The mechanical behavior of polymers caused a substantial loading condition and time

dependency of the compliance curves, and as a direct consequence, no distinct association for crack length as a feature of dynamic compliance can be discovered. Standardization of the dynamic compliance with an observable modulus partially decreased the difference. However, it still did not generate a distinct operational definition, because the variances between calibration curves seemed to be associated to stress-induced physical aging during the experiment. While performing crack propagation tests, the optical measurement method is used to determine the crack length. Because of its inconvenient use, they evaluated that the compliance results should be interpreted with caution [79].

Ewest et al. (2016) studied a new compliance method for single edge bending specimens. They described a modified compliance approach to the compliance method described in, for instance, ASTM E-647 that is perfectly served for high loads, divergent temperatures, and accounting for deviation in Young's modulus. To explore the impact of crack initiation regions on reliability of the method, an analytical finite element was conducted for a single edge bending specimen containing notch. The variation in cracked region versus change in stiffness for three different scenarios showed that curves declined to one curve, revealing that crack initiation way had no considerable effect on the compliance results. The numerical investigation was carried out and the results of different tests using various materials were made by heat encolouring. Eventually, they asserted a new compliance model for single edge bending specimens based on new geometry function [80].

Khor (2018) studied crack tip opening displacement measurements on his thesis. The measure of crack tip opening displacement was investigated as a means of assessing fracture toughness as determined in the single edge bending specimens having notch. Crack propagation tests were performed with constant displacement measurements on casting specimens. Then, the experiments clarified the findings of finite element models. Digital image correlation was used to acquire surface measurements, which were then evaluated to surface measurements via crack tip opening displacement from specimens. In addition to the experiments and finite element analysis, test data from databases was compared to demonstrate quantitative variabilities between crack tip opening displacement equations. Eventually, the findings of this study allowed for the precise

fracture evaluation of a variety of metallic materials with low and high strain hardening behavior [135].

Many breakthroughs have been achieved in recognizing the fatigue crack propagation mechanisms over the last 50 years. Throughout this time, the profession of fracture mechanics has evolved with mathematical and computational techniques capable of dealing with cracks of nearly any dimension and form in any type of materials. The introduction of TEM and SEM, as well as developments in testing machines such as servo-hydraulic systems, have significantly improved our knowledge of the principles that control the growth of a fatigue crack under constant and variable amplitude loading conditions [136]. Analytical methods have progressed to the point where incredibly detailed post-failure analysis is now standard practice for fractography [137].

Secondary cracks can be described as a result of a high and uneven stresses at the time of catastrophic failures. It is important to note that the existence of ratchet marks is directly correlated with fatigue. Ratchet marks seem to be tiny cracks that initiate and propagate in planes at the maximum shear stress. Fatigue failure indication can be revealed on SEM analysis by observing ratchet marks, secondary cracks and fatigue striations [138]. Striations on fracture surfaces can emerge as a result of a number of circumstances such as fatigue, slow crack growth, and quick brittle rupture. These curved lines are separated from each other in a fracture region that can be correlated with crack arrest and crack propagation through the sample. Fatigue striations are the most common clue for deformation marks on fracture surface of ductile metallic alloys at stable crack growth region of the da/dN curve. Laird's model is the most well-known for striation mechanism among other models [139]. Laird regarded striations as a form of consecutive blunting and re-sharpening of the crack tip under stable crack growth. Because of the Laird model's convenience in practice, striation distance has been readily employed as an estimation principle for crack propagation rate. But even so, striations are sometimes not usable in order to establish a direct proportionality between fatigue striation distance and fatigue crack growth rate [140]. Under high ΔK loading, it triggers irregular fatigue striation because of drastically increase of fatigue crack growth rate [141]. Li et al. explain this as

the dimples appear during high stress intensity loading [142]. As the crack propagates, the quantity of dimples increases, revealing that dimples have progressively become the dominant fracture mechanism at this crack growth rate. In case of reaching threshold region, fatigue crack growth is associated to the blunting and re-sharpening mechanism. On the other hand, the composition of fatigue striation is caused by the interaction of the crack tip and slip bands according to the dislocation-based model [143]. Under high ΔK loading, stress ahead of crack tip increases then it results in formation of micro-cracks with deformation. The dislocations released from the crack can also enhance the plastic strain under fatigue stress, leading to the growth and coalescence of micro voids. The transgranular crack growth is extremely planar and crystallographic in behavior, with facets on the fracture surfaces coherent with slip along most close-packed planes for many superalloys with low stacking-fault energy. Clearly, this can be observed when the cyclic plastic zone size approaches the average grain size, especially around the threshold region [144]. Each stress cycle doesn't create a striation at low ΔK , and there is an intensifying mismatch between striation spacing and microscale crack-growth rates with lowering ΔK , with striation spacings being roughly the same for plenty of materials which is around 80-300 nm [145]. It is generally believed that each striation is also generated by one stress cycle around threshold region as in the Paris region. Additionally, an enormous number of stress cycles are needed as reaching threshold before crack propagation, blunting and re-sharpening event takes place respectively since a dislocation pile up, or some other microstructural obstacles, must promote ahead of the crack wedge before crack propagation phase [146]. Nevertheless, it is probable that crack development can happen on each cycle across some segments of the crack front, with adequate crack blunting and re-sharpening arising at crack front to create striation just after cracks have propagated by a quite small distance identical to slip-band spacing [147].

For the sake of example, brittle failures cause almost no material deformation throughout the fracture region. Ductile failures, on the contrary, can cause significant deformations. The ductility portion visible on the fracture surface is a significant aspect of the stress or

environment effect to which the specimen was subjected under loading. Relatively high stresses, in particular, result in greater ductility and roughness; on the other hand, lesser stresses typically have lower ductility and roughness on the fracture surfaces. Lesser stresses and brittle failure are intimately connected with smoother fracture surfaces. Such a surfaces might also occur as a result of extreme environmental stress cracking. Slow crack growth failures under alternating loading can also result in very smooth fracture surfaces. In case of exposed higher stresses, the fracture surface typically results in increasingly rougher surfaces [148]. A biaxial stress state occurs on the exterior portion of the crack tip, because the stress element perpendicularly to the free surface would disappear.

The main purpose of a failure analysis is to identify the underlying problem behind of failure. Regardless of the type of material, one of the following reasons may be the root cause: geometry, manufacturing process, service conditions, or material nature. In case of combination of these reasons, it may result as cataphoric failure. For example, increased stress concentration due to geometry and inappropriate material choice may cause early failure. Typical fatigue failures indicate striations, beach marks and ratchet marks on the fracture surface of metals that makes easier to examine crack origin and crack propagation direction [149]. The delivery of clues after failure and the choice of suitable component for SEM investigation are part of the initial processes of fractography analysis. On-site investigation, a historical background of the failure, material quality, an evaluate of maintenance and replacement documents and the percentage of previous failures for this particular element must all be included as additional considerations.

The analysis will begin with a naked eye macroscopic visual inspection of the fracture surface of the component prior to microscopic investigations. Optical microscope will aid in revealing fracture surface features, confirming crack initiation regions and failure mechanisms, and revealing microstructural defects that cause crack initiation. More comprehensively, scanning electron microscopy would help in determining the aspect of fracture and identifying the origin of crack nucleation [150]. Fractography is essential to assess fatigue crack growth by presenting mechanism behind of the failure. An ultrasonic

bath was used to clean the fracture surface. After that, the specimen was examined under a scanning electron microscope. The measurements were taken in the plane strain region generally since the characteristics can vary considerably near the edges in plane stress. Images were captured at low magnifications at various crack lengths to present history of test. Distribution of striations on fracture surface depends on what stress ratio it happens. Therefore, it is expected that striations decrease by increasing stress ratio [151]. Fatigue crack surfaces visible to the human eye have an almost flat fracture surface that is indicative of fatigue. It was eventually perpendicular to the applied stress direction. As the crack propagation rate increases near unstable crack growth region, the shear lips extend. Once the shear lips completely covered the specimen cross sectional area, it typically results in catastrophic failure as a shear crack [152].

CHAPTER 4

EXPERIMENTAL PROCEDURE

4.1. MATERIAL

AISI 4340 steel with a chemical composition of .38% C, .65% Mn, .7% Cr, 1.65% Ni, .2% Mo, .025% P and S, bal. Fe in weight % was chosen as a research material to investigate the fatigue and fracture behavior of the steel which has high toughness and fatigue performance.

4.2. SAMPLE PREPARATION

Within the scope of this thesis; two specimen configurations were manufactured. The first specimen type was the round fatigue specimens with 130 mm length and 8 mm gage diameter as shown Figure 16 to evaluate fatigue limit behavior of AISI 4340 steels.

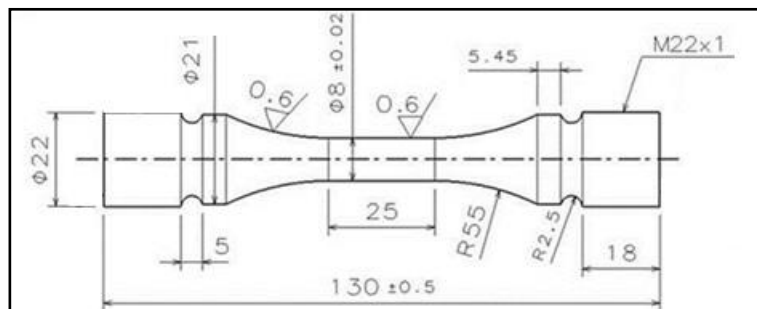


Figure 16 Technical drawing of the round specimens

Manufacturing process for smooth fatigue specimens starting from raw material to final product can be seen on Figure 17.

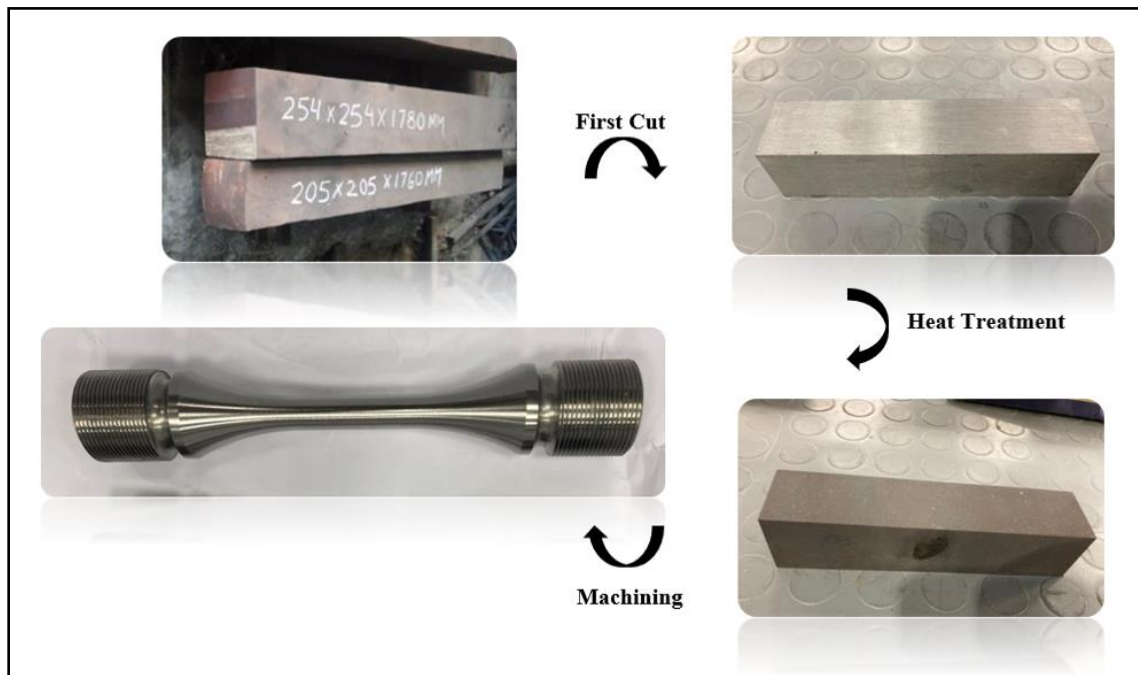


Figure 17 Manufacturing process of fatigue specimens

After the material was out of stock, heat treatment was applied according to AMS 2759-1D [153]. Accordingly, the rectangular bars were initially normalized at 900 °C for 90 minutes next air cooled, then austenitized at 816 °C for 60 minutes, afterward rapidly quenched in oil, and finally tempered at around 600 °C for 3 hours as shown in Figure 18.

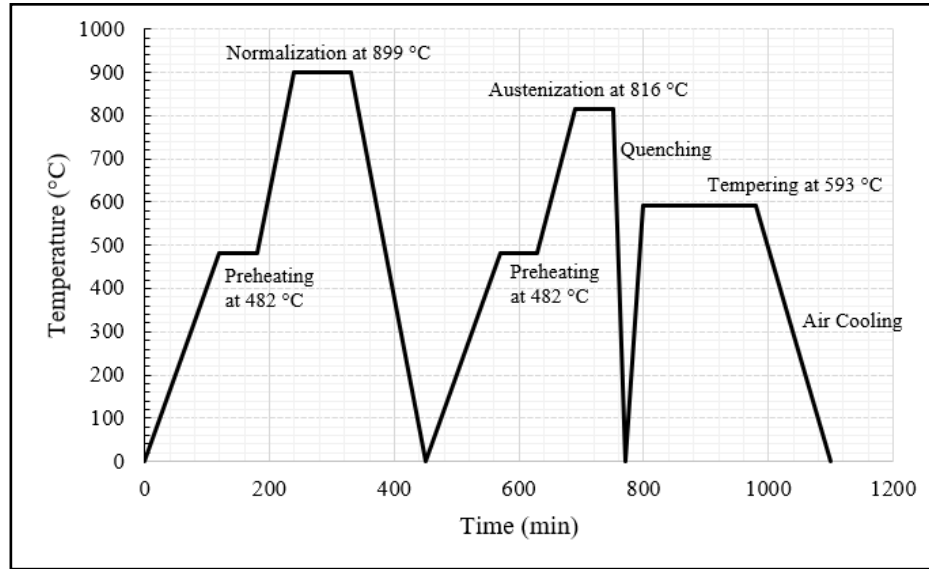


Figure 18 Heat treatment procedure for smooth fatigue specimens

After heat treatment, fatigue test specimens were manufactured according to ASTM E466-96 [154] standard using machining parameters given on Table 2 and surface roughness was measured as 0.81 μm Ra on average after machining.

Table 2 Machining parameters of the AISI 4140 steel samples

Rough Turning		Semi-Finish Turning	
Feed Rate (mm/rev)	Cutting Speed (rev/min)	Feed Rate (mm/rev)	Cutting Speed (rev/min)
0.18	850	0.02	850

Fatigue behavior of the AISI 4340 steel was estimated using in total 14 identical fatigue specimens. They all extracted from the Rolling Direction-R90 orientation. In connection with that, crack initiation was observed in the R90-Transverse plane perpendicular to the applied stress along the Rolling Direction as shown in Figure 19.

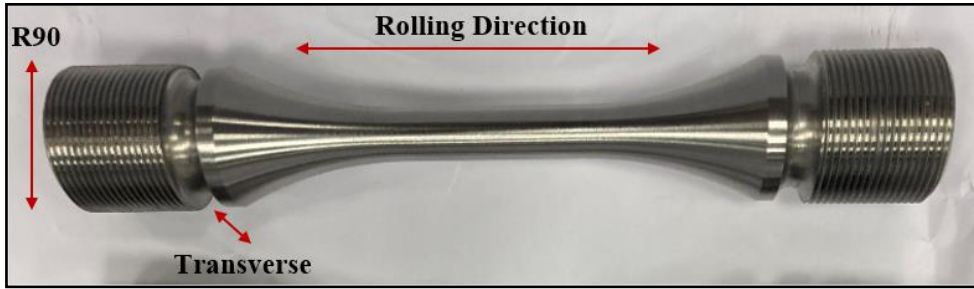


Figure 19 Sampling of round fatigue specimens with extracted orientation

The other specimen configuration was Single Edge Bend (SEB) specimens to evaluate crack growth behavior of material, as illustrated in Figure 20. The sample configuration was chosen as SEB for the following reasons: When performing crack growth tests, the extended geometry provides additional workspace. When compared to other sample configurations, it involves less force for the same stress density factor value. When mounting the specimen for the test rig, no gripping is required. This is quite favorable for crack growth tests since gripping has an effect on compliance measurements.

The dimensions of specimens were 110 mm in length, 24 mm width and 12 mm thickness by ensuring plain strain condition specified on ASTM E-647. Additionally, 8 mm wide notch section was manufactured by the Electro Discharge Machining (EDM) method in the center of specimens. It provides very precise dimensions and accuracy in terms of positioning because of nature of electrochemical operation.

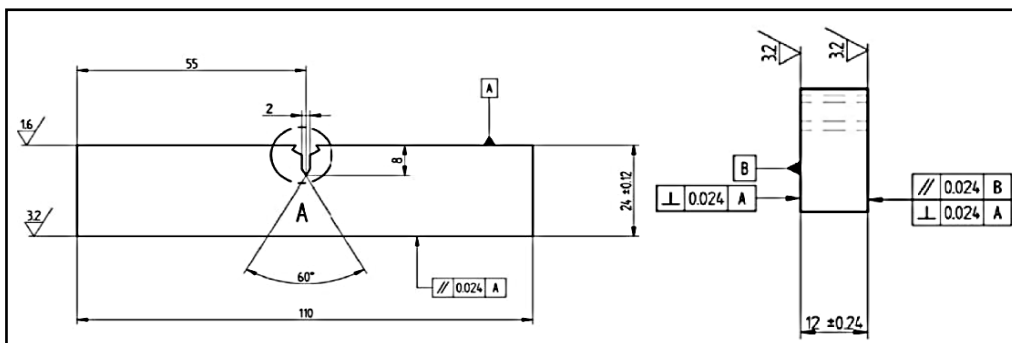


Figure 20 SEB specimen dimensions with EDM notch on center of the specimen

Manufacturing process for crack growth specimens starting from raw material to final product can be shown on Figure 21.

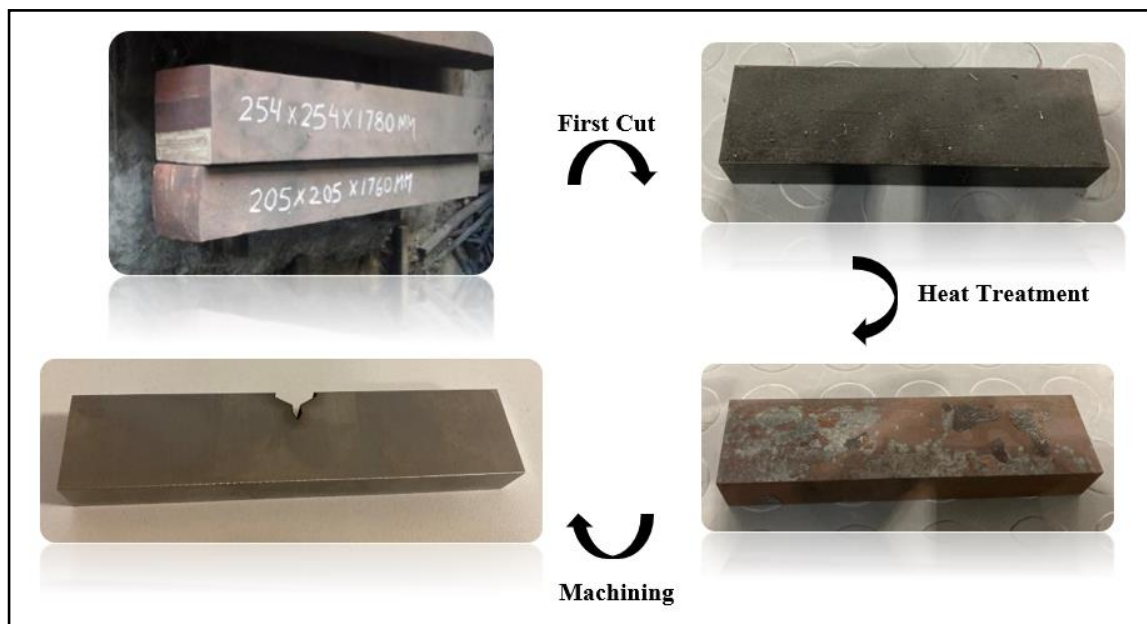


Figure 21 Manufacturing process of crack growth specimens

After the material was out of stock, heat treatments were applied according to AMS 2759-1D. Accordingly, two different heat treatments were processed in the scope of this specimen configuration because of assessing the effect of heat treatment on fatigue crack growth. Heat treatment variables were chosen as tempering and annealing of specimens. For tempered condition, some parts of the rectangular bars were initially normalized at 900 °C for 90 minutes next air cooled, then austenitized at 816 °C for 60 minutes, afterward rapidly quenched in oil, and finally tempered at around 600 °C for 3 hours as described in the round fatigue specimens above. Differently, some parts of rectangular bars were annealed as shown in Figure 22. Accordingly, specimens were firstly normalized until at 900 °C for 90 minutes next air cooled, then annealed at 843 °C for 60 minutes and furnace cooled around 4 hours until 427 °C to provide slow cooling allowing phase transformation and it was eventually air cooled until room temperature.

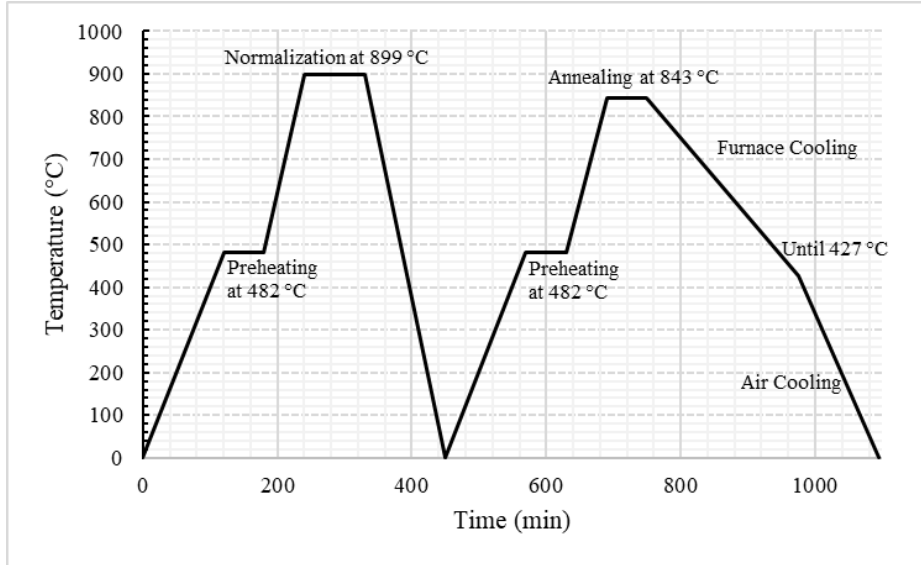


Figure 22 Heat treatment procedure for annealed crack growth specimens

After heat treatment, fatigue crack growth test specimens were manufactured according to ASTM E-647 standard using optimized machining parameters aforementioned above. Crack growth behavior of the AISI 4340 steel was estimated using in total 15 SEB specimens. They all extracted from rolling direction as shown in Figure 23.

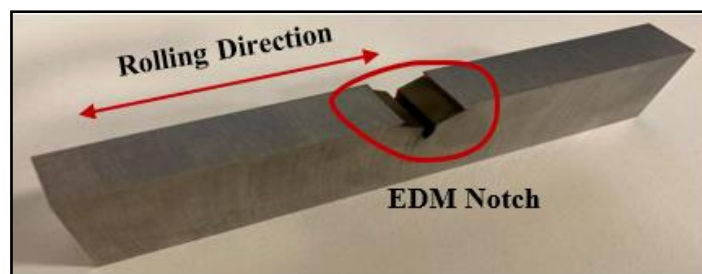


Figure 23 Sampling of crack growth fatigue specimens with extracted orientation

To observe fatigue crack on optical microscope, crack growth specimen surfaces were polished before starting testing. BUEHLER Beta Grinder-Polisher was used for metallographic polishing purpose as shown in Figure 24. P600, P800 and P1000 sand paper was used for fine grinding respectively. Eventually, surface finish was gradually

done with 1 μm polycrystalline diamond suspension abrasives. A lower force applied to the specimens resulted in a smaller chip size during polishing.

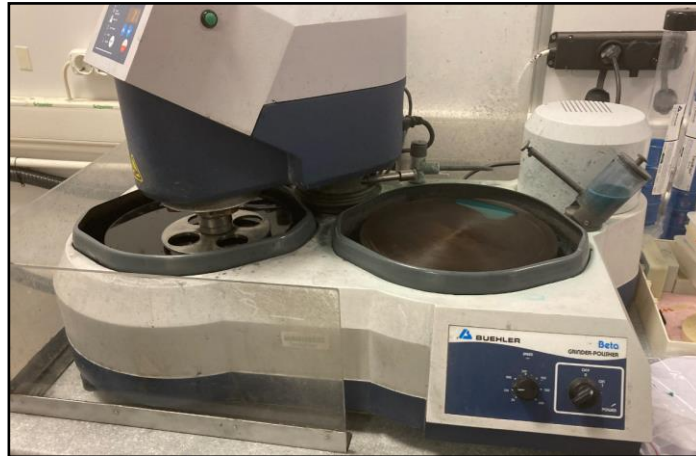


Figure 24 BUEHLER polishing machine

4.3. FATIGUE TEST PARAMETERS

Smooth fatigue specimens were alternatively loaded under constant amplitude to determine endurance limit of material by constructing SN curves with minimal standard deviation. In terms of statistical analysis of test results, two methods were basically taken into consideration depending on different approaches.

On the other hand, crack growth test results contain some anomalies because of preferred test procedure and defined test parameters before starting tests. To clarify this phenomenon because of the nature of fatigue behavior of material, following test variables were chosen to observe their effects on crack growth behavior of steel specimens. Firstly, compression precracking tests were performed at different stress ratios. It was objected to determine most reliable stress ratio during compression-compression precracking comparing long crack threshold values. Another issue was to determine effect of load ratio on crack growth behavior near threshold region. Therefore, crack growth tests were performed at different load ratios and dependence of stress ratio on long crack threshold

were investigated. Furthermore, crack growth measurement was performed with different sensor to observe effect of measuring device on compliance results. Aforementioned test parameters were summarized on Table 3.

Table 3 Test variables defined for thesis study

Corresponding Tests	Test Parameters			
SN Curves	Staircase Method		Curve Fitting	
Compression Precracking	R=10	R=20	R=40	Not Precracked
Crack Growth Tests	R=0.7		R=0.1	R=-1
Compliance Measurements	COD Gage			

4.4. TEST EQUIPMENTS

Smooth fatigue specimen tests were carried out on an axial resonance testing equipment (RUMUL Testronic) at laboratory environment with an alternating frequency of around 120 Hz and the stress ratio of 0.1; in other words, tests were performed under tensile-tensile cyclic loading. The load cell capacity of test bench was 100 kN under static and dynamic loading. Test control channel was arranged as load controlled for all performed tests. Throughout testing, the mean and oscillatory loads were held constant. The test bench's alignment was accredited to be less than 5% bending under specified maximum loading by ASTM E1012 [155] and calibrated per ISO7500-1 Class-1 [156]. During the tests, the controlled environment was adjusted to the temperature of 25 ± 3 °C and the relative humidity of 50 ± 5 %. Round fatigue specimens and compression-compression precracking tests were tested on resonant fatigue machine as shown in Figure 25. Test frequency of round specimens was around 120 Hz.

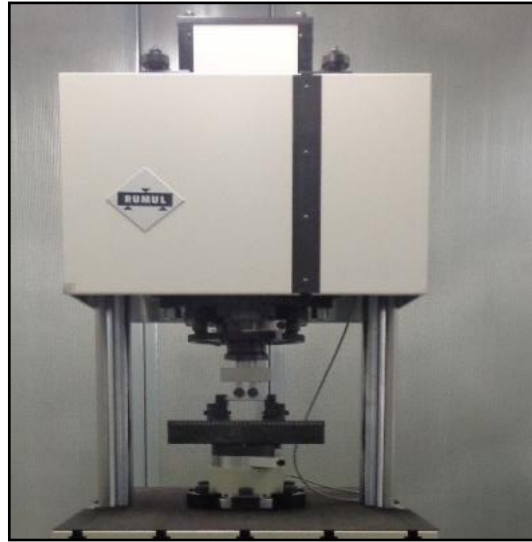


Figure 25 RUMUL Testronic resonant fatigue machine (performed at TAI M&P Lab.)

Crack growth tests were carried out on RUMUL Cracktronic resonant testing system providing bending moment on fatigue specimens as shown in Figure 26. Tests were performed at laboratory environment ensuring that the temperature of 25 ± 3 °C and the relative humidity of 50 ± 5 %. The machine is composed of the basic control unit with the resonant drive and the drive for the static load. The operating frequency can be changed by adding more masses. Test frequency of crack growth specimens was around 80 Hz.

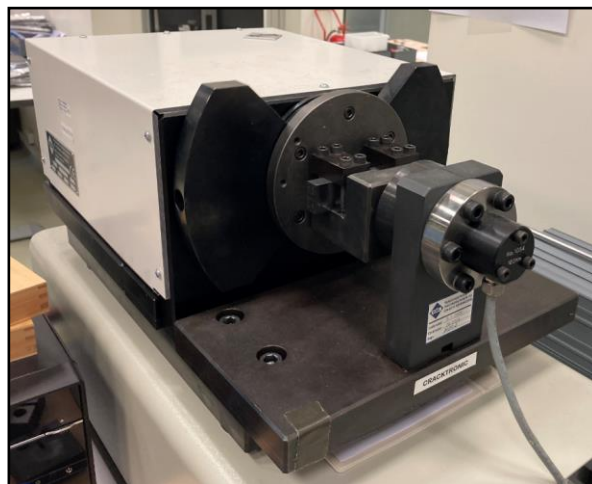


Figure 26 RUMUL Cracktronic resonant fatigue machine (performed at TAI M&P Lab.)

Static test was performed on Instron 8801 servo hydraulic test system at laboratory environment with force controlled as shown Figure 27. A system comprised of servo drives and servomotors that provides load transfer in a closed loop manner. Test control system provides stiffness based PID before starting testing to optimize command and feedback signal. Grip pressure was adjusted as 120 bar before starting tests and crosshead pressure provided by hydraulic power unit was 210 bar. The test bench's alignment was accredited to be less than 5% bending under specified maximum loading by ASTM E1012 and calibrated per ISO7500-1 Class-1. During the tests, the controlled environment was adjusted to the temperature of 25 ± 3 °C and the relative humidity of 50 ± 5 %.



Figure 27 Instron 8801 servohydraulic test bench (performed at TAI Structural Test)

Failure analysis was performed on ZEISS EVO Scanning Electron Microscope (SEM) at Turkish Aerospace as seen in Figure 28. After performing crack growth fatigue tests, the fatigue specimens were fractured by hammer impact after exposure to liquid nitrogen for several minutes to provide brittle fracture and not damage the fracture surface. Then, fracture surfaces were examined to observe crack initiation and propagation direction under SEM. It has also provided knowledge about test history thanks to color contrast during each phase of loading on crack growth tests.



Figure 28 Scanning Electron Microscope (examined at TAI M&P Lab.)

CHAPTER 5

RESULTS AND DISCUSSIONS

5.1. MICROSTRUCTURE OF THE SAMPLE

Two different heat treatment procedures were applied to the fatigue test specimens to observe effect of microstructure on crack growth behavior of material. Of these, tempering was the first heat treatment method. Before tempering, material was normalized to reduce internal tension and to achieve microstructural homogeneity. In terms of strength and hardness, austenitizing and tempering produced the desired microstructure. The martensite phase was formed as a result of rapid cooling after quenching, which does not allow enough time for carbon atom diffusion due to the resulting BCT crystal structure. Following tempering, the martensite phase transforms into the tempered martensite phase, resulting in the microstructure consisting of cementite and ferrite phases. As a direct consequence, the crystal structure after this transformation is BCC. Figure 29 presents the material's microstructure. After heat treatment, the mechanical properties of tempered condition resulted in a final strength of 1080 MPa and a hardness of 29 HRC.

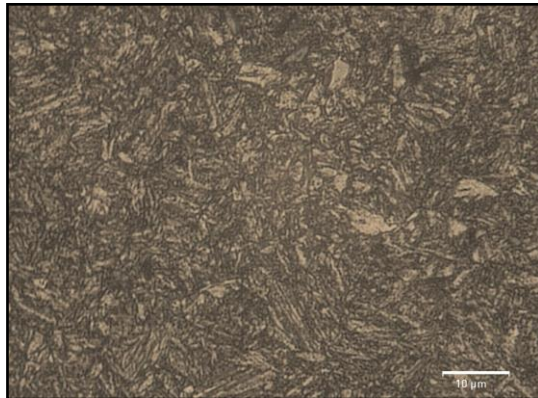


Figure 29 Micrograph of the tempered fatigue specimens

The other heat treatment condition was the annealing. Because of slow cooling, the annealed structure seemed to have explicit pearlitic colonies with larger interlamellar spaces between the coarser pre-eutectoid ferrite and pearlite formation stages. Figure 30 presents the annealed microstructure of microstructure. After heat treatment, the material's mechanical properties resulted in a final strength of 827 MPa and a hardness of 17 HRC. The fracture toughness of tempered and annealed conditions is between 76-78 MPa√m and 88-90 MPa√m respectively [171].

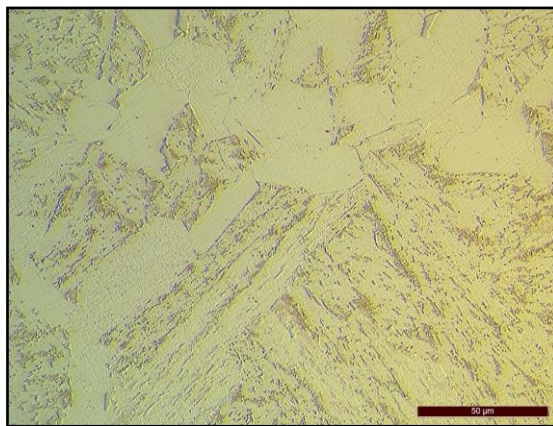


Figure 30 Micrograph of the annealed fatigue specimens

5.2. ENDURANCE LIMIT TEST RESULTS

SN curves were established in the scope of this thesis using various methods assessing data points for finite and infinite life regions. Endurance limit tests were carried out for only tempered condition specimens; fatigue limit for annealed specimens were estimated by correlation between fatigue limit and hardness. A total of 14 tempered fatigue specimens were sequentially tested, with eight of them assigned to determine the material's fatigue strength by applying a lower stress range and six of them assigned to focus on the finite fatigue zone. Fatigue tests were carried out under constant amplitude cyclic loading in a laboratory environment ($23\pm 2^{\circ}\text{C}$ and 50 ± 5 RH) in accordance with ASTM E466-96. A sinusoidal cyclic waveform with a stress ratio of 0.1 (tensile-tensile loading) were applied to round fatigue specimens under constant amplitude loading on the RUMUL resonance test system with a constant test frequency of 150 Hz.

Basically, two common approaches to fatigue data were used in order to generate SN curves: Staircase and Curve fitting methodologies.

5.2.1. STAIRCASE METHODS

The staircase or up-and-down method is a widely accepted method for determining the fatigue limit of a material at a given fatigue life. Before starting fatigue testing, the run-out criterion firstly needs to be clarified (say, ten million cycles), and the first specimen is nearly tested around the mean value. If the specimen fails at this stress level, the next specimen will be tested at a lower stress level with a defined stress increment. In the event of a run-out that means specimens endures until ten million cycles, the stress level will be increased with a defined stress increment. As a result, the applied stress for the next specimen is determined by the results of the previous tests. The standard deviation is generally used to calculate the stress increment, and the rest of the specimens are tested in this manner to construct SN curve.

5.2.1.1. DIXON-MOOD METHOD

The Dixon-Mood method, which is based on Maximum Likelihood theory, is a highly regarded method for determining the endurance limit of materials. The tests are performed by increasing or decreasing the stress level with a defined increment based on the standard deviation and generating the sequence, which is also known as the up-down method. The primary objective is to concentrate on the median value in order to decide accurate fatigue strength with defined confidence levels. The following equations can be used to calculate the sample mean (S) and standard deviation (σ):

$$S = S_0 + d * \left(\frac{A}{F} - \frac{1}{2} \right) \text{ when less periodic event becomes failures} \quad (5.1)$$

$$S = S_0 + d * \left(\frac{A}{F} + \frac{1}{2} \right) \text{ when less periodic event becomes run-outs} \quad (5.2)$$

$$\sigma = 1,62 * d * \left(\frac{F*B-A^2}{F^2} + 0,029 \right) \text{ in case of } \frac{B*F-A^2}{F^2} > 0,3 \quad (5.3)$$

$$\sigma = 0,53 * d \text{ in case of } \frac{B*F-A^2}{F^2} < 0,3 \quad (5.4)$$

where S_0 is the lowest stress level in the data set, d is the stress increment, $F = \sum f_i$, $A = \sum i * f_i$, $B = \sum i^2 * f_i$, i is the stress level numbering, and f_i is the number of samples equivalent to that stress level.

If the estimated stress increment is significantly greater than the standard deviation, the sample mean will be higher than the physical real value, and the standard deviation will be lower. In the case of an opposite circumstance, the standard error will be greater and the sample mean will be smaller. Before beginning the test, it was expected to select a stress increment between $2/3\sigma$ and $3/2\sigma$.

According to the equations given above, the sample mean with a 50% confidence level and standard deviation for the Dixon-Mood method were calculated as 585 MPa and 23.2 MPa, respectively, and the variables are shown in Figure 31. Because each set of test samples will have different mean values due to scattering, the confidence interval for the sample mean will provide that conservative data are depicted for the endurance limit. The

95% confidence interval can be used to preserve the sample mean safe, which means that 95% of the test results will be greater than the mean value. The coefficient of variance is assessed according to the unknown confidence interval t-distribution, which means that the defined confidence interval $((1 - \alpha) * 100 \text{ percent})$ is symmetric around the experimental sample mean, and the lower margin is expressed as the equation below.

$$S_{X\%} = S - t_{\alpha, n-1} * \frac{s}{\sqrt{n}} \quad (5.5)$$

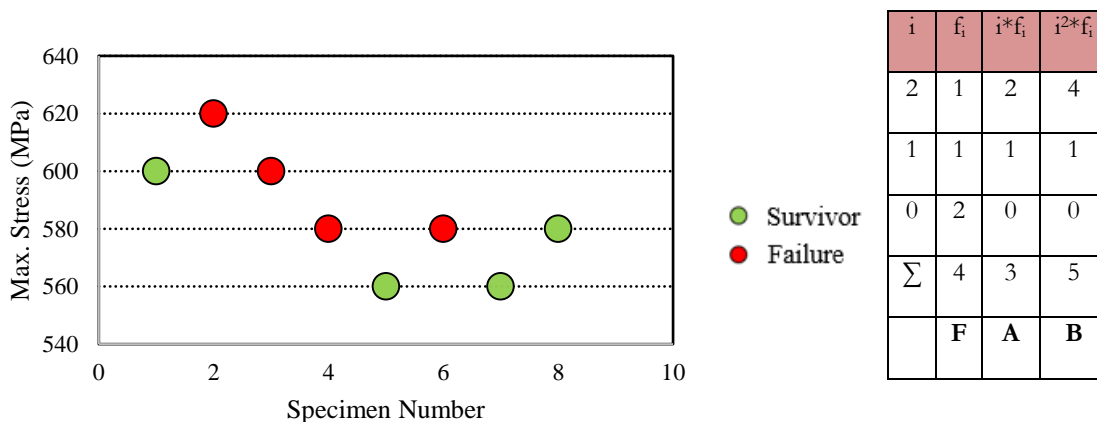


Figure 31 Staircase based on Dixon-Mood method

As a result, probability of failure limits was taken into account, along with a lower endurance limit. According to this, the mean value can be calculated as 563.8 MPa with a 95 percent confidence interval.

Similarly, the confidence interval for the standard deviation must be evaluated to validate the bounded confidence level and the standard deviation below the upper limit of the experimental standard deviation from the fatigue test data. The chi-square is calculated using the given equation and fits the right-tailed probability of distribution.

$$S_{X\%} = \sqrt{\frac{n-1}{\chi^2_{\alpha, n-1}}} * S \quad (5.6)$$

Eventually, the standard deviation can be estimated 56.9 MPa using the 95 percent confidence interval, as shown in Figure 32. This value will be used to determine the material's fatigue limit as well as the probability of failure.

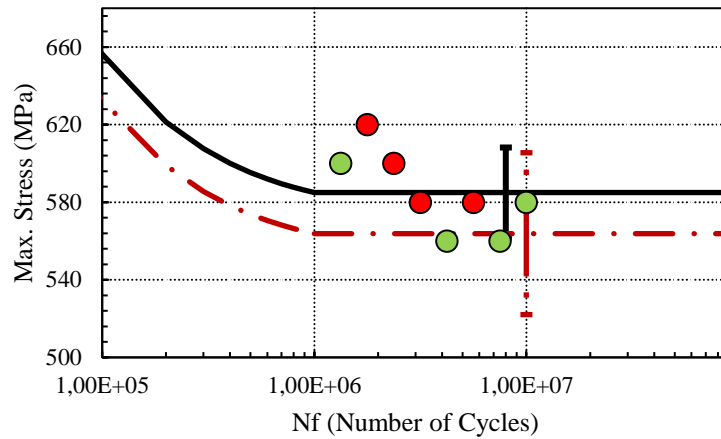


Figure 32 Mean value with 50% probability of failure and standard deviation provided by 95% confidence level

5.2.1.2. IABG METHOD

The IABG method proposed by Hück [157] is another effective approach among the staircase methods. In terms of data evaluation, it is similar to the Dixon-Mood method. Difference is that the IABG method begins with the data from the second test sample, and the first is discarded and not evaluated; fictitious data is then added to the end of the dataset, as shown in

Figure 33. Foregoing data will be evaluated in the same manner as the given equations addressed by the IABG method [118].

$$\log(S) = \log(S_0) + \log(d) * \frac{A}{F} \quad (5.7)$$

$$k = \begin{cases} \frac{F*B-A^2}{F^2} & \text{if } \frac{F*B-A^2}{F^2} \geq 0,5; \\ 0,5 & \text{else} \end{cases} ; a = 4,579494 * F^{-0,889521} ; b = 7,235548 * F^{-0,405229} \quad (5.8)$$

$$\log(\log(s)) = \log(d) * 10^a * k^b \quad (5.9)$$

Here, S and s symbolize the data set's mean and standard deviation, respectively, d represents the stress increment in the logarithmic base, and k , a , and b are auxiliary variables.

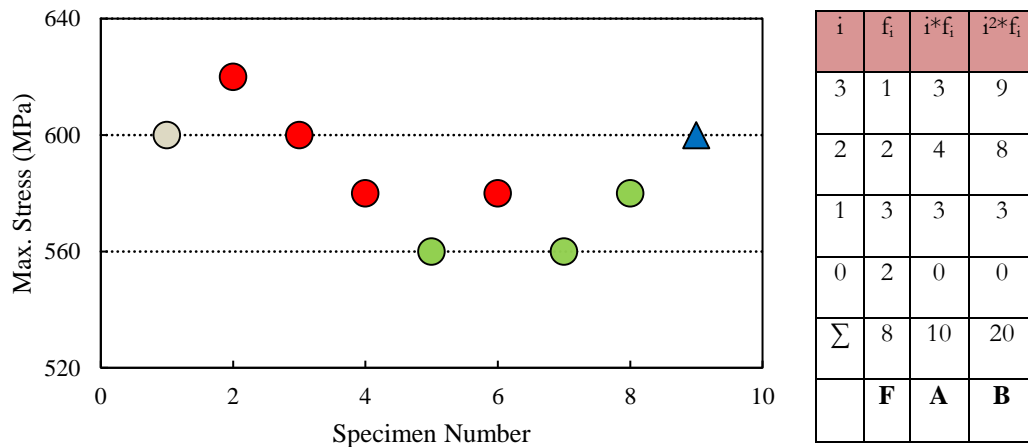


Figure 33 IABG method (Δ : fictitious data)

Based on the calculations provided equations above and shown logarithmically in Figure 34, the mean value with 50% confidence level and standard deviation for the IABG method are 585.1 and 14.5 MPa, respectively.

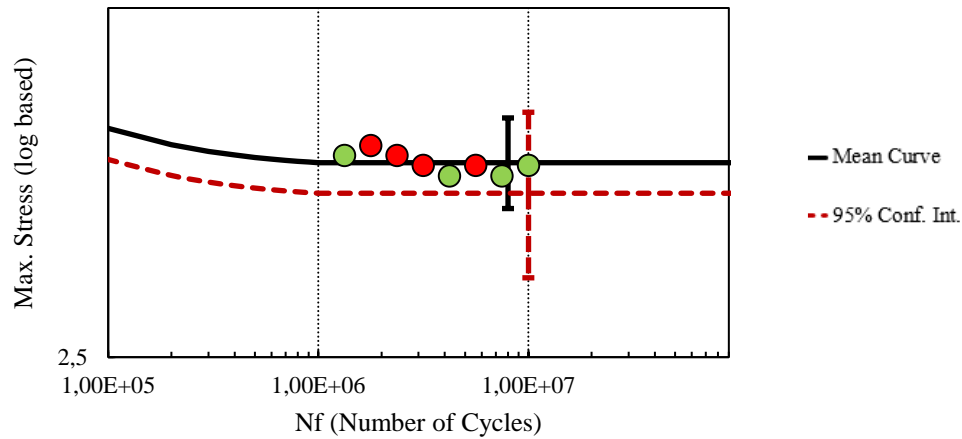


Figure 34 Estimation of mean value and standard deviation with given 95% confidence level via IABG method

5.2.1.3. BOOTSTRAPPING METHOD

Another approach is Efron's [158] bootstrapping method, which is based on data simulation, that is, resampling from the original data, which gives a variety of arbitrary data. Because the standard deviation of a random distribution of a population is inherently uncertain, the most common approach is to use the estimated standard error and associated standard deviation. Because the bootstrapping covers all applicable information about the distribution, evaluating the dataset's standard error may be a wise option. Figure 35 depicts the normal distribution of samples. The approach's goal is to reduce scatter by allowing for less biased standard error.

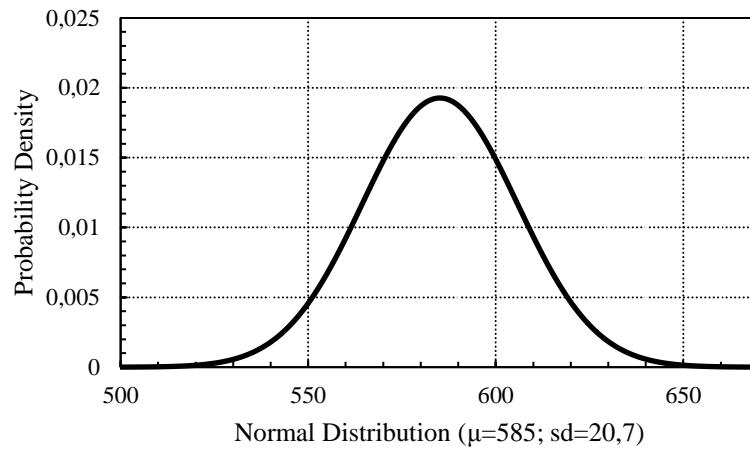


Figure 35 Gauss distribution of staircase data based on Bootstrapping method

The bootstrapping method originating from Monte-Carlo approach is based on estimation of standard error through redistribution of samples. Re-sampling from the original data is enlarged at least 200 times to approximate the population with a larger sample size. During the analysis, the original data was re-sampled 200 times, and only 10 of them are shown in **Error! Reference source not found.**

Table 4 (Cont'd) Bootstrapping algorithm (10 out of 200 re-sampling)

b	X(1)	X(2)	X(3)	X(4)	X(5)	X(6)	X(7)	X(8)	X*
1	580	580	600	580	580	580	600	600	587,5
2	580	620	600	620	600	560	600	580	595
3	580	580	560	620	580	620	560	620	590
4	560	560	580	580	560	560	580	560	567,5
5	560	600	600	580	560	580	580	560	577,5
6	560	560	600	560	560	560	560	560	565

7	580	580	580	600	560	560	580	580	577,5
8	600	580	620	580	560	620	600	600	595
9	620	560	600	600	600	560	600	600	592,5
10	580	600	580	620	580	620	560	560	587,5

Mean value (\bar{X}) and estimated standard deviation (s) of bootstrapping replications can be calculated via following equations;

$$\bar{X} = \frac{1}{B} \sum_{i=1}^B X_i^* \quad (5.10)$$

$$s = \left(\frac{1}{B-1} \sum_{i=1}^B (X_i^* - \bar{X})^2 \right)^{\frac{1}{2}} \quad (5.11)$$

Similarly, standard deviation (s) of Monte Carlo approximation based on bootstrapping replications can be calculated by equation below;

$$s = \left(\frac{1}{n^2} \sum_{i=1}^n (X_i - \bar{X})^2 \right) \sqrt{n} \quad (5.12)$$

The bootstrapped standard error of the arithmetic mean is the standard deviation of 200 mean values. After bootstrapping analysis, the mean value with 50% probability of failure was calculated as 585.1 MPa, and the estimated standard deviation is 7.1, as seen in Figure 36. The standard deviation calculated using the Monte Carlo approximation is 9.2, which is close to the bootstrapping method. Confidence intervals for a given population could be established using bootstrapping re-sampling. The following equations can be used to calculate the bootstrap t -interval ($t_{\alpha, n-1}$) and the standard confidence interval ($I-\alpha$).

$$t_{\alpha, n-1} = \frac{(\bar{X} - X_{lower})}{s} \quad (5.13)$$

$$X_{lower} = \bar{X} - z_{\alpha/2} * s \quad (5.14)$$

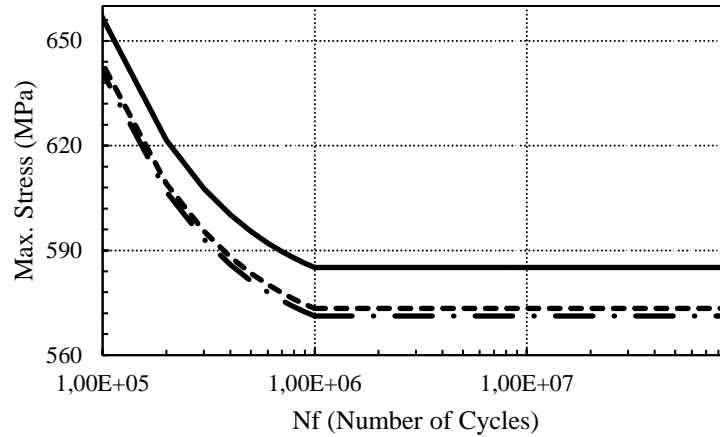


Figure 36 Mean curve with 50% probability of failure (solid line), including 95% bootstrap t-interval (dash line) and standard lower confidence limit (long dash dot)

5.2.1.4. WEIBULL METHOD

Fatigue data can be correlated to random variable function with an unknown parameter. When compared to the normal distribution, the Weibull distribution makes it easier to estimate low failure probabilities, and the 2-parameter Weibull distribution can also be used to determine the fatigue limit (in case of not used location parameter). The maximum likelihood estimator, which correlates variables with the most likely observed data, is the most used optimal technique for estimating scale (α) and shape (β ; Weibull slope) parameters. During analysis, all data (failure and runout) can be assessed, and the MLE method does not require specifying a constant stress increment. As a result, the advance of MLE is the correct treatment of censored data with any distribution.

Maximized likelihood function (L) is given below equation for staircase tests;

$$L = \prod_{i=1}^n F(S_{\alpha}^i, \{p\}) \cdot \prod_{j=1}^m [1 - F(S_{\alpha}^j, \{p\})] \quad (5.15)$$

where n and m are failed and run-out samples respectively, $\{p\}$ is the parameters defining distribution and F is the cumulative density function.

The Newton Raphson method, which is an iterative methodology for Weibull distribution function, may be used to estimate scale and shape parameters by optimizing L . As a result, α and β can be predicted using the asserted iteration approach as illustrated in Figure 37.

$$\beta_{k+1} = \beta_k - \frac{\frac{1}{\beta} + \frac{\sum_{i=1}^n \ln x_i}{n} - \frac{\sum_{i=1}^n x_i^\beta \ln x_i}{\sum_{i=1}^n x_i^\beta}}{\left(-\frac{1}{\beta^2} + \frac{(\sum_{i=1}^n x_i^\beta \ln x_i)^2}{(\sum_{i=1}^n x_i^\beta)^2} - \frac{\sum_{i=1}^n x_i^\beta (\ln x_i)^2}{\sum_{i=1}^n x_i^\beta} \right)} \quad (5.16)$$

$$\alpha = \left(\frac{\sum_{i=1}^n x_i^\beta}{n} \right)^{1/\beta} \quad (5.17)$$

$$\mu = \alpha \Gamma\left(1 + \frac{1}{\beta}\right) \quad (5.18)$$

$$\sigma = (\alpha^2 \Gamma\left(1 + \frac{2}{\beta}\right) - \mu^2)^{1/2} \quad (5.19)$$

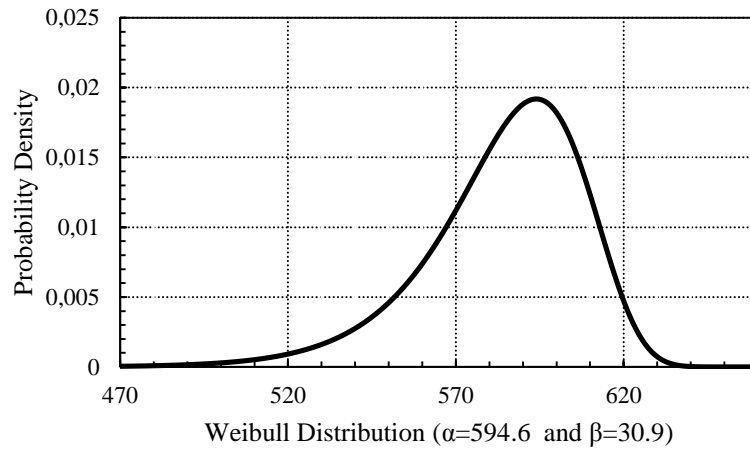


Figure 37 Weibull distribution of staircase data based on Newton Rapson technique

Mean value with 50% probability of failure (μ) and standard deviation (σ) can be calculated as 584.1 and 23.6 respectively based on Weibull distribution estimation.

5.2.1.5. JSME METHOD

The JSME (Japan Society of Mechanical Engineers) approach, which requires 14 specimens for assessment and produces the entire SN curve, is also used as a standard.

Eight of them are employed in the linear region, and six specimens are sufficient to calculate the data set's fatigue limit. The highest non-failed (run-out) data point in the data set is used as the first stress point. The rest are built using an up-and-down procedure based on past test results multiplied by a particular stress increment. By assuming that standard deviation equals stress increment, the stress increment for a staircase sequence may be calculated. The parameters (α , β) listed below are associated with the linear region.

$$\log(N) = \alpha + \beta * S \quad (5.20)$$

$$\beta = \frac{\sum_{i=1}^8 (S_i - \bar{S}) * (\log(N_i) - \log(\bar{N}))}{\sum_{i=1}^8 (S_i - \bar{S})^2}, \log(\bar{N}) = \frac{1}{8} \sum_{i=1}^8 \log(N_i) \text{ and } \bar{S} = \frac{1}{8} \sum_{i=1}^8 S_i \quad (5.21)$$

Mean (S) and standard deviation (s) can be calculated by given equations below;

$$S = \frac{1}{6} \sum_{j=2}^7 S_j \quad (5.22)$$

$$s = \frac{1}{|\beta|} \sqrt{\frac{1}{6} * \sum_{i=1}^8 (\log(N_i) - (\alpha + \beta * \log(S_i)))^2} \quad (5.23)$$

After calculation, arithmetic mean with 50% probability of failure and standard deviation were calculated as 583.3 and 26.1 respectively.

5.2.2. CURVE FITTING ANALYSIS

SN curves are created on behalf of engineering materials by linear regression of stress versus life data with a corresponding standard deviation. Curve fitting of fatigue data using goodness-of-fit is another name for this approach. For determining the fatigue life of metallic materials, the Weibull and log-normal distributions are appropriate. The fatigue limit can be computed using a statistical fatigue life model after modeling the SN curve and building design curves with an estimated confidence band.

5.2.2.1. BASQUIN METHOD

Initially, Wöhler generated an SN curve with regression variables to obtain a linear correlation between stress and fatigue life. In the finite region, the SN curve is characterized by a linear correlation between stress and life on a logarithmic scale. Later, Basquin suggested another more common approach, which relates stress as a function of life.

$$\sigma_a = \sigma_f \cdot (2N_f)^b \quad (5.24)$$

$$CoV = \sqrt{10^{b^2 s^2 - 1}} \quad (5.25)$$

The Basquin equation is based on the log-normal distribution, with σ_a , σ_f , and b representing the applied stress, fatigue strength coefficient, and fatigue strength exponent, respectively. The relationship of the fatigue strength coefficient and the standard deviation are used to calculate the coefficient of variance. The standard deviation is calculated dividing $\log(2N_f)$ by $\log(\sigma_a)$. The least square technique can be used to estimate an SN curve with finite life with 50% accuracy. As a result, the mean value for 50% probability of failure on ten million cycles (identified as the run-out criterion) and standard deviation were 592.9 and 34.7, respectively as shown in Figure 38.

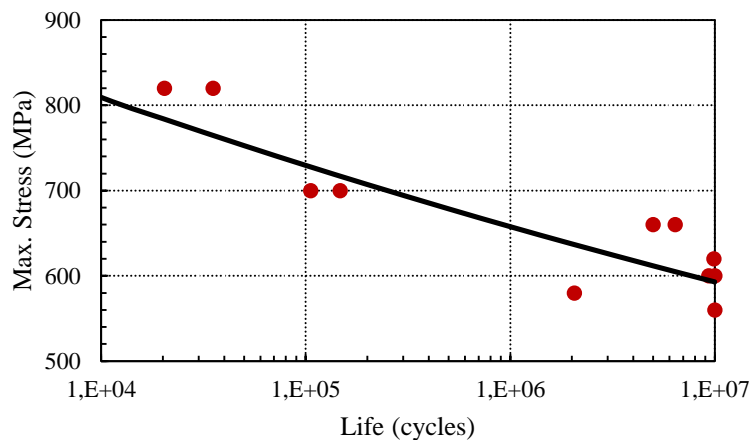


Figure 38 SN curve estimation using Basquin method

Strohmeyer proposed a new model for evaluating stress by adding a term even though there is no endurance limit at corresponding stress [169].

$$\sigma = \alpha * (N_f)^\beta + \sigma_\infty \quad (5.26)$$

where; σ : applied stress, α and β : fitting parameters, N_f : the number of cycles and σ_∞ : infinite stress.

Stromeyer's model, unlike Basquin's, is not linear based on this assumption. It is essentially smoothing linear models by including a new parameter that complicates estimation. Palmgren and Weibull later proposed new methods by including a dependent term and static stress, respectively [14]. The idea behind those methods is to provide a smoother curve with assigned fitting parameters to estimate material fatigue behavior.

5.2.2.2. ASTM E739-91 METHOD

ASTM E739-91 characterizes a linear correlation between stress and life by sizing experimental data and not extrapolating outside of data with corresponding confidence intervals. The linear relationship is established with only failed specimens and assessed on a logarithmic scale. It implies that at least 12 specimens are required to obtain reliable results for acceptable convenience.

$$\log(N) = a + b * \log(\sigma) \quad (5.27)$$

$$b = \frac{\sum_{i=1}^n (\log(\sigma_i) - \log(\bar{\sigma})) * (\log(N_i) - \log(\bar{N}))}{\sum_{i=1}^n (\log(\sigma_i) - \log(\bar{\sigma}))^2} \quad (5.28)$$

$$s = \frac{\sum_{i=1}^n (\log(N_i) - \log(\bar{N}))^2}{(n-2)} \quad (5.29)$$

The random variable in the given equation is life (N), the fitting parameters are a and b , and the independent variable is stress (σ). Finally, regression is used to ensure linear fit.

The confidence intervals for the entire SN curve are calculated for 95 % probability of failure.

$$a + b * \log(\sigma) \pm \sqrt{2 * F_p} * s * \left[\frac{1}{k} + \frac{(\log(\sigma) - \log(\bar{\sigma}))^2}{\sum_{i=1}^n (\log(\sigma_i) - \log(\bar{\sigma}))^2} \right]^{1/2} \quad (5.30)$$

where Snedecor distribution value (F_p) computed per degree of freedoms on ASTM E739-91.

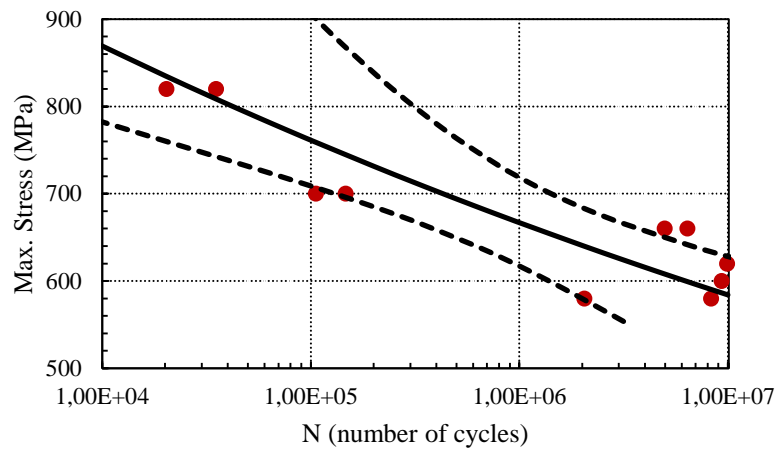


Figure 39 SN curve estimation using ASTM E731-91 method

After the calculations were implemented, the mean value for the 50% probability of failure on ten million cycles (taken as the run-out criterion) were calculated to be 584.1, and the 95% confidence intervals are displayed on Figure 39.

5.2.2.3. KIM AND ZHANG METHOD

In a different manner, Kim and Zhang introduced the new fatigue damage concept while establishing the SN curve. Hereof, the fatigue damage rate is related to the maximum stress and the defined fitting parameters. Fitting parameters can be obtained by using the best fit between damage rate and stress in logarithmic base. SN curves are estimated using

only finite data points. The damage rate ($\Delta D_{f(i)}/\Delta N_{f(i)}$) is calculated using the equation below.

$$D_f = \left(1 - \frac{S_{max}}{S_{ultimate}}\right) \quad (5.31)$$

$$\frac{\Delta D_{f(i)}}{\Delta N_{f(i)}} \approx \alpha * (S_{\max(i)})^\beta \quad (5.32)$$

where i describes each stress level on a finite region, and the average value can be used if there are multiple data points on each stress level to obtain the best fit relation. $\Delta D_{f(i)} = D_{f(i-1)} - D_{f(i)}$ for the case of $D_{f(i-1)} > D_{f(i)}$ and similarly $\Delta N_{f(i)} = N_{f(i-1)} - N_{f(i)}$ for $N_{f(i-1)} > N_{f(i)}$. To estimate fitting parameters (α and β); $\log (\Delta D_{f(i)}/\Delta N_{f(i)})$ and $\log (S_{\max(i)})$ are plotted then slope gives β value and ten to power of intercept gives α value. After calculating fitting parameters; SN curves are calculated using the equation below.

$$S_{max} = S_{ult.} * \left(\frac{\alpha * (\beta - 1) * (N_f + N_0)}{S_{ult.}^{-\beta}} + 1\right)^{\frac{1}{1-\beta}} \quad (5.33)$$

where N_0 is a fictitious value that represents the life of a material under alternating loading at S_{max} equals $S_{ult.}$. And the value ranges from zero to one. After all calculations were completed, the mean value for the 50% probability of failure on ten million cycles were 592.1 MPa, as shown in Figure 40.

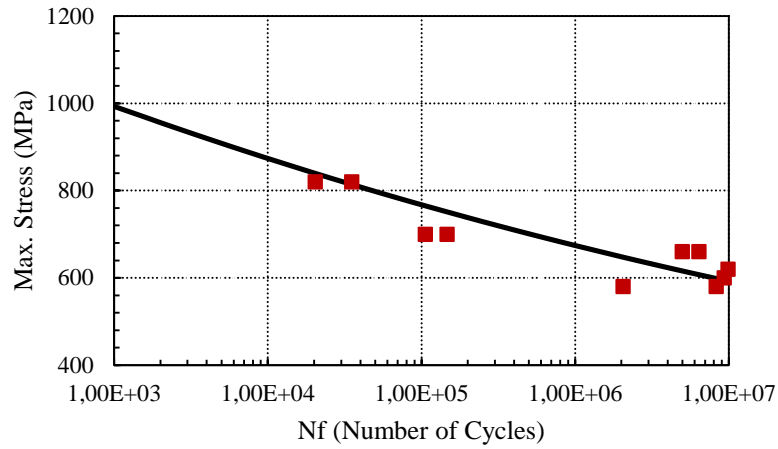


Figure 40 SN curve estimation using Kim and Zhang method

5.2.2.4. BILINEAR METHOD

The bilinear random fatigue limit model was regarded as an alternative method to the random fatigue limit method, which satisfies parameters to achieve the best fit using the maximum likelihood method. It is assumed that the SN curve is divided into two distinct regions, and the linear region can be projected using the Basquin method by implementing the number of cycles at the transition region and fatigue limit terms into the stress calculations.

$$S = -m * (\log N^* - N) + S_{limit} \quad \text{for } N < N^* \quad (5.34)$$

$$S = S_{limit} \quad \text{for } N \geq N^* \quad (5.35)$$

where m is the slope of the curve in the low cycle region and N^* is the number of transition cycles between the finite and infinite parts of the SN curve.

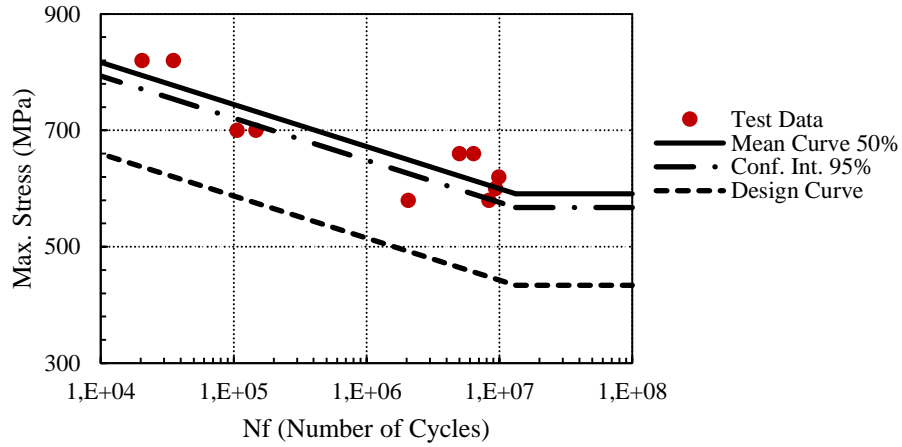


Figure 41 SN curve estimation using Bilinear method

It is generally recommended to use large amounts of experimental data to achieve desired curve fitting. As a result of the lack of a smooth transition, it is only a rough estimate of the fatigue limit with small data sets. On account of this, there is a limited relationship between high cycle and low cycle fatigue regions. According to the bilinear method, the fatigue limit value for 50% probability of failure was 592 MPa, as shown in Figure 41. As a result, regression models with strong estimation of fatigue data offer less bias.

5.2.2.5. STUSSI METHOD

Non-linear methods show unbiased estimation by regression analysis in terms of incorporating run-out data on assessed data. Stussi recommended a nonlinear model for predicting the SN curve in the low and high cycle fatigue regions by implementing tensile strength and fatigue stress at infinity into the equation [159]. This formulation is based on a log-log scale and is adapted through parameter fitting. Thereby;

$$S = \frac{R_m + \alpha * N^b * S_\infty}{1 + \alpha * N^b} \quad (5.36)$$

where R_m is the tensile strength of material, α and b are fitting variables and S_∞ is the infinite fatigue stress.

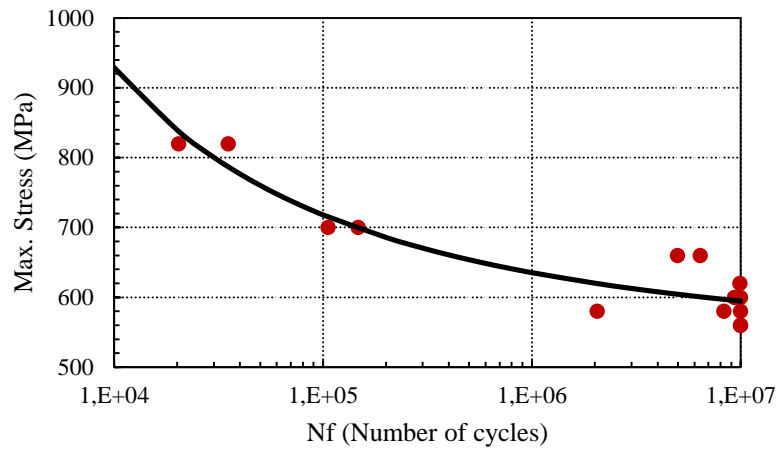


Figure 42 SN curve estimation using Stussi estimation

In comparison to the previous methods presented, this approach works well with the 3-parameter Weibull distribution and offers well-fitting not only in the endurance region but also in the low cycle fatigue region. According to this method, the mean value for the percent 50 probability of failure on ten million fatigue cycles was 594.6 MPa, as shown in Figure 42.

5.2.2.6. AGARD-AG-292 METHOD

The other method is AGARD-AG-292, a comprehensive manual for helicopter design, in which sub-chapter 4.4 describes statistical analysis of small sample sets by introducing 4 parameters regression covering censored data and taking into account constant variations of fatigue data along all regions of the SN curve. As a result, it is presumed that fatigue data is well fit by the Weibull distribution with four parameters. The regression analysis method is used to perform best fit and log scale is used to make parameters in linear form; however, increasing the number of fitting parameters increases the difficulty in calculating variables. Because the evolution of the curve outside of the data points cannot be conservative for the material's endurance limit, data must be used with a reduced curve and a confidence interval.

$$S = S_{\infty} + A * (N + B)^C \quad (5.37)$$

where S_{∞} is stress at infinite fatigue life, A , B and C are fitting variables, N is the number of fatigue cycles.

When evaluating the reduced curve, a two-sided confidence interval (value of Student variable T) can be used. As a consequence, the mean and standard deviation were evaluated assuming a normal distribution of the population. After which, T variable was estimated using the given equation;

$$\mu = \bar{x} \pm t_{\alpha} * \frac{s}{\sqrt{n-1}} \quad (5.38)$$

To evaluate 95 percent confidence interval of the distribution, SN curves were plotted for each specimen using the same fitting parameters and ensuring passing over the observed test data for corresponding specimen. Finally, the standard deviation was calculated on 1.0E+07 (the run-out criterion) using regarded stress points from each curve.

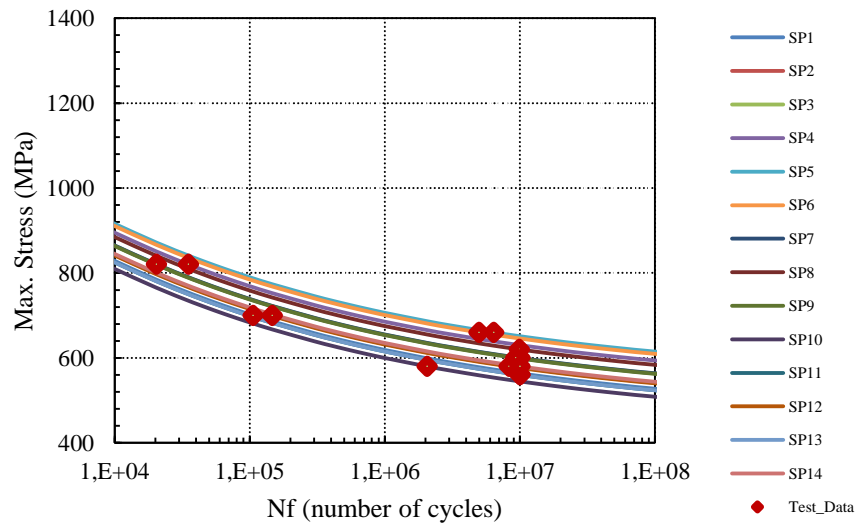


Figure 43 SN curve estimation using AGARD-AG-292 method

As a result, the mean value with a 50% probability of failure is 593.4 and the standard deviation is found as 33.3 as shown Figure 43. Using the T-variable for the 95 percent confidence interval, the fatigue limit was estimated to be 574.3 MPa.

5.2.3. FATIGUE RELIABILITY ANALYSIS

It is critical to convey accurate data without bias using theoretical data after assessment that meets the requirement of a component's intended lifetime. The term "reliability" refers to the likelihood of data not failing in real circumstances. Fatigue life is evaluated using statical evaluation to avoid fatigue failure during service with accurate estimation. There is a negative relationship between fatigue life and reliability in that reducing reliability leading to higher fatigue life, which means that probability reduces and fatigue failure variation intensifies.

In logarithmic base, the SN curve can be adapted to show a linear relationship between life and applied stress. The methodology minimizes error by adjusting estimation by using linear regression. Outliers for accurate data should be characterized after estimation of observation by determining residuals, which is the variation between test data and prediction. To keep things simple, standardized residuals are defined for each data point as the respective error (e_i) divided by an estimate of standard deviation.

$$r_i = \frac{e_i}{\sqrt{MSE(1-h_{ii})}} \quad (5.39)$$

$$MSE = \frac{1}{n} \sum_{i=1}^n e_i^2 \quad (5.40)$$

$$h_{ii} = \frac{1}{n} + \frac{(x_i - \bar{x})^2}{\sum_{i=1}^n (x_i - \bar{x})^2} \quad (5.41)$$

where r_i designates standardized residuals, h_{ii} symbolizes leverage, x_i denotes specimen fatigue life, and MSE represents mean square error. Outliers can be identified by examining residuals, and an influential point is accepted as an outlier if the standardized residuals are greater than three as an exact value. Because the presence of a potential

outlier in the data set affects the regression model and leads to biased predictor coefficients, studentized residuals are described by removing the i_{th} observation from the regression model. The formula is then as follows:

$$t_i = \frac{e_i}{\sqrt{MSE_{(i)}(1-h_{ii})}} \quad (5.42)$$

$$MSE_i = \left(MSE - \frac{e_i^2}{(1-h_{ii})(n-k-1)} \right) \frac{(n-k-1)}{(n-k-2)} \quad (5.43)$$

where k represents the number of independent variables, n denotes the number of specimens, and e_i is the difference between estimation and observed data. Figure 44 demonstrates that there are no outliers in this data set.

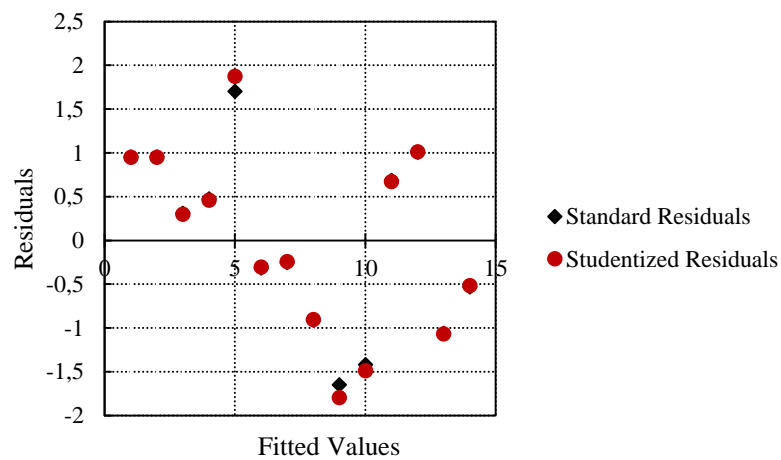


Figure 44 Comparison of standardized residual and studentized residuals

A normal probability plot can also be used to detect outliers. The points along the normal probability plot line project standard variation, but the data outside of the line is sceptical or outlier. The normal probability plot essentially displays the relative cumulative rate of fatigue data. The samples are arranged in increasing order, and the cumulative distribution function is calculated as $F(S) = [(S - \mu)/\sigma]$ where S , μ and σ represent stress in logarithmic base, mean value, and standard deviation, respectively. The probability plot is built by plotting log-stress versus $z_i = F^{-1}(p_i)$, which is the inverse function of the

cumulative distribution function. p_i is known as the plotting position, and the most common explanation proposed by Hazen [160] is as follows;

$$p_i = \frac{i-0,5}{n} \quad (5.44)$$

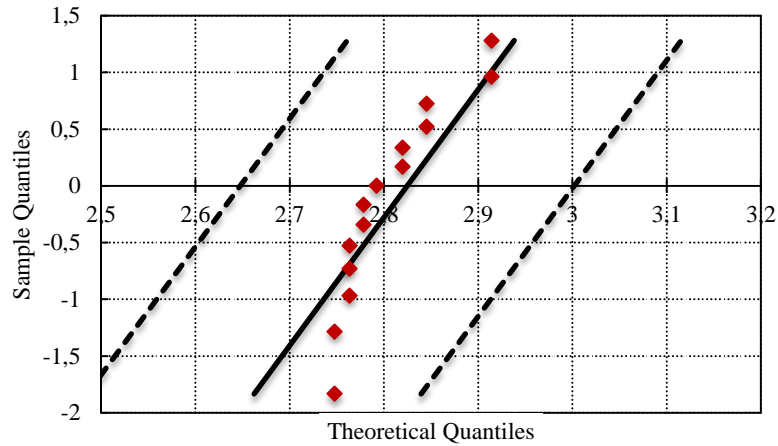


Figure 45 Normal probability plot assessment

As a result, theoretical data were presented with a 95% confidence interval, as shown in Figure 45, and no outliers are applicable for the normal probability plot.

Because of the nature of the material, fatigue data involves scatter, and the scatter band is surrounded by the confidence interval. Similarly, fatigue lifetime is outlined at a given probability of survival that specifies required service time by asserting a constant standard deviation across the entire curve. As a result, fatigue curves for a probability of survival can be established by addressing standard deviation to the Gaussian log-normal distribution in Table 5.

Table 5 Variation of probability of survival with standard deviation

Probability of Survival (%)	Standard Deviation Factor
99,9	-3
97,7	-2
84	-1
50	0
16	1
2,3	2
0,1	3

It is clear that having a higher probability of survival resulted in higher data reliability. In industrial applications, SN curves are generally associated with 97.7% probability of survival, which means that offsetting from the mean curve (50% probability of survival) by 2 times standard deviation to achieve fatigue data in a conservative manner rather than the 95 percent probability of survival stated in ASTM E739-91.

When calculating prediction of limits, 97.7% probability of survival is commonly used in design curves, which is involved with a one-sided distribution. The mean and standard deviation of the sample were expected to be the same for the entire population. As a result, a design curve was created using the Bi-linear method as an example, and a 26.5 % reduction in fatigue limit was observed, as seen in Figure 46. Similarly, reduced fatigue limit can be calculated for other methods.

$$N_{97,7} = N_{50} * 10^{-2*s} \tag{5.45}$$

where s denotes the standard deviation and N_{50} indicates the working curve's life at the corresponding stress range.

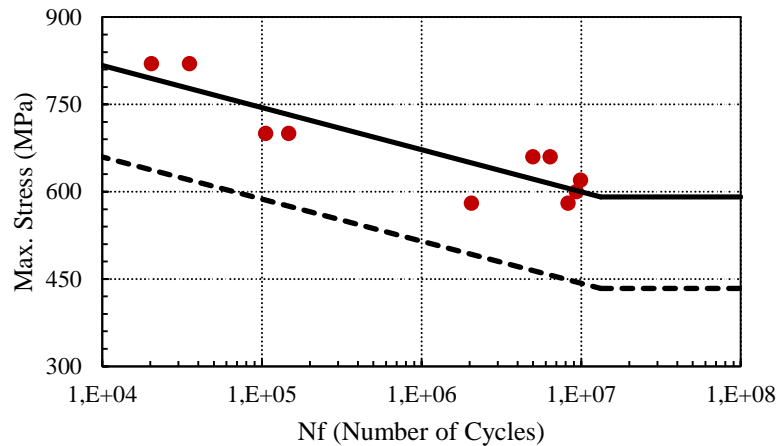


Figure 46 SN curve estimation with probability of failure using Bilinear method

5.2.4. FATIGUE LIMIT EVALUATION

Because of the material's cyclic plasticity and isotropic properties, fatigue damage in metals usually begins on the surface and propagates perpendicular to the applied load. The fatigue mechanism underlying crack initiation is a surface phenomenon, whereas propagation is a bulk phenomenon. Because the fatigue limit, as clarified by the SN curve, acts as a threshold below which crack initiation occurs, it is associated with the crack initiation phenomenon. Because of the randomly distributed nature of fatigue data, determining the fatigue limit of a material is effectively impossible; however, the distribution of fatigue limit with correct bias can be approximated. To achieve a good estimate of the mean value with a very small interval, large specimens must be handled while determining the fatigue limit of the material; conversely, the evaluation will be biased if small samples are used. Nonetheless, provided methodologies have been suggested to improve the accuracy of results with a smaller number of specimens. Mainly, staircase methods are simple to use when evaluating the mean value of a data set with a 50% probability of failure; conversely, standard deviation is challenged due to the small

data set and must be greatly decreased with a safety factor to obtain a conservative value. Various methods were used to analyze staircase test results, such as determining distribution parameters that maximize the probability of test data. When compared to the other methods, the Maximum Likelihood Estimation (MLE) method is the most accurate method in terms of estimation, with the lowest standard deviation. When compared to normal approximated intervals for staircase methods, MLE usage provides a higher confidence level to nominal ones. It is recommended to choose stress increments between 0.5 and 1.5 when handling the staircase because small intervals result in waste occurrences while increasing stress intervals results in lower precision of mean. The Bootstrapping method produced too small a standard deviation around the mean, implying a lower frequency of occurrence and a lack of optimal confidence intervals. Because the IABG method omits the first specimen's test results during analysis, a smaller sample size has been used with bias correction than the Dixon-Mood method. In addition, the Weibull distribution produced more accurate standard deviation determination than the Dixon-Mood method. Even so, the Dixon-Mood method provides excellent results when the data set has a very large coefficient of variance. While ASTM E739 is recommended for metallic materials with efficiency in the medium and high cycle regions, Stussi is also applicable in the low cycle fatigue region.

In industrial applications, it is assumed that fatigue strength and respective life guide a log-normal or Weibull distribution; thus, linear regression was used to identify the SN curve, which also makes it possible for the estimation of the fatigue limit. Curve fitting methods were used to optimize fitting variables in the correlation between fatigue life and stress. By increasing the number of parameters to boost the adaptability of the approach, attempting to solve the equation becomes more challenging due to the increased iterative process by least square method and requires the time and energy. Regression analysis produces a mean value with a 50% probability of failure, and the data must be reduced with an identified probability of survival and confidence interval for the generated design data. If the provided distribution does not fit the data exactly, the reliability assessment

will be inaccurate. Because of limited functionality in the case of adding ultimate strength of data as an input, the Basquin equation evaluated poorly, whereas regression models give good estimation with correlation. For materials with a sharp transition between infinite and finite regions and reasonably consistent scatter through the SN curve, a bilinear model can be preferred. Other approaches performed better in the medium and high cycle fatigue regions. Because of the lack of data on the low cycle fatigue region, Kim and Zhang approach was found a high covariance, implying that this method is better suited for stress levels greater than four on a finite region. Nonetheless, the predicted fatigue limit data was in reasonable agreement with the observed data.

Scatter band is impacted by nonuniform defect size in material microstructure, production, environment, operator, and test specimen misalignment on test machine. In general, scatter is expected to be greater in the low cycle fatigue region of the SN curve and lower in the infinite region. The probability distribution of fatigue specimens was investigated in order to evaluate reliability. There is an inverse relationship between fatigue life and reliability; higher fatigue life diminishes fatigue reliability. For reliable data in structural design, residual model is required after estimating fatigue data in terms of stress and life relation. Outliers can be identified at this point in order to reveal more accurate data by using the standard deviation for the normal probability plot and standard/studentized residuals, which are determined by least square estimation based on minimizing the sum of squared deviations. For this data analysis, the significance level was set at 0.05, indicating a 5% risk of missing data, and the confidence level and probability of survival for fatigue lifetime were calculated to be 95% and 97.7%, respectively.

In this study, the endurance limit of AISI 4340 steel with tempered heat treatment condition was determined using the staircase and curve fitting methods, and the results are summarized in Table 6.

Table 6 Different Approaches to determine fatigue limit of material

	Method	Formula	Fatigue Limit (MPa)	St. Dev.
Staircase	Dixon-Mood	$S = S_0 + d * \left(\frac{A}{F} - \frac{1}{2}\right)$ when less event failure $S = S_0 + d * \left(\frac{A}{F} + \frac{1}{2}\right)$ when less event run-outs	585.0	31.7
	IABG	$\log(S) = \log(S_0) + \log(d) * \frac{A}{F}$	585.1	14.5
	Bootstrapping	$\bar{X} = \frac{1}{B} \sum_{i=1}^B X_i^*$	585.1	7.1
	Weibull	$\mu = \alpha \Gamma\left(1 + \frac{1}{\beta}\right)$	584.1	23.6
	JSME	$S = \frac{1}{6} \sum_{j=2}^7 S_j$	583.3	26.0
Curve Fitting	Basquin	$\sigma_a = \sigma_f \cdot (2N_f)^b$	592.9	34.7
	ASTM E739-91	$\log(N) = a + b * \log(\sigma)$	584.1	43.9
	Kim and Zhang	$S_{max} = S_{ult.} * \left(\frac{\alpha * (\beta - 1) * (N_f + N_0)}{S_{ult.}^{-\beta}} + 1\right)^{\frac{1}{1-\beta}}$	592.1	57.2
	Bilinear	$S = -m * (\log N^* - N) + S_{limit}$ for $N < N^*$ $S = S_{limit}$ for $N < N^*$	591.0	40.6
	Stussi	$S = \frac{R_m + \alpha * N^b * S_{\infty}}{1 + \alpha * N^b}$	594.6	32.1
	AGARD-AG-292	$S = \frac{R_m + \alpha * N^b * S_{\infty}}{1 + \alpha * N^b}$	593.4	33.3

To eligible to apply fatigue test data providing after coupon tests, design curves must be established using a reduction factor to reveal conservative data, as illustrated in Figure 47. As a result, the probabilistic origin of fatigue data can be accurately determined by accounting for scatter effects.

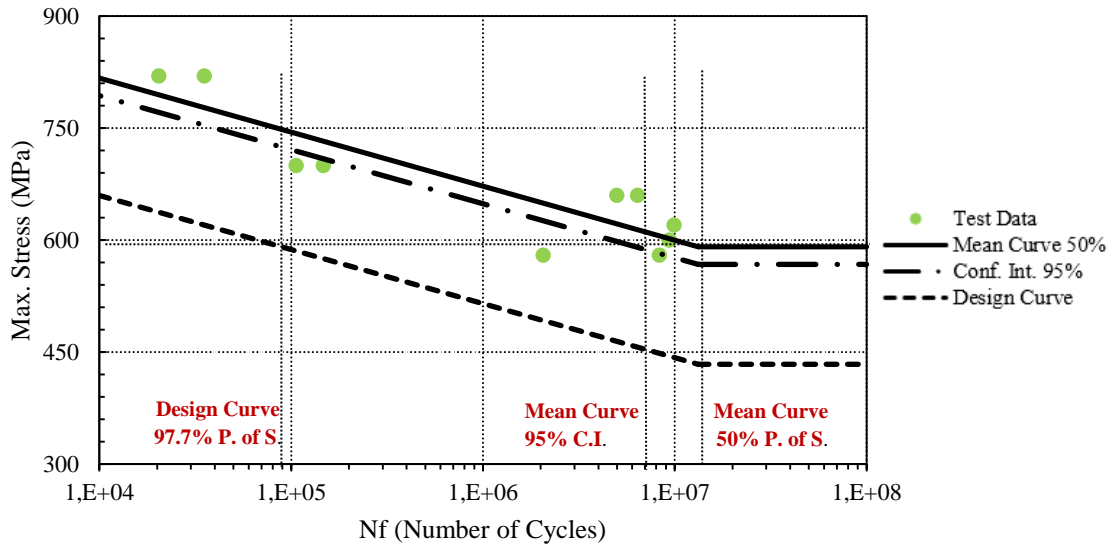


Figure 47 Alteration in the design curve as a result of probabilistic analysis (C.I.: Confidence Interval, P. of S.: Probability of Survival)

5.2.5. FATIGUE LIMIT CORRELATION

Rather than running new test sets for different heat treatment conditions, a functional correlation between endurance limit and hardness can be developed. For steels, hardness has a linear relationship with fatigue limit [161]. Steels with hardness values less than 500 Brinell hardness show relative variation in terms of endurance limit and stress amplitude versus fatigue life on a logarithmic scale, as shown in Figure 48.

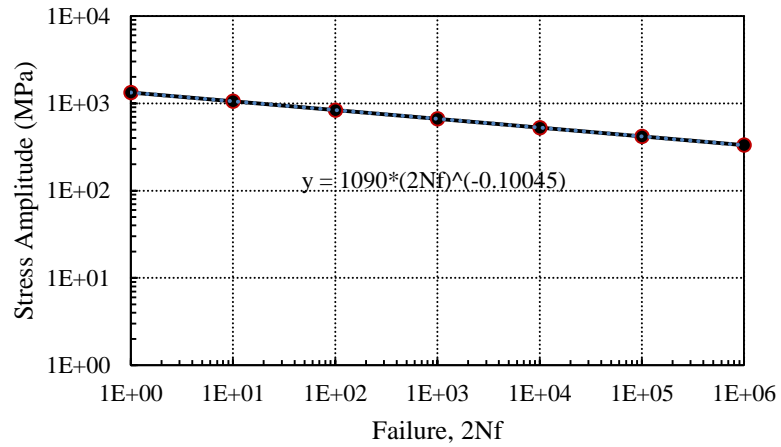


Figure 48 Variation of stress amplitude and failure cycle

The following equation [162] model the relationship between ultimate and oscillatory stress.

$$\frac{\Delta\sigma}{2} = (S_u + 345) * (2N_f)^b \quad (5.46)$$

where $\Delta\sigma/2$ denotes stress amplitude, S_u symbolizes ultimate stress, N_f indicates failure cycle, and b indicates fatigue strength exponent. As shown in Figure 49, the corresponding endurance limit for similar material with known hardness value can be correlated by estimating the stress amplitude.

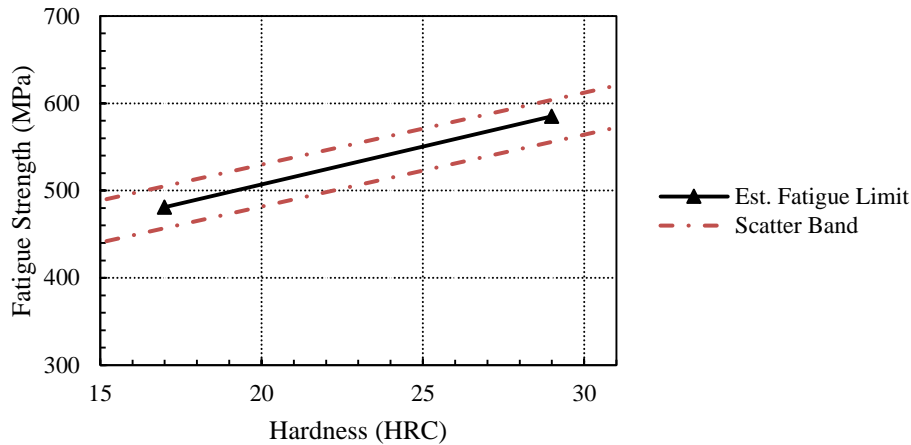


Figure 49 Variation of endurance limit and hardness

As a result, fatigue limit of AISI 4340 can be estimated as 481 MPa for annealed condition with 17 HRC hardness value under R of 0.1 loading condition.

5.3. CRACK GROWTH TEST RESULTS

Fatigue limit can be described as material resistance in terms of nucleated crack growth. On the other hand, relating threshold stress for fatigue limit needs to overcome microstructural obstacles for crack growth process. As a result, the fatigue limit is summarily related to microstructure characteristics such as grain dimensions at the onset of fatigue initiation and the initial growth phase is also known as the microstructural threshold. Controlling the microstructure of a material by heat treatment allows for advanced fatigue properties as well as transcendent mechanical properties.

Crack growth test specimens were produced from AISI 4340 steel with annealed and tempered conditions to investigate the crack propagation behavior of the steel, which has high toughness and fatigue performance, make it a great candidate for aerospace quality steel. Crack propagation tests were performed in accordance with ASTM E-647 under laboratory conditions (23 ± 2 °C and 50 ± 5 % RH). Specimens were cyclically loaded on

the RUMUL cracktronic test system with different stress ratios using an exciting sinusoidal wave form at an 80 Hz test frequency.

Determining the long crack threshold as a selection criterion after crack growth tests is not a distinctive research topic; nevertheless, some discrepancies in the literature due to diverse testing procedures keep it vogueish. For structural components with small crack sizes, inaccurate assessments may lead to substantial variation in the associated endurance stress. In comparison to traditional approaches, an acknowledged approach is to apply compression-compression precracking before crack propagation tests, thereby history effects can be eliminated and long crack threshold value can be precisely estimated. Load history effects may occur as a result of the specimen configuration and test procedure used. The magnitude of yielding during precracking should not be ignored, and residual stresses have an effect on crack growth rates, even if they are limited by stress relief in the plastic region. Naturally formed precrack grows until the size of the associated tensile zone responsible for crack growth decreases.

5.3.1. COMPLIANCE METHOD

Crack length can be measured using a variety of techniques, including compliance, potential drop, laser interferometry, and ultrasonic isoscanning. Among these, the compliance technique is the most commonly used method for estimating crack length. By analyzing load and displacement data to assess crack propagation, the compliance method is applicable to isotropic materials such as metals that reflect linear elastic behavior. The basic idea behind this approach is based on the idea that stiffness decreases as crack length on a specimen grows. As a result, the calibration curve reflects the relationship between crack length and compliance. The compliance method is implemented for a narrow range of normalized crack size. It is also referred to as specimen elastic compliance due to the introduction of an unloading portion of the elastic-plastic range, and it is a function of crack length. As a result, the compliance value varies by changing the crack length, which is inversely proportional to the specimen size.

The fatigue crack closure mechanism is based on steadily closing from the crack tip, leading to plasticity induced crack closure that adjusts compliance uniformly on the load-displacement curve. Friction caused by mating surfaces and plastic deformation cause hysteresis on the compliance curve, therefore determining the opening stress makes more difficult. The load ratio effect on fatigue crack growth can be substantially reduced by implementing K_{eff} rather than using K and R (load ratio) together. As is well known, the main mechanism for having different crack growth rates under various load ratios is plasticity-induced crack closure. It was discovered that the moment a crack opens causes a change in compliance measured data.

The compliance method is appropriate for monitoring the crack length of structures subjected to cyclic loading. It produces a justified opening stress value from the load-displacement curve in the range of 0.3 to 0.65 times the sample width in terms of crack length. For constant amplitude loading conditions, the following expression [52] can be used to approximate opening stress:

$$\frac{S_0}{S_{max}} = A_0 + A_1 * R + A_2 * R^2 + A_3 * R^3 \quad \text{for } R \geq 0 \quad (5.47)$$

$$\frac{S_0}{S_{max}} = A_0 + A_1 * R \quad \text{for } -1 \leq R < 0 \quad (5.48)$$

$$A_0 = (0.825 - 0.34 * a + 0.05 * a^2) [\cos(\pi * S_{max}/2\sigma_0)]^{1/a} \quad (5.48)$$

$$A_1 = (0.415 - 0.071 * a) * (S_{max}/\sigma_0) \quad (5.49)$$

$$A_2 = 1 - A_0 - A_1 - A_3 \quad (5.50)$$

$$A_3 = 2A_0 + A_1 - 1 \quad (5.51)$$

where σ_0 is the flow stress, S_0 is the opening stress, S_{max} is the maximum applied stress, R is the stress ratio, a is the constraint factor, and A_0, A_1, A_2 and A_3 are the coefficients.

To determine the stress state prior to the crack tip, the constraint factor must be outlined. Related factor is 1 for plain stress conditions and 3 for plain strain conditions. Variation

of opening stress with stress ratio can be seen on Figure 50, Figure 51 and Figure 52 when constraint factor is equal to 1, 3 and $S_{max}/\sigma_0=1/3$ respectively.

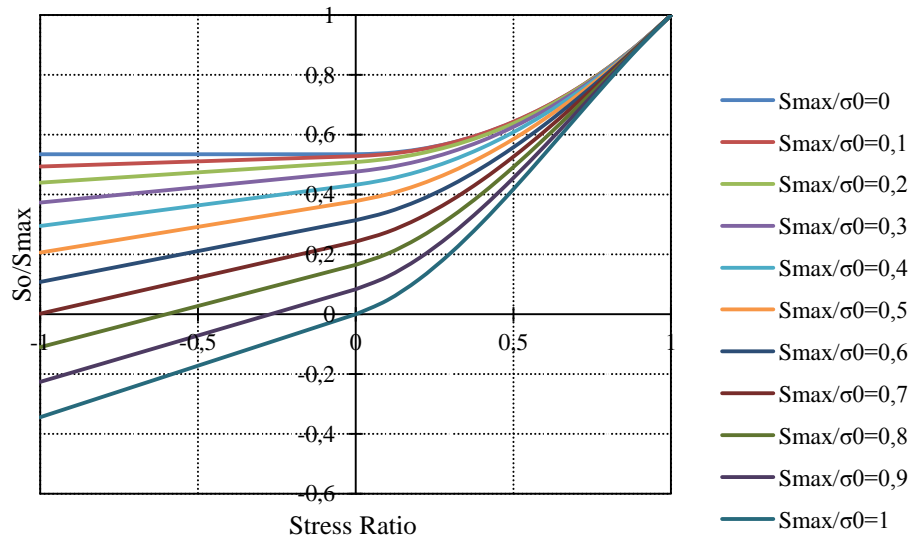


Figure 50 Normalized crack opening stress varies with stress ratio in case of constraint factor is equal to 1

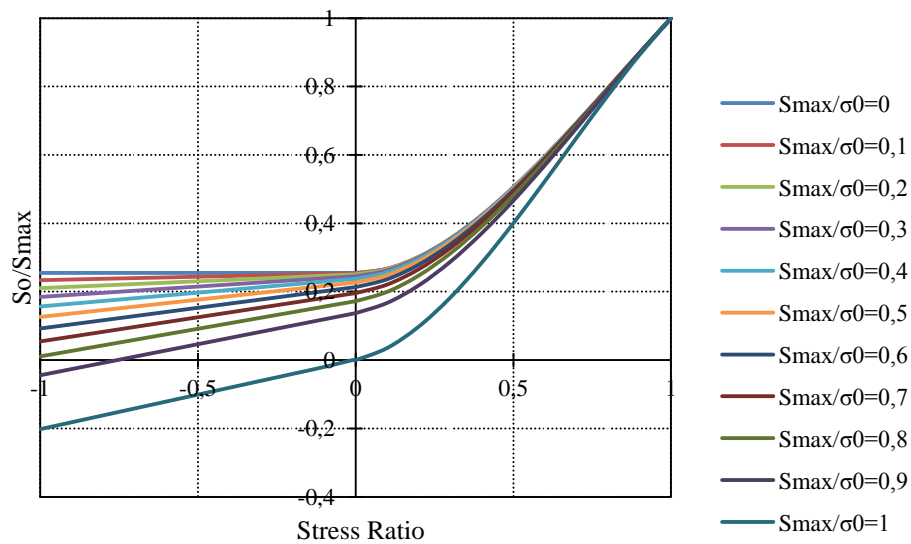


Figure 51 Normalized crack opening stress varies with stress ratio in case of constraint factor is equal to 3

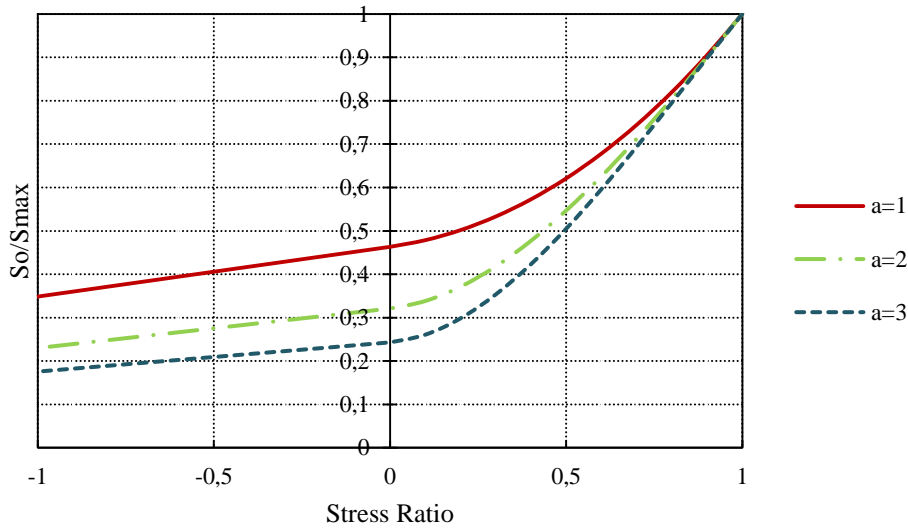


Figure 52 Normalized crack opening stress varies with stress ratio in case of $S_{max}/\sigma_0=1/3$

As shown in the Figure 52, normalized crack opening stress, independent of stress ratio, decreases with increasing constraint factor.

Identifying compliance by elastic unloading was suggested by Clarke [163] in order to measure crack length and plastic work component ahead of crack tip. Compliance can also be referred to as the inverse stiffness function of crack length. As a result, the relationship between crack length and compliance is expressed in terms following equation:

$$EBC = f\left(\frac{a}{w}\right) \quad (5.52)$$

where E is the elastic modulus of the material, B is the thickness, C is the compliance, w is the width, and a is the crack size

If the normalized crack size (a/w) for SEB specimens is between 0.05 and 0.45, the following equations can be used for specimens with shallow cracks [164]. Least square polynomial regression is used to accomplish this correlation.

$$\frac{a}{w} = 1.01878 - 4.5367 * u + 9.0101 * u^2 - 27.333 * u^3 + 74.4 * u^4 - 71.489 * u^5 \quad (5.53)$$

$$u = \frac{1}{\sqrt{\frac{BWCE}{S/4} + 1}} \quad (5.54)$$

where u is dimensionless compliance and S is span length of specimen.

During the tests, crack sizes were monitored at regular intervals and their relationship with the compliance term was investigated, as shown in Figure 53.

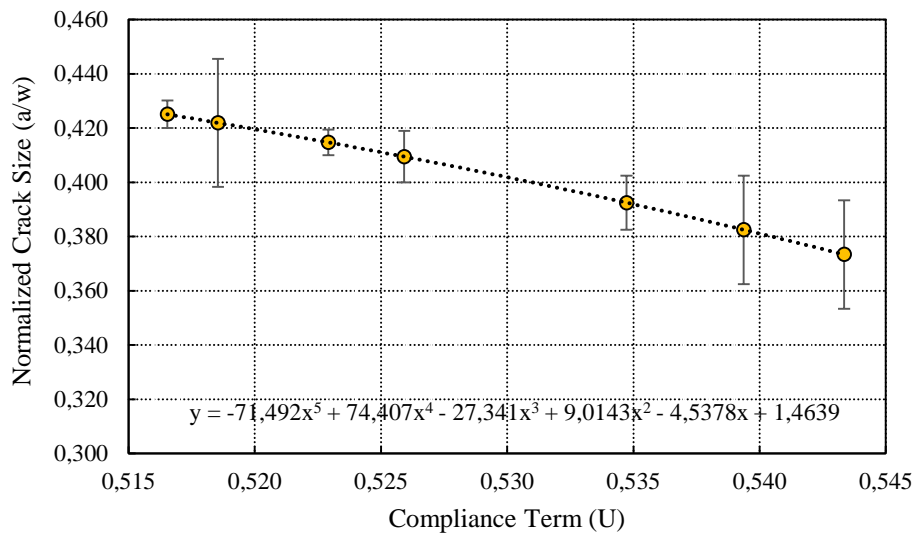


Figure 53 Evaluation of crack Size by compliance method

Compliance measurements were taken on an unloaded specimen to avoid errors caused by inelastic strains when calculating the slope of displacement versus load data. Compliance can also be identified as the inverse stiffness of a material, and the relevant data has nonlinear behavior at maximum and minimum values. As a result, 10% of the upper and lower parts of the curve were skipped to avoid nonlinear effects, and the slope was calculated using least square regression fits on the unloading part of the curve. The commonly accepted method is to use the fifth order polynomial fit proposed by Hudak and Saxena [86]. Despite the fact that compliance change may not be observed at high

stress intensity factors due to stabilized cracks, compliance variation can be obtained at low stress intensity factors, particularly near thresholds.

A sampling rate of 100 data pairs per cycle is required to acquire a correct compliance value. The unloading part, which consists of 50 data pairs, is used to predict opening stress. To calculate opening stress, the fully open crack slope value is first decided using least squares. To decide compliance value, the ASTM method employs the least square fit on the upper part of the load-displacement curve, which is in the range of about 25% as illustrated in Figure 54.

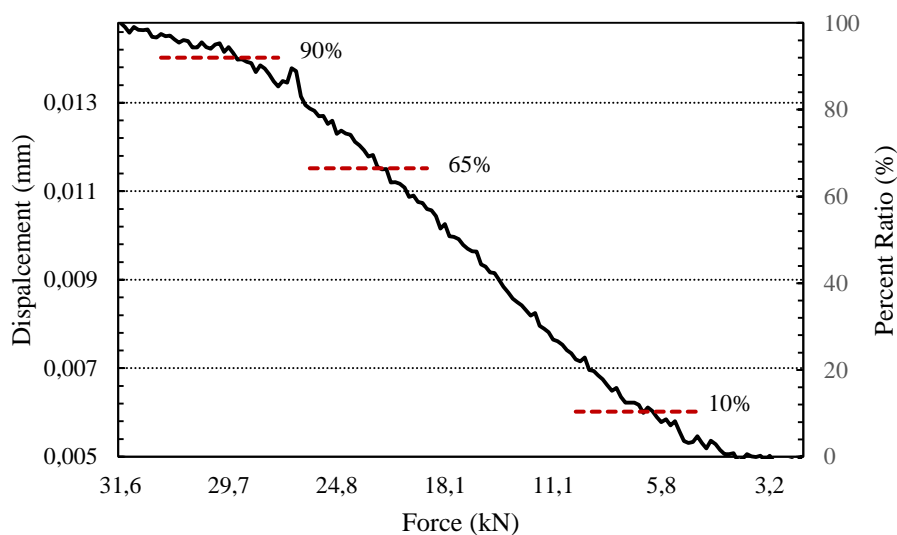


Figure 54 Unloading part of load-displacement curve

By establishing a loading segment and an overlapping range, the compliance offset method was used to calculate opening stress. In this study, a loading segment was designated as 10% sliding on a fully open part, with a 5% overlapping range between each segment, and variation from this slope gives opening stress by implementing a specific deviation on slope value. This deviation varies with sampling rate, so a higher sampling rate yields more consistent results.

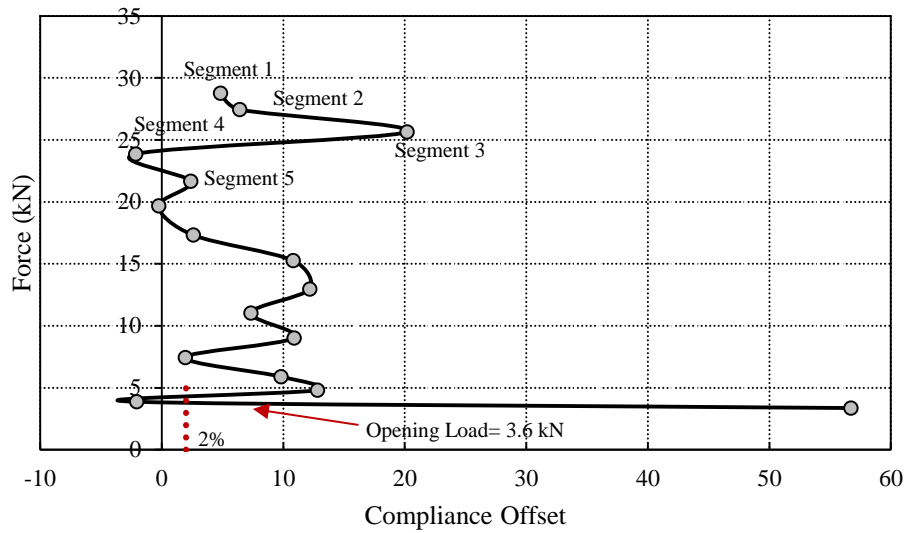


Figure 55 Compliance offset method

The scattering in the data resulted in high variability in the compliance offset data; however, the opening load can be found as 3.6 kN per ASTM assumption of 2 percent deviation shown in Figure 55.

Despite the fact that compliance change may not be observed at high stress intensity factors due to stabilized cracks, compliance variation can be achieved at low stress intensity factors, particularly near thresholds. Compliance measurements were taken throughout the threshold tests, and Figure 56 depicts the variation of crack size with compliance.

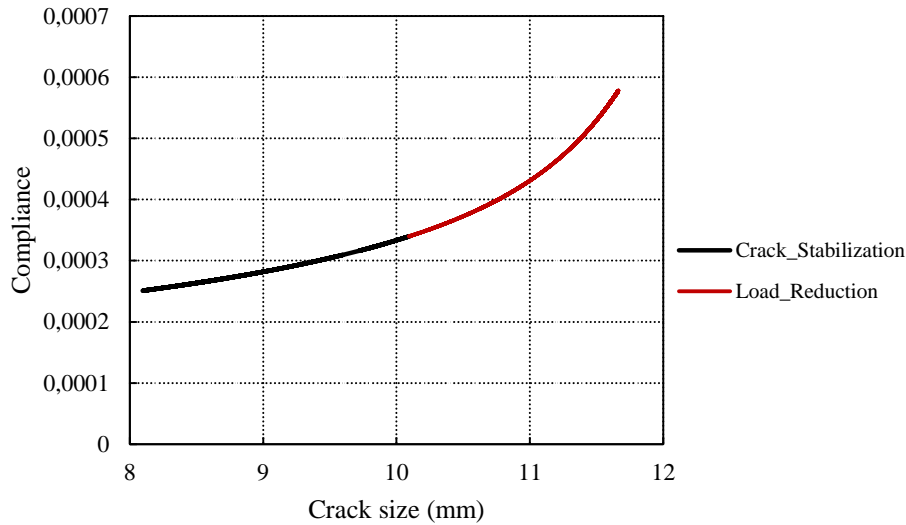


Figure 56 Compliance change with increasing crack size during each phase of test

5.3.1.1. COMPLIANCE EVALUATION

The precision of compliance verifies a correct correlation about crack closure responsible for stress ratio impact on fatigue crack growth rate, which reveals effective stress intensity factor. In small crack length circumstances, the compliance value increases as the load increases, whereas at larger crack lengths, the compliance begins to diverge. Due to hysteresis and measurement noise on data, determining opening stress using the compliance method is difficult and confusing. Compliance variation is caused by changes in crack size, which alters the contacted region, as well as changes in the size of the plastic zone. It is broadly acknowledged that using a 2 percent deviation from the compliance offset yields reasonable results. More than 3% deviation on the load displacement curve can be associated to crack opening stress using the compliance method. Opening stress can be calculated taking into account a 1.5 percent offset on the load-displacement curve. When the total variation of the load displacement curve is very small; in other words, when the slope change is not easily visible, determining the opening stress can be difficult and results in a large scatter. In such cases, an ASTM compliance offset of 2% results in

a lower opening stress value when compared to a larger variation of compliance instances with a clearly different slope change. A tendency for a larger deviation, such as 10% on the compliance offset value, results in less scatter on the data but shifts the effective stress intensity curve to higher values. ASTM is recognized as a compliance offset method, among others. However, the method's drawback is that its lack of precision results in a high scatter on compliance measurements.

Crack closure becomes stabilized as it grows from a small to a long crack, and it increases as the crack length increases until it reaches a steady state. Closure in terms of crack wake plasticity is increased in this region, but its influence decreases as effective stress increases. The existence of crack closure allows for contact of crack flakes during unloading, resulting in a change in slope on the compliance curve. By increasing the load ratio for long cracks, the crack closure effects reduce when R of 0.7 condition is reached. Crack closure for small cracks gradually increases as crack size increases, implying that the threshold stress for small cracks increases until a certain value is reached at which point the small crack approaches the length of a long crack.

5.3.2. COMPRESSION PRECRACKING

Compression precracking is a technique that provides fatigue crack growth data by minimizing the effects of load history. Load history effects caused by test procedure, specimen size, and test configuration are the most common causes of misleading threshold values. Remote closure occurs when precracking loading is applied at a higher level, reducing driving force and resulting in a higher threshold value. The benefit of compression precracking is that stress intensity is under zero while the crack is closing during the pre-cracking period, so the crack will open straightforwardly and will not be influenced by load histories under constant amplitude fatigue crack growth testing. During compression precracking, a monotonic compressive zone develops after the first static loading case, and tensile yielding ahead of the notch occurs after unloading, followed by the formation of a tensile plastic zone within the compressive zone. As

fatigue testing progresses, a cyclic plastic zone forms, resulting in small scale yielding and crack propagation. As the crack propagates, residual stress relaxes and the size of the cyclic plastic zone decreases. It proceeds until the crack reaches a monotonic compressive zone size, at which point it is stopped due to the decline in the driving force for crack propagation. The benefit of compression precracking is that it provides a fully open crack, which resolves the possibility of crack closure effects, resulting in lower crack growth rates at low stress intensities. Crack growth rate near the threshold is affected by increased stress intensity caused by crack propagation and advancing threshold due to arising crack closure effects. After a certain length of propagation near the threshold value, crack closure makes slower and an increase in stress intensity results crack extension irruptively.

Razor blade operation was used to concentrate stress around the crack tip prior to compression precracking. Due to the small plastic deformation for precracking, razor blades are welcomed as a useful method for forming sharp cracks around 20 μm . Following EDM notch preparation, the notch is sharpened with a razor blade via 1 μm diamond paste. For accurate dimensions, an EDM notch is machined with 30 μm wires in diameter. Precracking tests were performed using constant amplitude under compressive loading, which allows for tensile yield ahead of the crack tip, and this tensile zone is responsible for straight and natural cracks. Because of the relaxation of internal stresses caused by fatigue crack growth, the tensile cyclic plastic zone decreases and the crack stops after reaching the monotonic compressive zone. The amount of crack propagation for precracking can be strongly associated with the size of the compressive plastic zone.

Because there is no supplied driving force, an arrested crack is referred to as a non-propagating crack under compressive loading. Compressive precracking tests were carried out at stress ratios (R) of 10, 20, and 40 on an RUMUL resonant fatigue test system using a four-point bending setup under constant ΔK for each case. The test loads were calculated using the Irwin plastic zone assumption. For compression precracking tests, the lower and upper roller distances were configured as 24 mm in each case, and the

oscillating load was calculated to be 20 kN. As the stress ratio increases, the maximum force converges to zero and the minimum force converges to -20 kN in the case of a predetermined 10 kN amplitude loading condition, as shown in Figure 57. In other words, beyond a certain stress ratio, fatigue crack threshold values for compression precracked specimens especially with a higher stress ratio converge to close threshold values. As a result, R of 40 for compression precracking was chosen as the highest stress ratio because the threshold values for higher stress ratios will give similar results.

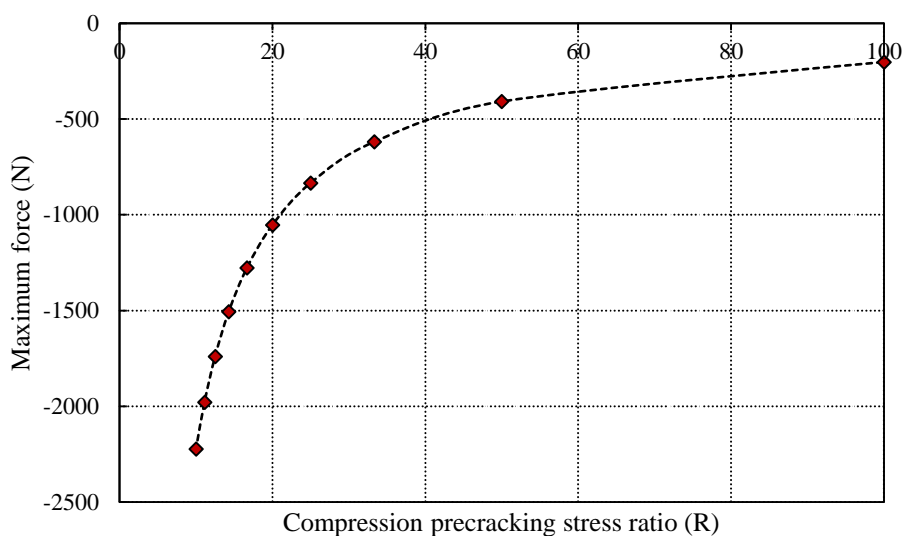


Figure 57 Variation of maximum compression precracking force with stress ratio

Three specimens were alternatively loaded under different stress ratios to examine the effect of compression precracking on the near threshold regime, as shown in Figure 58, and one specimen was not precracked for comparison. The compression precracking loading is calculated using an Irwin tip radius of 0.25 mm over plain stress condition. Following cyclic loading, the cyclic plastic zone size decreases due to the relationship of residual stresses, resulting in a decrease in driving force for crack growth and crack arrests around the monotonic compressive zone.

$$r_p, \text{ Plain Stress} = \left(\frac{1}{2\pi}\right) \left(\frac{K_{max}}{\sigma_y}\right)^2 \quad (5.55)$$

where r_p is Irwin radius, K_{max} is maximum stress intensity factor and σ_y is yield strength of material. The following equations can be used to calculate K_{max} .

$$K_{max} = \left(\frac{Y * M_{max}}{B * \sqrt{(W)^3}}\right) \quad (5.56)$$

$$Y_{SEB} = 6 * \left(\frac{\sqrt{\left(2 * \tan\left(\frac{a}{W}\right)\right)}}{\cos\left(\frac{a}{W}\right)}\right) * \left(0,923 + 0,199 * \left(1 - \sin\left(\frac{a}{W}\right)\right)^4\right) \quad (5.57)$$

where M_{max} is the maximum moment, B and W are the thickness and width of the specimens respectively, Y is the geometry factor, a is the crack size of the specimen including the notch length.

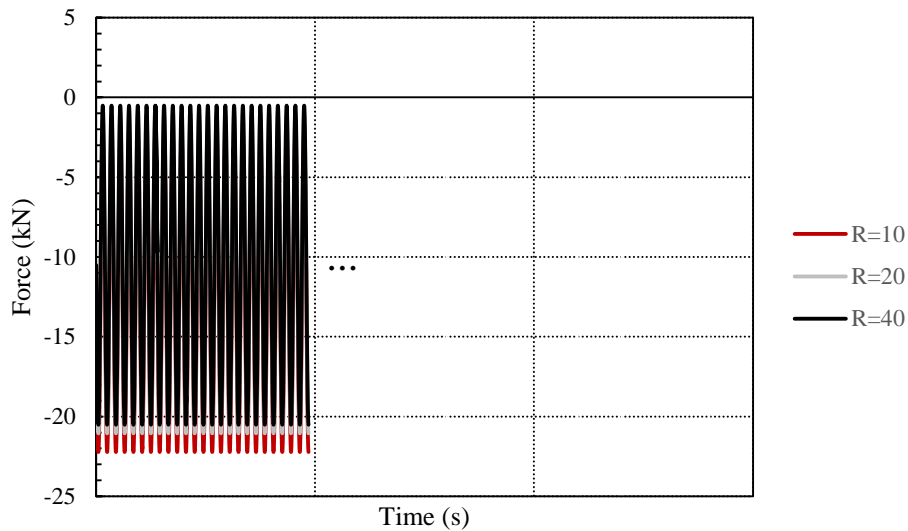


Figure 58 Load profiles for different stress ratios under of compression-compression precracking test

Compression precracking tests were progressed until two million cycles, at which point the non-propagating crack was measured using an optical microscope on each side

of specimen, as shown in Figure 59. To achieve steady state crack growth conditions after compression precracking, a non-propagating crack must progress at least three monotonic compressive zone sizes. The non-propagating crack size was around 0.2 mm or less, and precracking size is identified to be less than the cyclic tensile zone comprised of after unloading. To obtain accurate fatigue crack growth data, the precracking size must be outside of the monotonic compressive zone by establishing small scale yielding ahead of the crack tip. This is accomplished by tensile fatigue loading after compression precracking in order to be residual stress free. After determining optimized stress ratio for compression precracking, rest of the specimens were precracked under R of 40 loading condition.

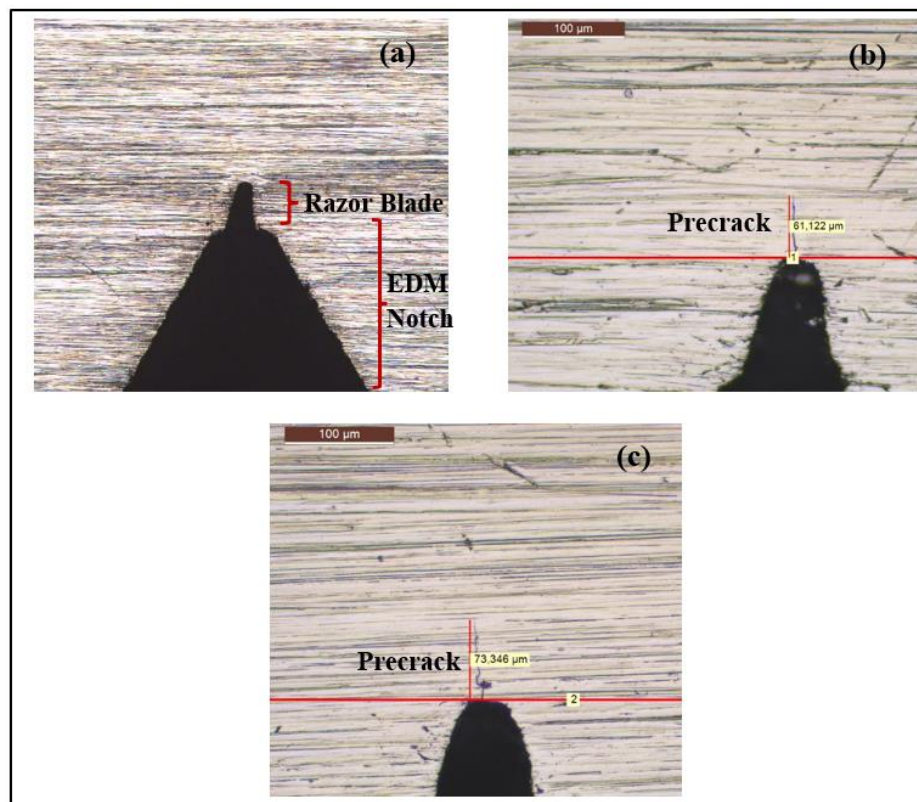


Figure 59 Non propagating crack formation after compression precracking: a) Razor blade application prior to precracking b) Front side micrograph c) Back side after formation of non-propagating crack

5.3.2.1. PRECRACKING EVALUATION

Compression precracking prior to crack growth tests results in faster crack growth rates than the load reduction procedure, resulting in a lower threshold value. Under the load reduction scenario, initial ΔK has an effect on threshold values. Natural crack, on the other hand, will form and be fully open following compression precracking and reach a steady state under constant amplitude loading. As a result, obtaining a stabilized crack before load reduction approaches crack growth to effective stress intensity and minimizes deviation around the threshold. Because of the challenges in controlling crack growth and maintaining a sufficient crack length with tensile-tensile precracking, compression precracking is advisable. The productivity of precracking is affected by grain boundary orientation in terms of aligned and elongated grains. It is preferable to use a low ΔK for precracking in order to reduce tensile residual stresses. Under cyclic compression, small scale yielding occurs ahead of the crack tip front after precracking. Non-propagating crack size is around 0.2 mm or greater, and precracking size is known to be less than the cyclic tensile zone consisting of after unloading. To achieve reliable fatigue crack growth data, the precracking size must be outside of the monotonic compressive zone by establishing small scale yielding ahead of the crack tip. This is accomplished by tensile fatigue loading after compression precracking in order to be residual stress free. Long cracks must be fully opened in the steady-state region before load reduction can be practiced to ensure an accurate threshold value by guaranteeing fatigue crack growth tests are conducted with residual stresses eliminated. Although compression precracking reduces load history effects, crack propagation is intended to ensure that closure effects are eliminated. Because of the roughness and oxide induced crack closure that is responsible for observing the rough crack flank, the ASTM E-647 load reduction procedure has a low crack growth rate and a high threshold value. To reduce residual stress effects ahead of the crack tip, the precracking stress value should be as low as possible.

The following condition must be met for crack growth to occur: Loading applied is greater than $K_{max,th}$ and K_{th} . Long crack threshold value is a property of a material that is unaffected by crack size or specimen geometry. On the other hand, small cracks propagate on regions with in-situ or pre-existing stress concentrations caused by slip bands, dislocation pile-up, or existing defects. Cyclic deformation causes fatigue damage through dislocation pile-up and the formation of persistent slip bands, presenting an available condition for the initiation phase of a crack. Short crack behavior can be explained as crack length dependence, higher crack growth rates, propagation even below long crack threshold value, and threshold variations with crack size.

Cracks may not be formed at the maximum allowable crack growth rates on load reduction stage for AISI 4340 steels; however, precracking allows for crack initiation around K_{th} by eliminating load history effects. Despite the fact that compression precracking is thought to provide more reliable fatigue crack growth data with less load history effects than traditional methods. To accomplish steady state crack growth conditions after compression precracking, a non-propagating crack must propagate at least three monotonic compressive zone sizes.

For long cracks under small scale yielding conditions, tensile part of loading causes crack closure. Plasticity, roughness, and oxide-induced crack closure all contribute to the crack closure effect in small scale yielding. Plasticity-induced crack closure is not indicated under plain strain conditions because local wedge formation near the crack tip occurs as a result of plastic shear deformation in the crack's wake. Internal stresses are caused by stress concentration regions such as notch, hole, microstructural defects, and so on. And as one moves away from the source, internal stress diminishes asymptotically. Even so, as crack length increases, applied stress increases, and total stress is competitive. If the applied stress is less than K_{th} and K_{max} , the crack is stopped because the total stress is inadequate for crack propagation. Fatigue crack growth behavior of long cracks is

associated to the removal of internal stress. Because of the presence of internal stresses, the local stress ratio will be greater at the crack tip than the remote stress ratio.

5.3.3. THRESHOLD TEST RESULTS

Constant amplitude loading is applied just below the threshold value until the crack propagation rate is partly advanced. The most difficult part at this point is to estimate the initial ΔK value because the initial data is directly impacted by tensile residual stresses from precracking. To grow the crack partially, tests were launched at low stress intensities. Load increment was elevated by 10% if crack growth was not recognized after five million cycles. This method was repeated until the rate of crack propagation has stabilized. After enabling 1-1.5 mm crack advancement, a crack size that is at least two or three times the plastic zone size allows for steady-state crack propagation under constant amplitude loading. During the propagation phase, the crack plane is yielded, and the resulting residual stresses influence the crack's propagation beyond the plastic zone. Residual stresses and loading below the threshold stress led to crack arrest. As a result, residual stress effects are eliminated for subsequent constant amplitude testing when the pre-crack size is close to the plastic zone size. For instance, ΔK initial was set to 4.5 MPa \sqrt{m} with a R of 0.1 for tempered specimens. The crack was then intended to propagate for a minimum of 1.5 mm to establish that it was stabilized.

Following crack stabilization as shown in Figure 60, load reduction method was used to determine a precise threshold value of around 10^{-10} m/cycle crack growth rate. At least five data points were witnessed before the test was terminated, supposing that the crack was not propagating around the near-threshold region due to dominant closure effects on crack growth rate.

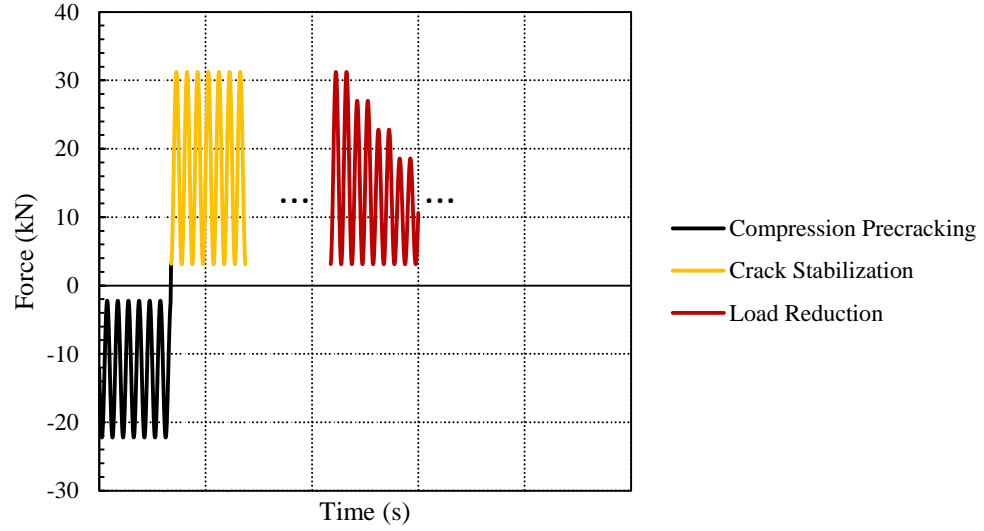


Figure 60 Loading sequence to reach threshold region

During data analysis post-processing, the NASGRO crack growth approach was used to estimate ΔK_{th} [165]. The expression is given by the equation below;

$$\frac{da}{dN} = C \left(\frac{(1-f)}{(1-R)} \Delta K \right)^n \frac{\left(1 - \frac{\Delta K_{th}}{\Delta K} \right)^p}{\left(1 - \frac{K_{max}}{K_c} \right)^q} \quad (5.58)$$

where the crack growth rate (da/dN) is affected by the following parameters: C and n are constants, f is the Newman's crack opening function, p and q are responsible for slope change in the threshold and unstable crack growth regions, ΔK is the stress intensity factor range, ΔK_{th} is the threshold stress intensity factor range, K_{max} is the maximum applied stress intensity factor, K_c is the critical stress intensity factor, and R is the stress ratio.

The following formula [52] can be used to calculate Newton's crack opening function.

$$f = \frac{K_{opening}}{K_{maximum}} = \begin{cases} \max R \text{ or } (A_0 + A_1 * R + A_2 * R^2 + A_3 * R^3) & R \geq 0 \\ A_0 + A_1 * R & R < 0 \end{cases} \quad (5.59)$$

By minimizing errors, the equation fits fatigue crack growth data using the logarithmic square method. The fitting parameters were the material constants C and n , with the parameter q set to zero because we were only engaged in the near-threshold region [69].

The NASGRO variables [166] can be used to calculate the threshold change as a function of the stress ratio. C_{th}^p , C_{th}^m and ΔK_1 are material constants estimated using least square fitting with fatigue threshold (ΔK_{th}) data. The stress intensity threshold range as the stress ratio approaches one is denoted by ΔK_1 . ΔK_1^* takes into account a small crack parameter known as a_0 [167].

$$\Delta K_{th} = \Delta K_1^* * \left[\frac{\left(\frac{1-R}{1-f}\right)^{(1+RC_{th}^p)}}{(1-A_0)^{(1-R)(C_{th}^p)}} \right] \quad R \geq 0 \quad (5.60)$$

$$\Delta K_{th} = \Delta K_1^* * \left[\frac{\left(\frac{1-R}{1-f}\right)^{(1+RC_{th}^m)}}{(1-A_0)^{(C_{th}^p - RC_{th}^m)}} \right] \quad R < 0 \quad (5.61)$$

$$\Delta K_1^* = \Delta K_1 * \sqrt{\frac{a}{(a+a_0)}} \quad (5.62)$$

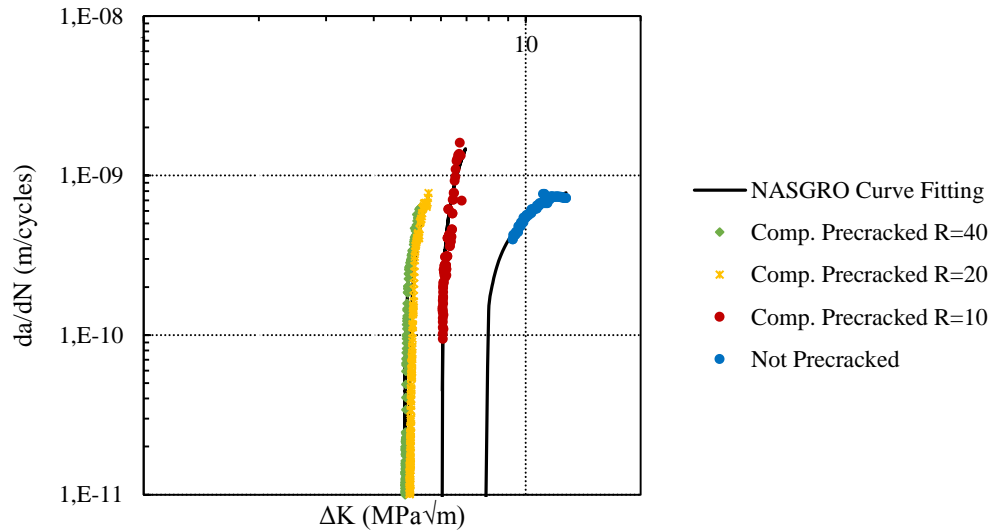


Figure 61 NASGRO curve fitting after crack growth tests

The least squares method for curve fitting aids in estimating the stress intensity threshold range. Consequently, the resulting curves were constructed only on near-threshold data using NASGRO curve fit, as illustrated in Figure 61. For non-precracked specimen, the initial ΔK was set as $5 \text{ MPa}\sqrt{\text{m}}$ and at least two million cycles loaded to recognize the fatigue crack. Nonetheless, fatigue cracks were not initiated at this stress level, despite the fact that enough stress concentration was developed through the razor blade. Because this was insufficient to initiate cracks ahead of the notch, ΔK was increased as a 10% of the predetermined initial ΔK value. This procedure was repeated until ΔK equaled $15 \text{ MPa}\sqrt{\text{m}}$. Then, a natural crack was formed on the notch region and stabilized after 1.5 mm propagation. Because of the high stress level, the crack propagated quickly during load reduction, and the crack length reached its limit due to specimen geometry. As a result, data points for crack growth around 10^{-10} m/cycle were not retrieved. Nonetheless, NASGRO curve fitting allows for the estimation of the long crack threshold value after least square for non-precracked specimen test. Eventually; long crack threshold values of 4.82, 4.96, 6.06, and $7.97 \text{ MPa}\sqrt{\text{m}}$ was determined for R of 40, 20, 10, and non-precracked specimens, respectively.

Long crack threshold values were determined for each case, and the effect of compression-compression precracking was assessed. As a result, R of 40 was determined to be the lowest threshold value, implying that a more accurate estimate of the threshold value can be made using that stress ratio as design criteria. Indeed, lowering load ratio for compression precracking resulted in remote closure and a reduction in driving force, resulting in a higher threshold value. For an accurate and reliable fatigue threshold value, it is recommended that a higher stress ratio for compression precracking be selected. If compression precracking was not conducted prior to beginning crack growth tests, the expected higher threshold was obtained due to load history effects unsurprisingly.

5.3.3.1. THRESHOLD EVALUATION

Based on influential research results, material strength and microstructure complexity are the most important factors in determining fatigue crack growth rate near the threshold. Lower crack growth rates in lower-strength steels have been indicated by reducing yield strength, and higher threshold values in steels and titanium alloys have been revealed by maximizing grain size. At high stress intensities, fatigue crack growth rates become sensitive to microstructure and stress ratio, consistent with the formation of static failure modes during striation growth. In the mid-range of crack growth rates, changes in microstructure and stress ratio have no effect on crack growth rate. Aside from these, the major influence of load ratio and microstructure on crack growth rates is observed at low crack growth rates; the highest sensitivity to stress ratio occurs in lower-strength steels, and the highest sensitivity to microstructure exists at low stress ratios.

Failure in steels is primarily caused by a transgranular ductile striation mechanism, with little involvement from microstructure and stress ratio in the middle range of the curve. Because of a shift away from striation growth and toward static fracture modes like cleavage and intergranular fracture as K_{max} approaches K_{IC} , crack growth rates become highly sensitive to both microstructure and stress ratio. Microstructure and stress ratio

have a comparable significant impact on growth rates at low crack growth rates near the threshold, as well as an extreme sensitivity to crack closure and environmental impacts.

The fatigue-crack growth threshold decreases as cyclic strength increases, either due to high initial monotonic strength or due to cyclic hardening. After cyclic softening, however, the softest condition arranged via tempering temperature results in the largest threshold. Tempering temperature clearly has an effect on threshold levels and, implicitly, near-threshold crack growth rates. As tempering temperature rises, the threshold ΔK_0 rises, accompanied by a decrease in tensile strength. At higher stress ratios, the same trend of increasing ΔK_0 with decreasing strength is still visible, but the influence is significantly reduced for the same loss of strength. Cyclic softening, defined as a decrease in dislocation density with cyclic loading, can be advantageous in terms of improving near-threshold crack growth resistance. Although the threshold stress intensity did not change, coarsening the prior austenite grain size was found to increase near-threshold crack growth resistance.

Microstructure has been found to have a significant influence in steels, where the formation of ferritic and martensitic microstructures can result in increased crack growth resistance at low stress intensities and material strength compared to industrially heat-treated steel. After appropriate heat-treatment procedures, dual phases microstructures with a prolonged martensitic phase that completely enclosed the ferritic phase were found to have greater strength and a significantly higher threshold than similar structures with the ferritic phase enclosing the martensite. The conclusion for the relationship between strength and near-threshold behavior is unexpected; however, it brings a very favorable way of increasing fatigue-crack growth resistance in terms of microstructure dependence.

A combination of shearable and non-shearable precipitates influences crack growth. As a result, slip bands formed by subsequent dislocations cutting through shearable precipitates soften if the effective size of the particles is small; on the other hand, strong precipitates that cannot be cut when their size reaches a critical limit and are relatively large compared

to shearable precipitates, and the inter-particle spacing of non-shearable precipitates dominate the effective crack length. Within the continuum mechanics framework, the maximum and cyclic plastic zone sizes near the threshold under plane strain conditions are evaluated. As a result, there is a significant improvement in fatigue crack growth resistance near the threshold when compared to Paris and unstable crack growth regions. In the Paris regime, where K is sufficiently high, the size of the cyclic plastic zone is on the order of tens of microns or greater, and thus exceeds grain size. As a result, cracks form across grain boundaries, making their growth rate unaffected by microstructural characteristics.

The material with the ferritic-pearlitic structure has a higher roughness in near-threshold regions than the material with the martensitic structure. In contrast to the pearlitic phase, which had no striation, the ferritic phase had a striation pathway. A different mechanism was involved in the martensitic material: it lacks striation but has fine secondary cracks near the threshold, whereas sharp cracks occur at high stress densities. The pearlite phase is stronger than the ferritic phase and directly limits ferrite deformation in the plastic zone during crack propagation. The pearlite structures are unable to maintain their strength after cyclic hardening due to plastic deformation, and the strength and plastic deformation are distributed to neighboring ferritic colonies. With each cycle, this sharp increase in deformation creates the image of micro crack increments in the ferrite colonies, eventually leading to their breakage. The higher roughness of the fracture surface of the pearlitic-ferritic microstructure compared to the martensitic one is another factor influencing crack growth characteristics. In the pearlitic-ferritic microstructure, striations dominate the crack growth region. On the fracture surface of the martensitic microstructure, however, there are several secondary microcracks rather than striation. The threshold levels in the annealed material were significantly higher than in the martensitic microstructure. Similarly, the bainitic and pearlitic-ferritic microstructures shared the martensitic microstructure.

5.4. FAILURE ANALYSIS

Failure analysis are necessary to determine the origin of the fracture, to assess the direction of crack growth, and to determine the corresponding fracture mechanism. This is accomplished by critically analyzing the marks existing on the fracture surface. Almost all failures are the consequence of more than one cause and are seldomly single. The comprehensive examination of the fracture surface facilitates the recognition of some fatigue failure attributes: ratchet marks, which demonstrate the results of several origins of fatigue crack initiation because of the high stress concentration, and beach marks, which represent the development of fatigue cracks and clearly show the alteration in crack propagation rate.

Fractography studies are indispensable to reveal the mechanism behind the failure by looking at the fracture surfaces. In this regard, fractography can determine crack initiation location, crack propagation direction, any involved defect on microstructure, environmental effect on failure, and the stress type to which material is exposed. Thus, fracture surface analysis was carried out for crack growth specimens to evaluate fracture mechanism and clarify test history by examining each phase. Stereo microscopy was used to obtain the fracture surfaces of the failed specimens as shown Figure 62 and Figure 63. As expected, multiple crack initiation was observed in the precracking stage of crack growth test due to severe loading condition.

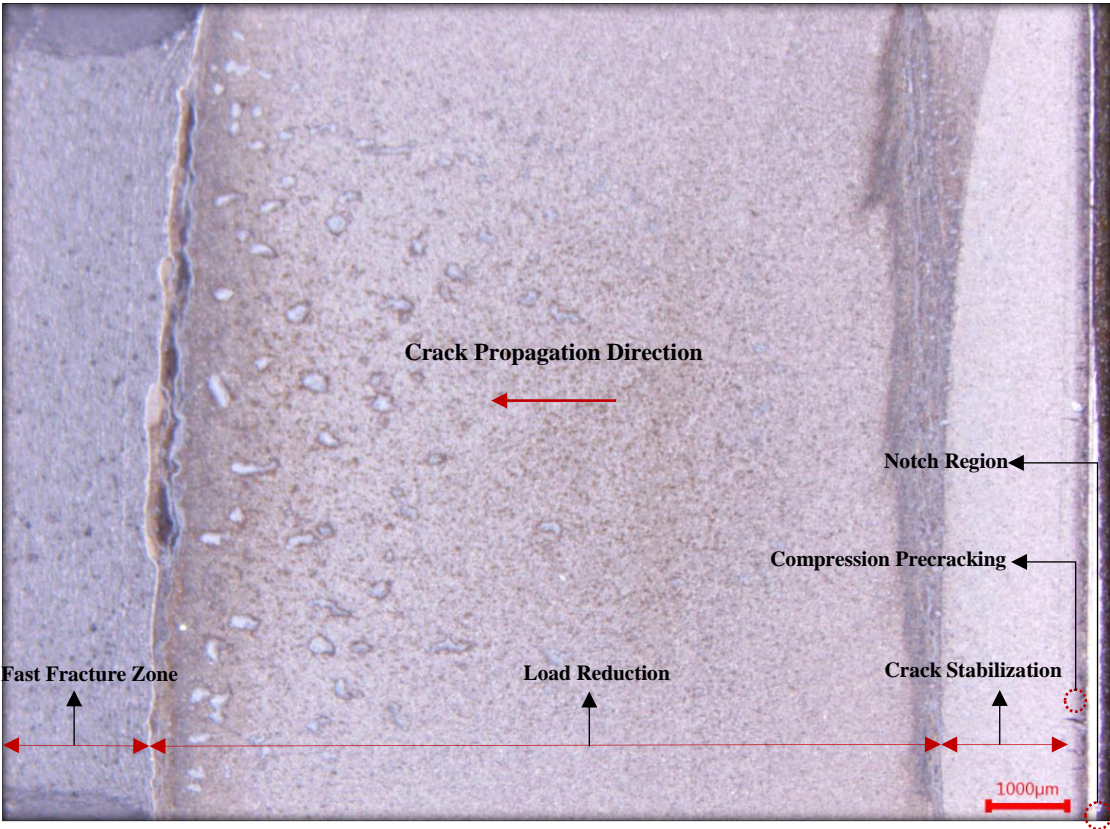


Figure 62 Micrograph of fracture surface of the crack propagation test

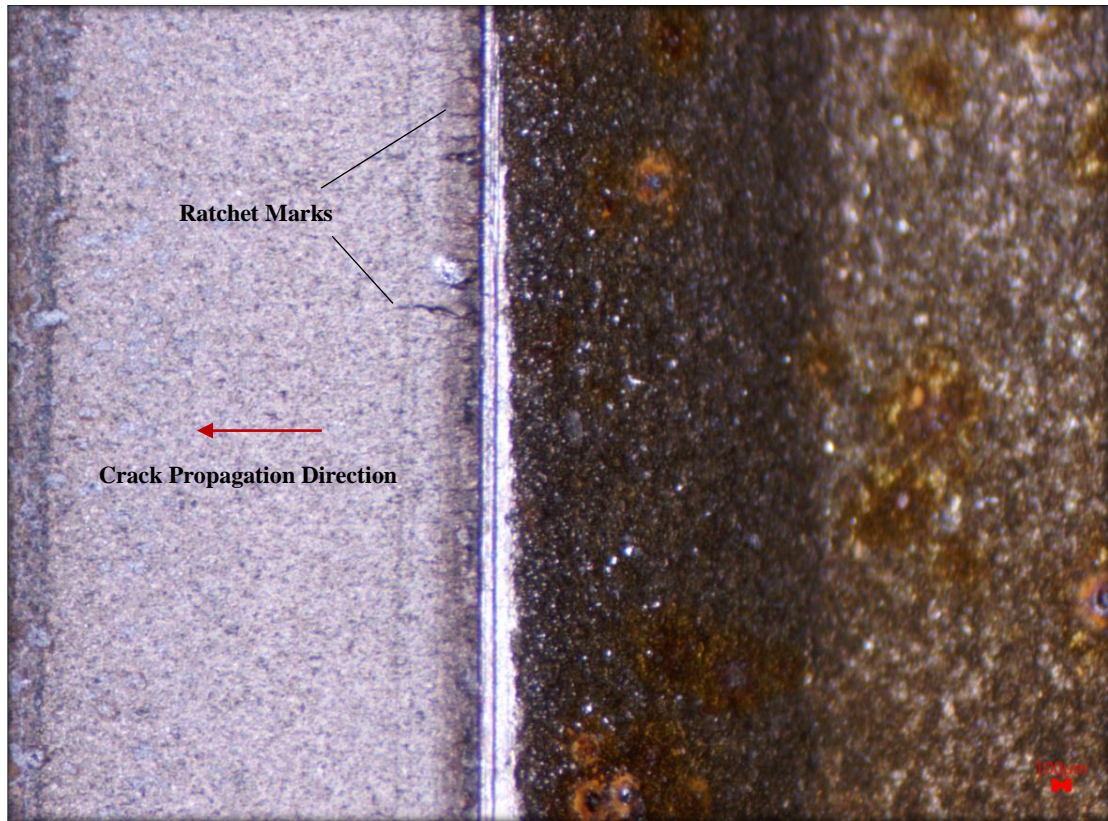


Figure 63 Multiple crack initiation during precracking loading

The following captures were taken after SEM investigation for each microstructure. Failure analysis were carried out on Turkish Aerospace under Zeiss modular SEM platform. It allowed the crack initiation points and failure modes after rupture to be clearly revealed.

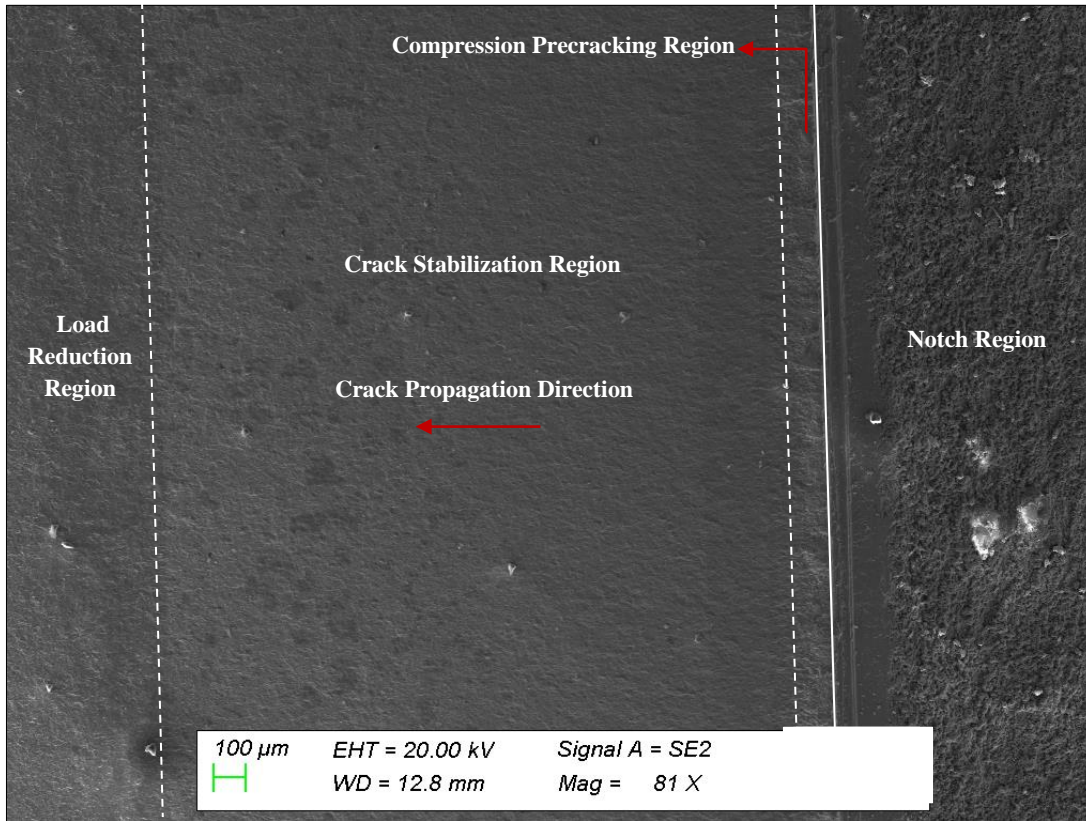


Figure 64 Crack growth sequence for tempered specimen

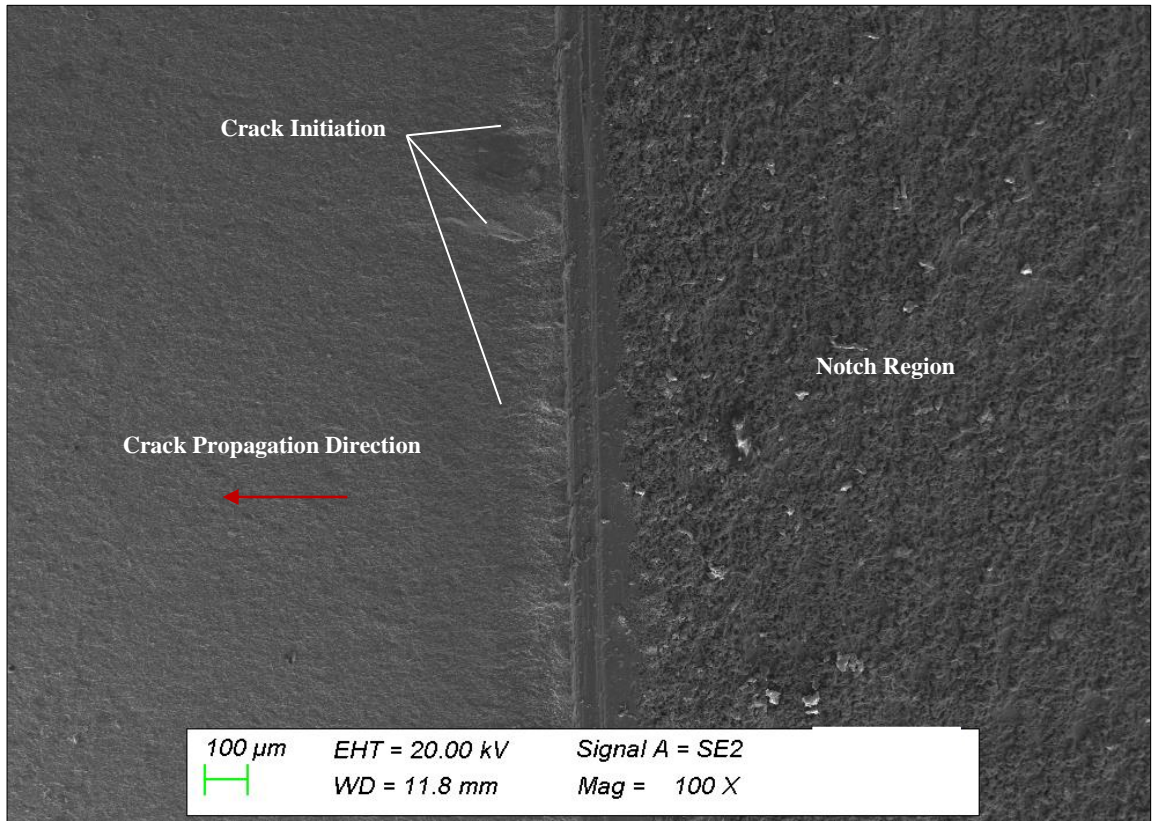


Figure 65 Compression precracking stage for tempered specimen

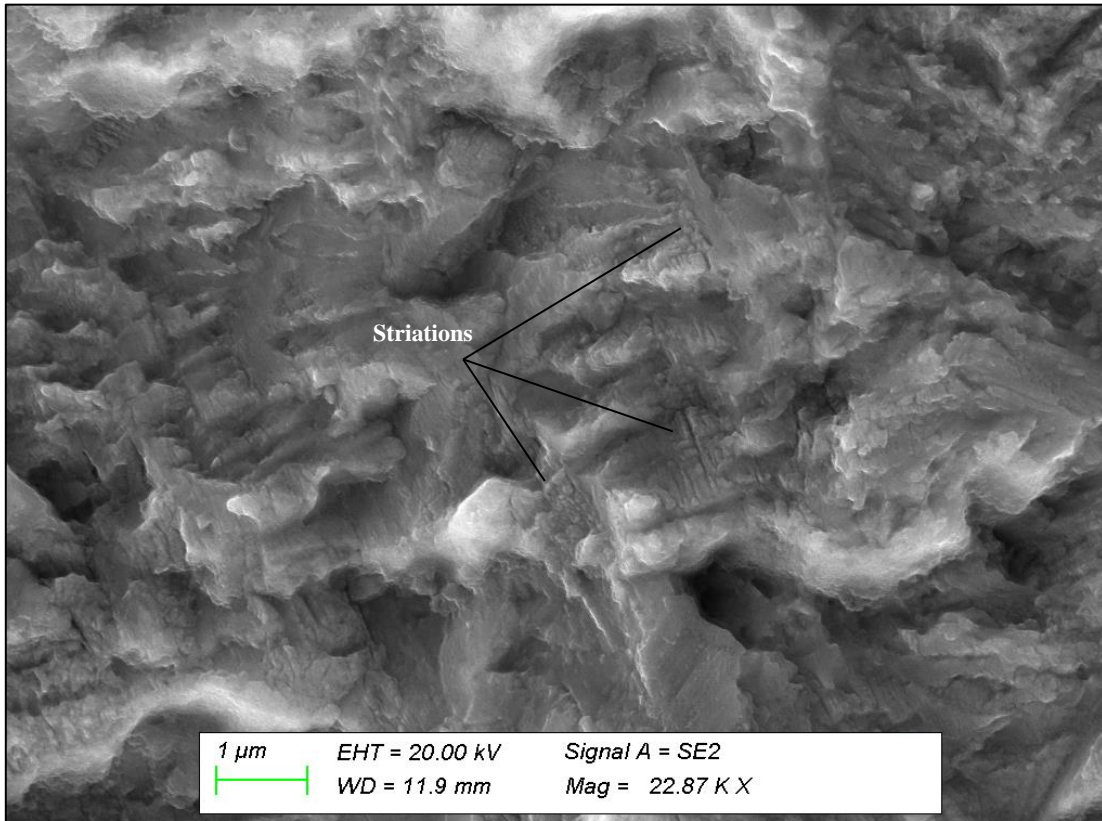


Figure 66 Crack growth region for tempered specimen in high magnification

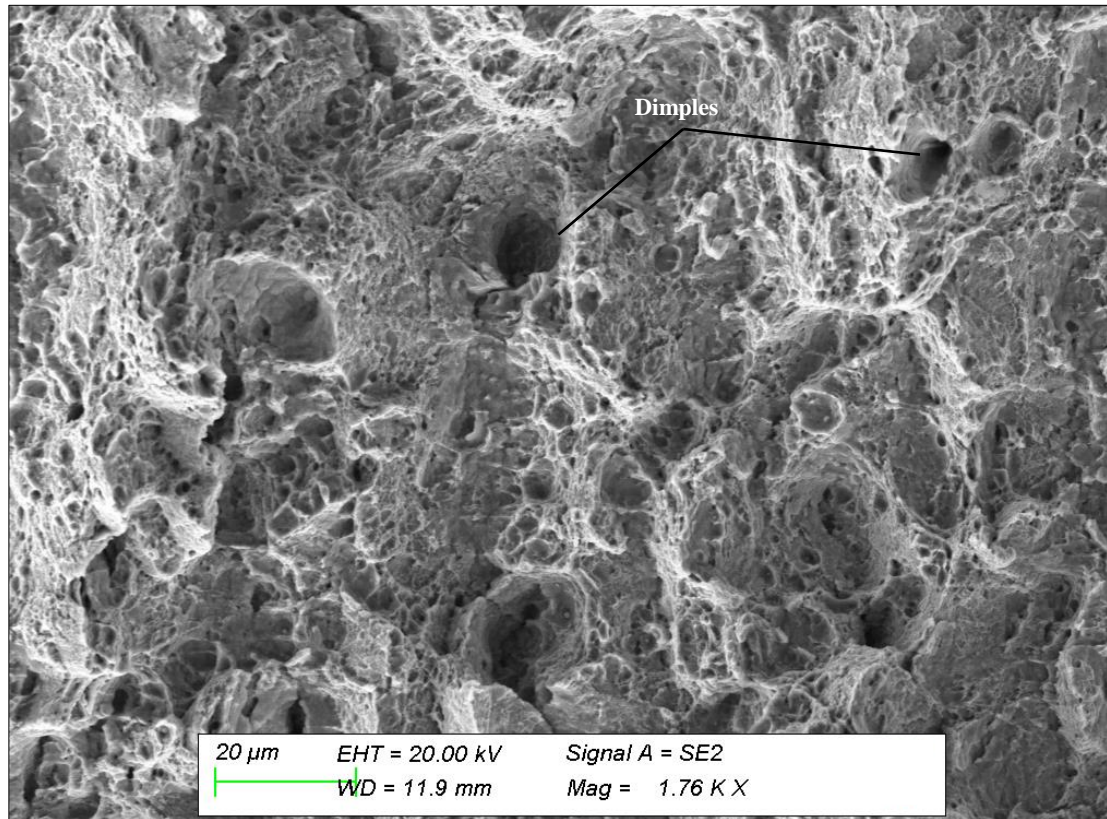


Figure 67 Fast rupture for tempered specimen

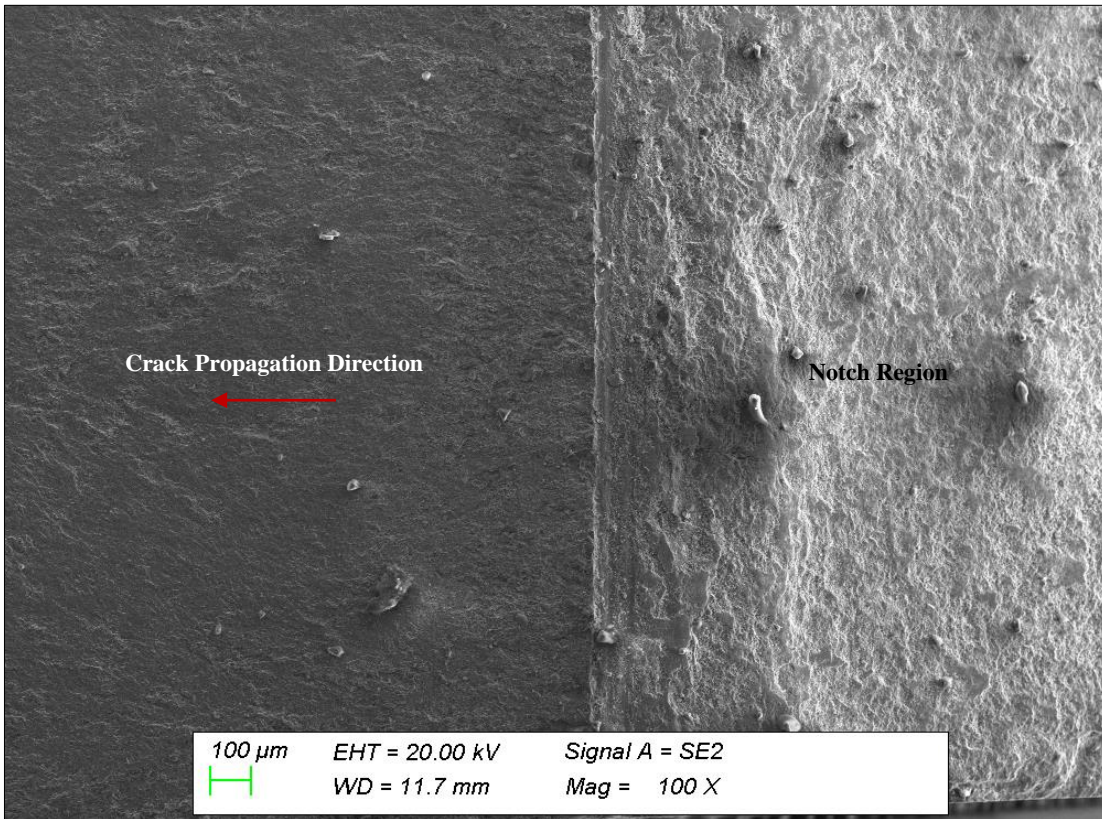


Figure 68 Compression precracking stage for annealed specimen

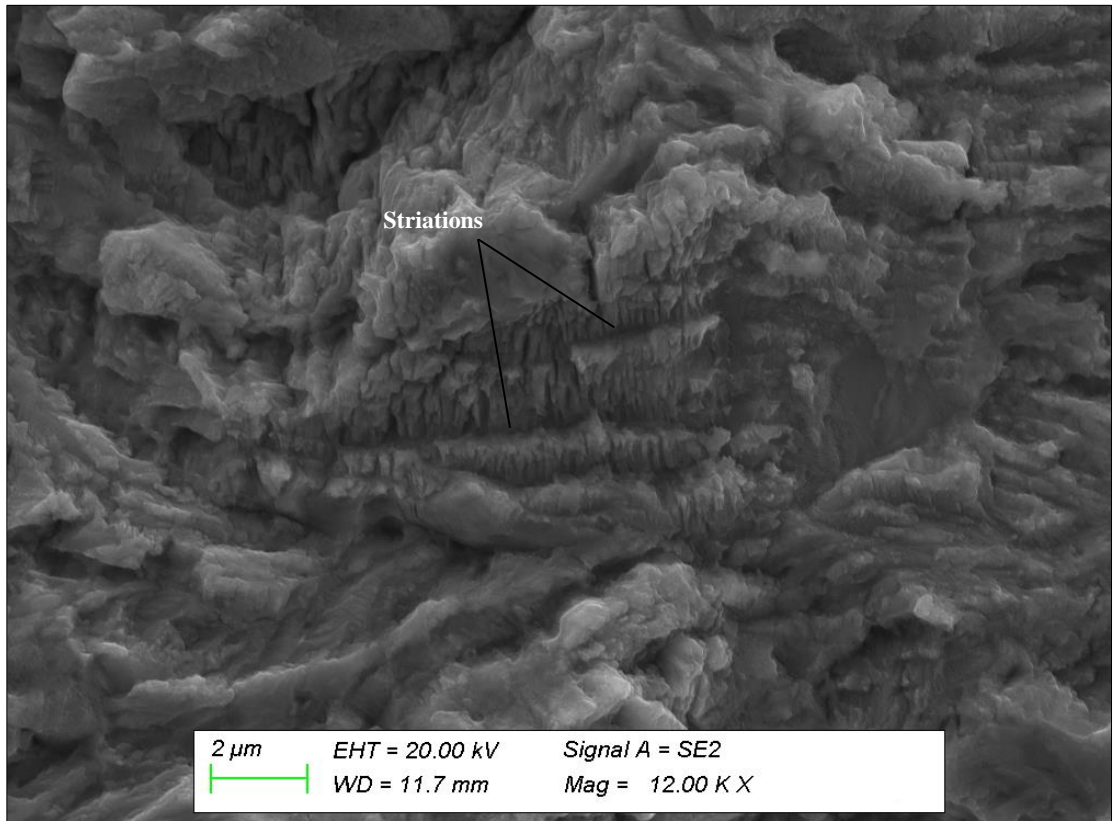


Figure 69 Crack growth region for annealed specimen in high magnification

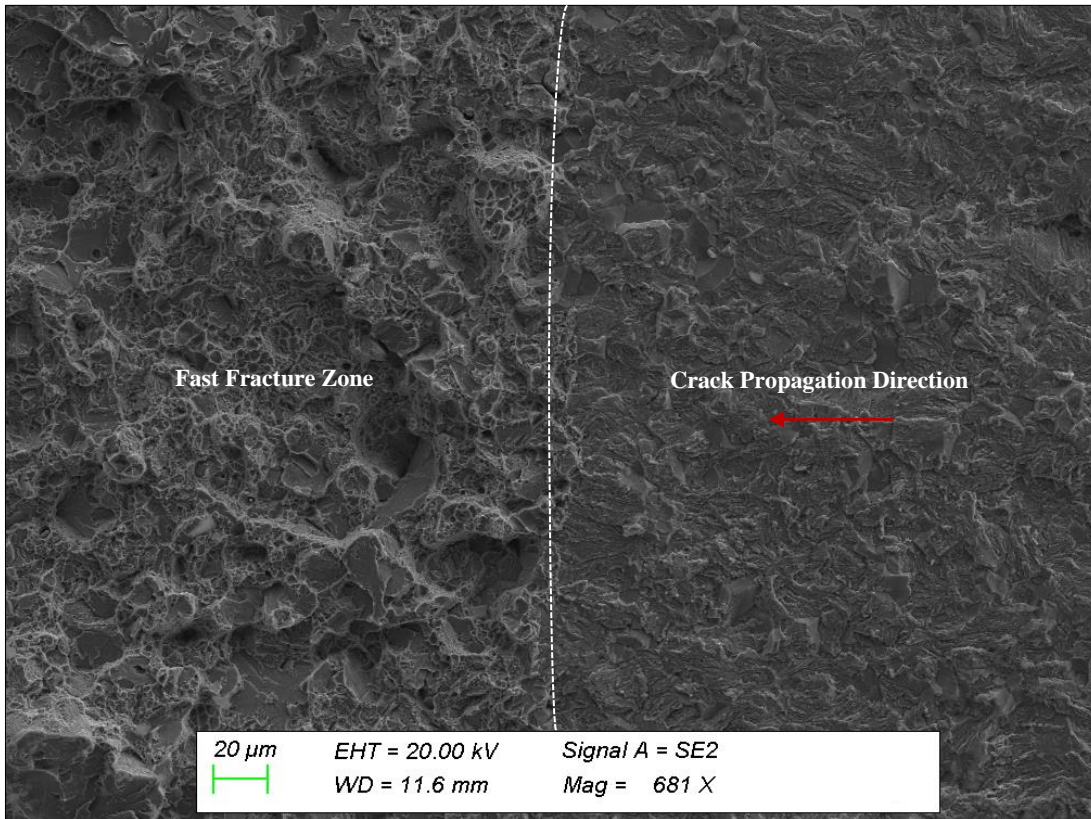


Figure 70 Transition region for crack growth test of annealed specimen

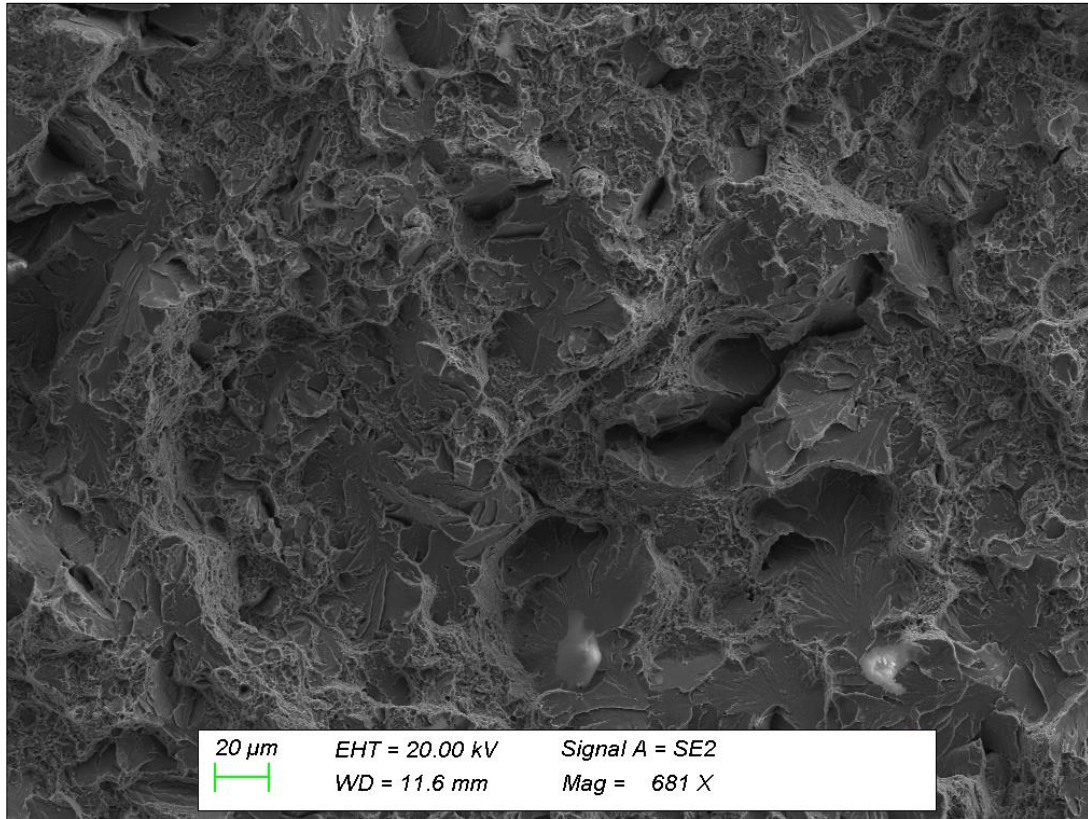


Figure 71 Fast fracture region for the annealed specimen

Because of severe compression loading during precracking stage of crack growth test, multiple crack initiation was observed for tempered and annealed specimens. Striations were so fine for both microstructures as expected. Final rupture is quasi-cleavage for tempered specimens and cleavage for annealed specimens. The number of dimples were mostly observed on tempered fracture zone compared to annealed ones. Elongation of dimples was not evident since fast rupture occurred under axial loading in other words shear component was not available during rupture.

5.5. RESULTS OF FATIGUE TESTS

Long crack threshold tests were carried out at different stress ratios under annealed and tempered condition of AISI 4340 steel. The effect of microstructure resulting from heat

treatment and effect of stress ratio can be seen on Figure 72. Bounce effect (oddly increasing rate of decreasing crack growth) was only observed in the annealed data with R of -1 condition because of reduced remote closure effect and this can be associated with the compression precracking stage.

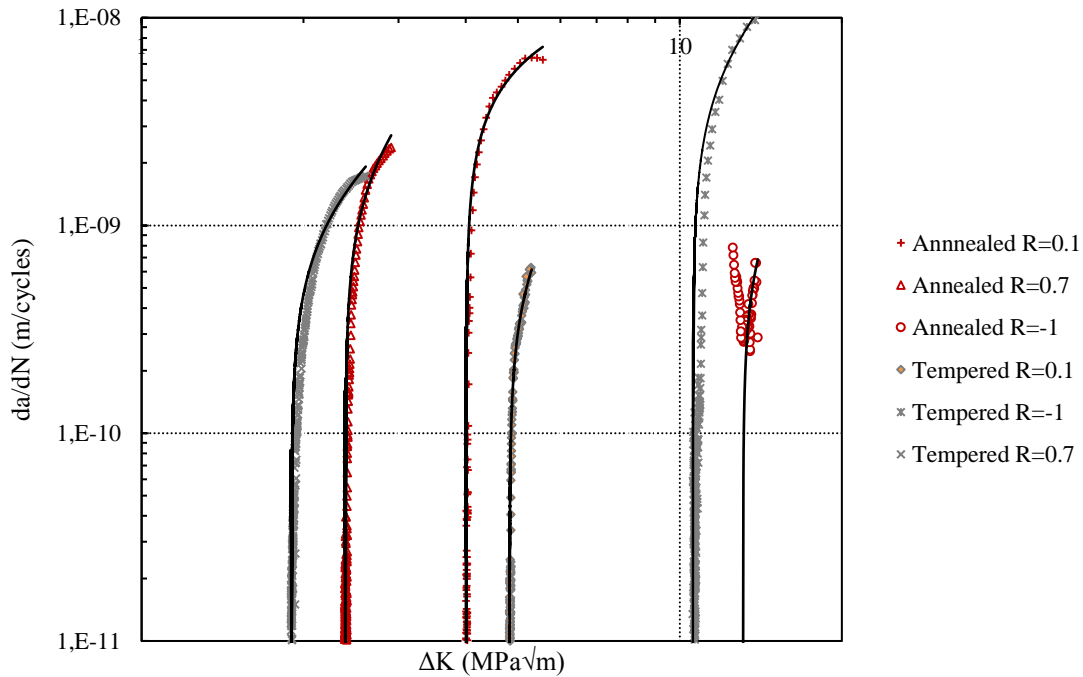


Figure 72 Variation of long crack threshold data

The following table summarizes the curve fitting results for all crack growth data. To determine threshold value; two tests were performed for each parameter and the average of these data was taken as the corresponding threshold value to set a singular value. There are two competing mechanisms for crack growth tests: one based on cyclic plastic zone ahead of crack tip, which is inversely proportional with yield strength and the other based on fracture toughness influence because of microstructure. For instance, tempered microstructure is expected to have a higher threshold value because of the increased fracture toughness of tempered martensite compared to annealed one. On the other hand, tempered one has a lower plastic zone size ahead of crack tip that decreases threshold. To summary, two mechanisms are always in competition each other. In our study, the effect

of plastic zone size is dominant at low and high stress ratios; however, the fracture toughness effect dominates at the R of the 0.1 condition.

Table 7 Near threshold results for all fatigue crack growth tests

Stress Ratio (R)	Heat Treatment	Long Crack Threshold (MPa√m)
0.7	Tempered	1.89
0.1		4.89
-1		10.63
0.7	Annealed	2.38
0.1		4.01
-1		13.11

After determining endurance limit and long crack threshold for AISI 4340 steel; critical stress for small cracks can be estimated via El-Haddad equation [151] from corresponding tests carried out at same stress ratio.

$$\Delta K = Y\Delta\sigma\sqrt{\pi(a + a_0)} \quad (5.63)$$

$$a_0 = \frac{1}{\pi} * \left(\frac{\Delta K_{th}}{\Delta\sigma_{end.}} \right)^2 \quad (5.64)$$

where a_0 is intrinsic crack length, a is crack length, Y represents the geometry factor, $\Delta\sigma$ is stress amplitude, ΔK_{th} is long crack threshold value and $\Delta\sigma_{end.}$ is the corresponding endurance limit in defined stress range.

Figure 73 exhibits the normalized long crack thresholds ΔK_{th} in regard to the stress ratio. As expected, ΔK_{th} values increase uniformly from the positive stress ratio to the negative stress ratio for each microstructure. Normalized long crack threshold exhibits almost same values at negative stress ratio and approaches to stress ratio with no closure.

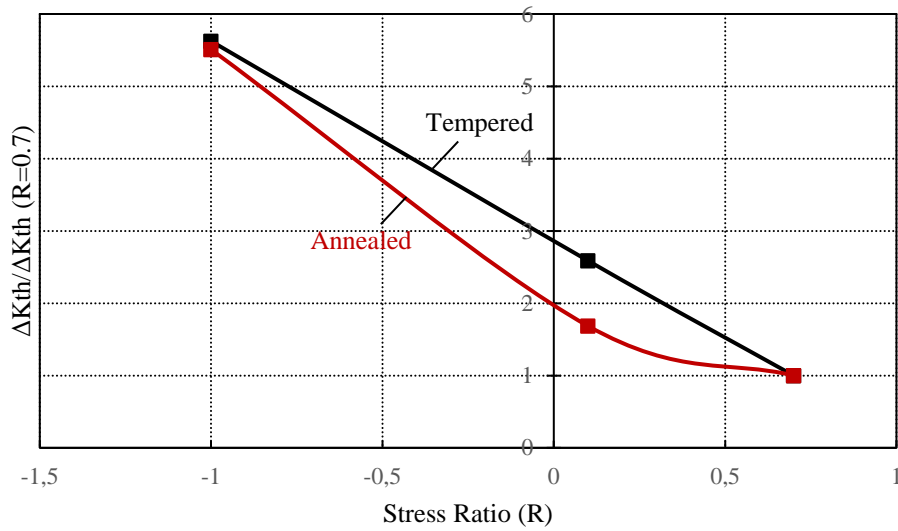


Figure 73 Variation of long crack threshold data with stress ratio

The Kitagawa diagram [168] can be constructed using endurance and crack growth data in which endurance and crack growth tests were performed at the same stress ratio. There is a positive relationship between the endurance limit and the threshold value for AISI 4340 steels under different heat treatment conditions for R of 0.1. Accordingly, higher fatigue strength resulted in higher crack growth resistance. The annealed microstructure resulted in lower thresholds and lower endurance limits. In contrast, higher fatigue strength was achieved for the tempered microstructure and this resulted in a low crack propagation rate as shown in Figure 74.

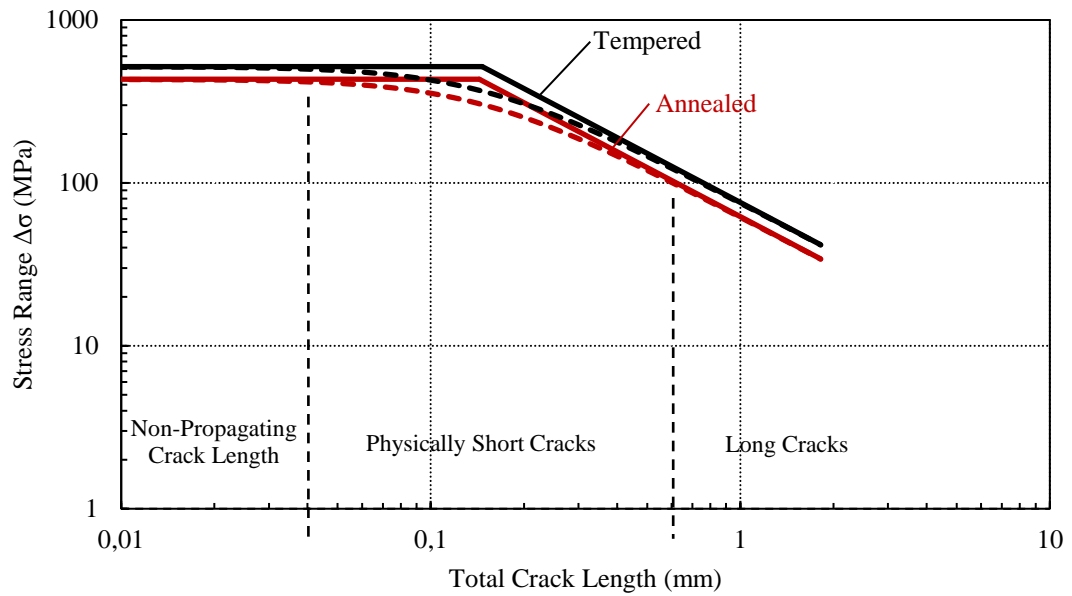


Figure 74 Kitagawa Diagram of AISI 4340 for different microstructures under R of 0.1

Non-propagating fatigue crack length was found to be approximately 40 μm for each microstructure, and it is assumed that fatigue crack did not propagate below this value. On the other hand, long crack length was observed to be higher than approximately 600 μm for each microstructure. Between these values, the endurance limit for materials with physically small crack can be estimated for each microstructure.

CHAPTER 6

CONCLUSIONS

The aim of this study is to investigate the effect of heat treatment on fatigue threshold in terms of microstructural features for AISI 4340 steels and to estimate small crack behavior by combining endurance limit of the material and long crack threshold data obtained from high cycle fatigue tests and crack growth tests respectively. In the region where fatigue cracks propagate near the threshold, microstructural characteristics play a significant role. The fatigue crack growth mechanism is restricted to a small region of the plastic zone. Microstructural variations, which are frequently directed to heat treatment methods, can affect yield strength and hardness, resulting in plastic zone size differences. As a result, crack growth under alternating loading may be affected, resulting in differences in threshold values. Threshold stress is extremely important for structures subjected to high cycle loading because the high percentage of life causes crack initiation and remaining short time causes crack propagation, so accurate threshold stress estimation is essential. The long crack threshold is primarily used for damage tolerant structures as design criterion, but small cracks have been shown to grow at different rates than long cracks. To perceive the differences in crack growth rate, the concept of crack closure needs to be well understood. The fatigue strength of a material can be evaluated statistically by analyzing the staircase or curve fitting approaches. The objective is to deliver more reliable data with predefined confidence intervals, so that conservative data can be used in design stage. By combining long crack threshold and fatigue limit data, corresponding

critical stress of small cracks can be estimated. As a result, the following conclusions can be drawn from this particular study:

- Fatigue tests were performed in a laboratory environment, and the results provide information about the fatigue behavior of the material; but even so, components in service may have unforeseen risks, which complicates scatter determination so further safety factors are required.
- A total number of 14 specimens were deemed well suited to plot the SN curve and allowed estimation of the endurance limit for analysis of the limited data set.
- The staircase methods are simple to use for assessing the fatigue strength of a material, and the conventional methods produce proximate limit values of 50% failure probability; nevertheless, standard deviation is complicated as a whole, so large safety factors are required to obtain reliable results for small sample sets.
- Curve fitting techniques can be used to assess the shape of the SN curve by allowing for the evaluation of fatigue strength for the associated number of cycles, and the projected fatigue limit on ten million cycles provided reasonable correlation with staircase methods.
- For the limited data set, the Weibull, IABG and Bootstrapping methods fit better than other methods due to the small standard deviation.
- The stress ratio and microstructure had a great impact on crack growth rates near the threshold region, with the remarkable sensitivity to stress ratio existing in lower strength conditions and the immense sensitivity to microstructure occurrence at low stress ratios.
- As the stress ratio increases, the crack growth rates around threshold accelerate and the long crack threshold value diminishes for each microstructure; ΔK_{th} is inversely correlated with the stress ratio.
- As yield strength of steel decreases, crack propagation rates near threshold region reduces because of increasing plastic zone size ahead of crack tip that increases

crack growth resistance, and the threshold value is inversely correlated to cyclic yield strength for low and high stress ratios.

- There are two competing mechanisms for crack growth tests: one based on cyclic plastic zone ahead of crack tip, which is inversely proportional with yield strength and the other based on fracture toughness influence because of microstructure. For R of 0.1 condition, the plastic zone size effect was less dominant than fracture toughness effect when compared to the annealed and tempered conditions.
- The fatigue limit and long crack threshold values were found to be 585 MPa and $4.89 \text{ MPa}\sqrt{\text{m}}$ for tempered specimens, and 481 MPa and $4.01 \text{ MPa}\sqrt{\text{m}}$ for annealed specimens.
- Crack size smaller than $30 \mu\text{m}$ is considered as non propagating crack and crack size larger than $600 \mu\text{m}$ is attributed as long crack for tempered specimen on R of 0.1 loading condition; any crack size between this range is considered as physically short crack and its endurance limit can be estimated.

REFERENCES

- [1] James, M. A., Forth, S. C., & Newman, J. A. (2005). Load History Effects Resulting from Compression Precracking. *Journal of ASTM International*, 2(9), 12025.
- [2] Pippin, R., & Hohenwarter, A. (2017). Fatigue crack closure: a review of the physical phenomena. *Fatigue & Fracture of Engineering Materials & Structures*, 40(4), 471–495.
- [3] Li, S., Zhang, Y., Qi, L., & Kang, Y. (2018). Effect of single tensile overload on fatigue crack growth behavior in DP780 dual phase steel. *International Journal of Fatigue*, 106, 49–55.
- [4] Taira, S., Tanaka, K. and Nakai, Y. (1978) A model of crack-tip slip band blocked by grain boundary. *Mech. Res. Commun.*, 5, 375–381.
- [5] Elber, W., "The Significance of Fatigue Crack Closure," *Damage Tolerance in Aircraft Structures*, ASTM STP 486, American Society for Testing and Materials, 1971, pp. 230-242.
- [6] Chapetti, M. D. (2002). Estimation of the Plain High-Cycle Fatigue Propagation Resistance in Steels. *Materials Research*, 5(2), 101–105.
- [7] Schijve, J., *Statistical Distribution Functions and Fatigue of Structures*, *International Journal of Fatigue*, pp. 1031-1039, 2005. <https://doi.org/10.1016/j.ijfatigue.2005.03.001>
- [8] Pascual, F. G., & Meeker, W. Q. (1999). Estimating fatigue curves with the random fatigue-limit model. *Technometrics*, 41(4), 277-289. <https://doi.org/10.1080/00401706.1999.10485925>

- [9] Rabb, B.R., 2003. Staircase testing – confidence and reliability. *Trans. Eng. Sci.* 40, 447–464.
- [10] Sutherland, Herbert & Veers, Paul. (2000). The Development of Confidence Limits for Fatigue Strength Data. *Wind Energy ASME/AIAA*. 10.2514/6.2000-63.
- [11] H. Li, D. Wen, Z. Lu, Y. Wang, F. Deng, Identifying the probability distribution of fatigue life using the maximum entropy principle. *Entropy* 18 (4), 111 (2016). <https://doi.org/10.3390/e18040111>
- [12] Sakai, T. (1997). Statistical distribution patterns in mechanical and fatigue properties of metallic materials. *Journal of the Society of Materials Science*. Volume 46 Issue 6 Appendix Pages 63-74. https://doi.org/10.2472/jsms.46.6appendix_63
- [13] Schneider, C. R. A., Maddox, S. J. (2003). "Best practice guide on statistical analysis of fatigue data", The Welding Institute, Cambridge, UK.
- [14] Barbosa, J. F., Correia, J. A., Freire Júnior, R., Zhu, S., & De Jesus, A. M. (2019). Probabilistic S-N fields based on statistical distributions applied to metallic and composite materials: State of the art. *Advances in Mechanical Engineering*, 11(8), 168781401987039. <https://doi.org/10.1177/1687814019870395>
- [15] Toasa Caiza, P. D., & Ummenhofer, T. (2018). A probabilistic STÜSSI function for modelling the S-N curves and its application on specimens made of steel S355J2+N. *International Journal of Fatigue*, 117, 121–134. <https://doi.org/10.1016/j.ijfatigue.2018.07.041>
- [16] Burhan, I., & Kim, H. (2018). S-N Curve Models for Composite Materials Characterisation: An Evaluative Review. *Journal of Composites Science*, 2(3), 38. <https://doi.org/10.3390/jcs2030038>

- [17] Kim, H. S., & Zhang, J. (2001). Fatigue damage and life prediction of glass/vinyl ester composites. *Journal of Reinforced Plastics and Composites*, 20(10), 834-848. <https://doi.org/10.1177/073168401772678959>
- [18] Lipski, Adam. (2018). Determination of the S-N curve and the fatigue limit by means of the thermographic method for ductile cast iron. *AIP Conference Proceedings*. <https://doi.org/10.1063/1.5066398>
- [19] ASTM E739-91(1998). (n.d.). Retrieved April 07, 2021, from <https://www.astm.org/DATABASE.CART/HISTORICAL/E739-91R98.htm>
- [20] Meggiolaro, Marco & Miranda, A. & Castro, Jaime. (2007). Short crack threshold estimates to predict notch sensitivity factors in fatigue. *International Journal of Fatigue - INT J FATIGUE*. 29. 2022-2031.
- [21] Yukitaka Murakami, Toshio Takagi, Kentaro Wada, Hisao Matsunaga, Essential structure of S-N curve: Prediction of fatigue life and fatigue limit of defective materials and nature of scatter, *International Journal of Fatigue*, Volume 146, 2021, 106138, ISSN 0142-1123. <https://doi.org/10.1016/j.ijfatigue.2020.106138>
- [22] Leonetti, Davide & Maljaars, Johan & Snijder, Bert. (2017). Fitting fatigue test data with a novel S-N curve using frequentist and Bayesian inference. *International Journal of Fatigue*, 105, 128-143. <https://doi.org/10.1016/j.ijfatigue.2017.08.024>
- [23] Pollak, R., Palazotto, A., & Nicholas, T. (2006). A simulation-based investigation of the staircase method for fatigue strength testing. *Mechanics of Materials*, 38(12). <https://doi.org/1170-1181>. 10.1016/j.mechmat.2005.12.005
- [24] Bathias. (1999). There is no infinite fatigue life in metallic materials. *Fatigue & Fracture of Engineering Materials & Structures*, 22(7), 559–565.

- [25] Dixon, W. J., & Mood, A. M. (1948). A method for obtaining and analyzing sensitivity data. *Journal of the American Statistical Association*, 43(241), 109-126. <https://doi.org/10.1080/01621459.1948.10483254>
- [26] Dixon, W. J. (1965). The up-and-down method for small samples. *Journal of the American Statistical Association*, 60(312), 967-978. <https://doi.org/10.1080/01621459.1965.10480843>
- [27] Lin, S. (2001). Evaluation of the staircase and the accelerated test methods for fatigue limit distributions. *International Journal of Fatigue*, 23(1), 75-83. [https://doi.org/10.1016/s0142-1123\(00\)00039-6](https://doi.org/10.1016/s0142-1123(00)00039-6)
- [28] Little, R. E., "Estimating the Median Fatigue Limit for Very Small Up-and-Down Quantal Response Tests and for S-N Data with Runouts", *Probabilistic Aspects of Fatigue*, ASTM STP 511, American Society for Testing and Materials, 1972, pp. 29-42. <https://doi.org/10.1520/stp35403s>
- [29] Loren, S. (2003). Fatigue limit estimated using finite lives. *Fatigue Fracture of Engineering Materials and Structures*, 26(9), 757-766. <https://doi.org/10.1046/j.1460-2695.2003.00659.x>
- [30] Minak, G. (2007). Comparison of different methods for fatigue limit evaluation by means of the Monte Carlo method. *Journal of Testing and Evaluation*, 35(2), 100122. <https://doi.org/10.1520/jte100122>
- [31] Nicholas Metropolis & S. Ulam (1949) The Monte Carlo Method, *Journal of the American Statistical Association*, 44:247, 335-341
- [32] Johnson, R. W. (2001) An introduction to the bootstrap. *Teach. Stat.* 23, 49–54.

- [33] Beretta, S., & Murakami, Y. (1998). STATISTICAL analysis of defects for fatigue strength prediction and quality control of materials. *Fatigue Fracture of Engineering Materials and Structures*, 21(9), 1049-1065. <https://doi.org/10.1046/j.1460-2695.1998.00104.x>
- [34] Suresh, S., & Ritchie, R. O. (1984). Propagation of short fatigue cracks. *International Metals Reviews*, 29(1), 445–475.
- [35] Tokaji, K.; Ogawa, T.; Harada, Y.; Ando, Z. *Fatigue and Fract. Engng. Mater. Struct.*, v. 9, n. 1, p. 1-14, 1986.
- [36] Sangid, M. D. (2013). The physics of Fatigue Crack Initiation. *International Journal of Fatigue*, 57, 58–72.
- [37] Lankford, J. 1977, “Initiation and Early Growth of Fatigue Cracks in High Strength Steels,” *Eng. Fract. Mech.* 9, pp. 617-624.
- [38] Park, H B, & Chopra, O K. (2000). A fracture mechanics approach for estimating fatigue crack initiation in carbon and low-alloy steels in LWR coolant environments. United States.
- [39] Sadananda, K., Nani Babu, M., & Vasudevan, A. K. (2019). A review of fatigue crack growth resistance in the short crack growth regime. *Materials Science and Engineering: A*, 754, 674–701.
- [40] McEvily, A. J. (1970). The growth of short fatigue cracks: a review. *Transactions on Engineering Sciences*, 13, 93–107.
- [41] Chowdhury, P., & Sehitoglu, H. (2016). Mechanisms of fatigue crack growth - a critical digest of theoretical developments. *Fatigue & Fracture of Engineering Materials & Structures*, 39(6), 652–674.

- [42] Wu, X. J., Koul, A. K., & Krausz, A. S. (1993). A transgranular fatigue crack growth model based on restricted slip reversibility. *Metallurgical and Materials Transactions A*, 24(6).
- [43] Ritchie, R. O. and Lankford, J., Overview of the Small Crack Problem, in *Small Fatigue Cracks*, ed. by R. O. Ritchie and J. Lankford, The Metallurgical Society, AIME, Warrendale, Pa., 1986, pp. 1
- [44] Tabernig, B., & Pippan, R. (2002). Determination of the length dependence of the threshold for fatigue crack propagation. *Engineering Fracture Mechanics*, 69(8), 899–907.
- [45] Ritchie, R. O., & Lankford, J. (1986). Small fatigue cracks: A statement of the problem and potential solutions. *Materials Science and Engineering*, 84, 11–16.
- [46] Sadananda, K., & Vasudevan, A. K. (1997). Short crack growth and internal stresses. *International Journal of Fatigue*, 19(93), 99–108.
- [47] Grasso, M., De Iorio, A., Xu, Y., Haritos, G., Mohin, M., & Chen, Y. K. (2017). An analytical model for the identification of the threshold of stress intensity factor range for crack growth. *Advances in Materials Science and Engineering*, 2017.
- [48] Lenets', Y. N. (1995). Near-threshold fatigue-crack growth: State of the problem and some anomalies. *Materials Science*, 30(3), 301–315.
- [49] Leis, B., Kanninen, M., Hopper, A., Ahmad, J., Broek, D. (1983). A Critical Review of the Short Crack Problem in Fatigue. *Engineering Fracture Mechanics*, 23(5), 883-898.
- [50] Oplt, T., Pokorný, P., Náhlík, L., & Hutař, P. (2017). The Effect of the Free Surface on the Singular Stress Field at the Fatigue Crack Front. *Strojnícky Casopis – Journal of Mechanical Engineering*, 67(2), 69–76.
- [51] Zerbst, U., Madia, M., Vormwald, M., & Beier, H. T. (2018). Fatigue strength and fracture mechanics – a general perspective. *Engineering Fracture Mechanics*, 198, 2–23.

- [52] Newman, J. J. (1984) A crack opening stress equation for fatigue crack growth. *Int. J. Fract.*, 24, R131–R135.
- [53] Lawson, L. (1999). Near-threshold fatigue: a review. *International Journal of Fatigue*, 21, 15–34.
- [54] Paris, P. C., "Testing for Very Slow Growth of Fatigue Cracks," *Closed Loop Magazine*, MTS Systems Corporation, Vol. 2, No. 5, 1970.
- [55] Saxena, A., Hudak, S. J., Jr., Donald, J. K. and Schmidt, D. W., "Computer-Controlled Decreasing Stress Intensity Technique for Low-Rate Fatigue Crack Growth Testing," *Journal of Testing and Evaluation*, Vol. 6, No. 3, 1978, pp. 167-174.
- [56] Newman, J.C. (1997). The Merging of Fatigue and Fracture Mechanics Concepts: A Historical Perspective. *Progress in Aerospace Sciences*, 34, 347-390.
- [57] Maierhofer, J., Kolitsch, S., Pippan, R., Gänser, H. P., Madia, M., & Zerbst, U. (2018). The cyclic R-curve–determination, problems, limitations and application. *Engineering Fracture Mechanics*, 198, 45-64.
- [58] Forth, S. C., James, M. A., & Johnston, W. M. (2004). Fatigue crack growth thresholds in D6AC steel. In *Proc. of the 15th European Conf. on Fracture*.
- [59] Hubbard, R.P., "Crack Growth Under Cyclic Compression," *Journal of Basic Engineering*, Transactions ASME, Vol. 91, 1969, pp. 625-631.
- [60] Stein, T., Wicke, M., Brueckner-Foit, A., Kirsten, T., Zimmermann, M., Bülbül, F., & Christ, H. J. (2017). Crack growth behavior in an aluminum alloy under very low stress amplitudes. *Journal of Materials Research*. 32. 1-8.
- [61] Forth, S., Newman, J., & Forman, R. (2003). On generating fatigue crack growth thresholds. *International Journal of Fatigue*, 25(1), 9–15.

- [62] Pearson, S., “Initiation of Fatigue Cracks in Commercial Aluminum Alloys and the Subsequent Propagation of Very Short Cracks,” *Engineering Fracture Mechanics*, Vol. 7, No. 2, 1975, pp. 235-247.
- [63] Newman, J.C., Jr., “A Nonlinear Fracture Mechanics Approach to the Growth of Small Cracks,” *Behavior of Short Cracks in Airframe Components*, AGARD Conference Proceedings, No. 328, 1983.
- [64] James, M., Forth, S., Johnston, W., Newman, J.A., & Everett, R. (2013). Effects of compression precracking on subsequent crack growth. 15th European Conference of Fracture Advanced Fracture Mechanics for Life and Safety Assessments (ECF15), Stockholm, Sweden.
- [65] Maierhofer, J., Pippan, R., & Gänser, H.-P. (2014). Modified NASGRO Equation for Short Cracks and Application to the Fitness-for-purpose Assessment of Surface-treated Components. *Procedia Materials Science*, 3, 930–935.
- [66] ASTM E647-15e1, Standard Test Method for Measurement of Fatigue Crack Growth Rates, ASTM International, West Conshohocken, PA, 2015, www.astm.org
- [67] Wang, S., Li, H., & Bowen, P. (2019). Investigation on Fatigue Threshold Testing Methods in a Near Lamellar TiAl Alloy. *Materials*, 12(21), 3487.
- [68] Zerbst, U., Vormwald, M., Pippan, R., Gänser, H.-P., Sarrazin-Baudoux, C., & Madia, M. (2016). About the fatigue crack propagation threshold of metals as a design criterion – A Review. *Engineering Fracture Mechanics*, 153, 190–243.
- [69] Patriarca, L., et al. “Short-Crack Thresholds and Propagation in an AISI 4340 Steel under the Effect of SP Residual Stresses.” *Fatigue & Fracture of Engineering Materials & Structures*, vol. 41, no. 6, June 2018, pp. 1275–1290.

- [70] Bohác, I., Dahl, W., & Pesek, L. (1995). Application of fatigue precracking methods and their influence on fracture toughness values. *Steel Research*, 66(12), 543–547.
- [71] Taguchi, K., Nakadate, K., Matsuo, S., Tokunaga, K., & Kurishita, H. (2018). Fatigue pre-cracking and fracture toughness in polycrystalline tungsten and molybdenum. *Journal of Nuclear Materials*, 498, 445–457.
- [72] Patterson, A. E., Chadha, C., Jasiuk, I. M., & Allison, J. T. (2019). Design and repeatability analysis of desktop tool for rapid pre-cracking of notched ductile plastic fracture specimens. *Engineering Fracture Mechanics*, 217, 106536.
- [73] Newman Jr., J. C., & Yamada, Y. (2010). Compression precracking methods to generate near-threshold fatigue-crack-growth-rate data. *International Journal of Fatigue*, 32(6), 879–885.
- [74] Newman, Isadore. (1999). *Analyses of Fatigue Crack Growth and Closure Near Threshold Conditions for Large-Crack Behavior*.
- [75] Bülbül, F., Kirsten, T., Wicke, M., Zimmermann, M., Brückner-Foit, A., & Christ, H.-J. (2018). Crack growth behaviour of aluminium wrought alloys in the very high cycle fatigue regime. *MATEC Web of Conferences*, 165, 20007.
- [76] Kitagawa H, Takahashi S. Applicability of fracture mechanics to very small cracks or the cracks in the early stages. In *Proceedings of the Second International Conference on Mechanical Behavior of Materials*. Metals Park, OH: American Society for Metals; 1976. pp 627–631.
- [77] El Haddad, M. H., Smith, K. N., & Topper, T. H. (1979). Fatigue crack propagation of short cracks.

- [78] Huang, Yifan, "Finite Element Analyses of Single-Edge Bend Specimens for J-R Curve Development" (2013). Electronic Thesis and Dissertation Repository. 1671.
- [79] Kanters, M. J. W., Stolk, J., & Govaert, L. E. (2015). Direct comparison of the compliance method with optical tracking of fatigue crack propagation in polymers. *Polymer Testing*, 46, 98–107.
- [80] Ewest, D., Almroth, P., Sjödin, B., Simonsson, K., Leidermark, D., & Moverare, J. (2016). A modified compliance method for fatigue crack propagation applied on a single edge notch specimen. *International Journal of Fatigue*, 92, 61–70.
- [81] Oh, C. (1997). Automated real-time measurements of fatigue crack length and crack opening load using unloading elastic compliance method. *International Journal of Fatigue*, 19(2), 169–176.
- [82] Carroll, J., Efstathiou, C., Lambros, J., Sehitoglu, H., Hauber, B., Spottswood, S., & Chona, R. (2009). Investigation of fatigue crack closure using multiscale image correlation experiments. *Engineering Fracture Mechanics*, 76(15), 2384–2398.
- [83] Song, J., Kang, J., & Koo, J. (2005). Proposal of modified (normalized) ASTM offset method for determination of fatigue crack opening load. *International Journal of Fatigue*, 27(3), 293–303.
- [84] Skorupa, M., Machniewicz, T., & Skorupa, A. (2007). Applicability of the ASTM compliance offset method to determine crack closure levels for structural steel. *International Journal of Fatigue*, 29(8), 1434–1451.
- [85] Keller, S., Horstmann, M., Kashaev, N., & Klusemann, B. (2019). Crack closure mechanisms in residual stress fields generated by laser shock peening: A combined experimental-numerical approach. *Engineering Fracture Mechanics*, 221, 106630.

- [86] Saxena, A., & Hudak, S. J. (1978). Review and extension of compliance information for common crack growth specimens. *International Journal of Fracture*, 14(5), 453–468.
- [87] Heine, L.-M., Bezold, A., & Broeckmann, C. (2018). Long crack growth and crack closure in high strength nodular cast iron. *Engineering Fracture Mechanics*, 192, 24–53.
- [88] Allison, J. E., Ku, R. C., & Pompetzki, M. A. (1988). A Comparison of Measurement Methods and Numerical Procedures for the Experimental Characterization of Fatigue Crack Closure. *Mechanics of Fatigue Crack Closure*.
- [89] Creel, J. A., Stover, S. M., Martin, R. B., Fyhrie, D. P., Hazelwood, S. J., & Gibeling, J. C. (2009). Compliance calibration for fracture testing of anisotropic biological materials. *Journal of the Mechanical Behavior of Biomedical Materials*, 2(5), 571–578.
- [90] Chung, Y.-I., & Song, J.-H. (2009). Improvement of ASTM compliance offset method for precise determination of crack opening load. *International Journal of Fatigue*, 31(5), 809–819.
- [91] Patriarca, L., Foletti, S., & Beretta, S. (2018). A comparison of DIC-based techniques to measure Crack closure in LCF. *Theoretical and Applied Fracture Mechanics*, 98, 230–243.
- [92] Song, J. H., & Chung, Y. I. (2010). A review of crack closure measurement by compliance technique and the normalized-extended ASTM method as a currently most refined, practical and simple one. *Procedia Engineering*, 2(1), 777–786.
- [93] Beretta S., Carboni M., Machniewicz T., Skorupa M.: Correlation between experiments and Strip Yield model results on fatigue crack growth in structural steel, *Proceedings ECF14, Krakow, Poland*, pp. 225-232, 2002.

- [94] Skorupa, M., Beretta, S., Carboni, M., & Machniewicz, T. (2002). An algorithm for evaluating crack closure from local compliance measurements. *Fatigue & Fracture of Engineering Materials & Structures*, 25(3), 261–273.
- [95] Ritchie, R. O. (1977). Influence of microstructure on near-threshold fatigue-crack propagation in ultra-high strength steel. *Metal Science*, 11(8-9), 368-381.
- [96] Masounave J, Bailon J P. *Scr Metall*, 1976; 10: 165.
- [97] McMahon Jr, C. J., Briant, C. L., & Banerji, S. K. (1978). The effects of hydrogen and impurities on brittle fracture in steel. In *Advances in Research on the Strength and Fracture of Materials* (pp. 363-385). Pergamon.
- [98] Washida, A., Tsuchida, E., & Kobayashi, H. (1986). Crack Growth and Threshold Characteristics of Surface Fatigue Crack in Plate Specimen of S 45% Carbon Steel. *Bulletin of JSME*, 29(254), 2403-2409.
- [99] Putatunda, S. K. (1988). Influence of material strength level on fatigue crack closure. *Engineering Fracture Mechanics*, 30(5), 627-639.
- [100] Keum, C. H., & Kwun, S. I. (1990). The Effect of Heat Treatment on the Fatigue Crack Propagation in SM40C Steel. *Journal of the Korean Society for Heat Treatment*, 3(2), 37-44.
- [101] Shin, H., Moon, Y. B., Kim, S. T., & Kwon, J. D. (1997). Microstructural Change and Near-threshold Fatigue Crack Growth Behaviors of Ni-Cr-Mo-V Steel by Tempering Treatments. *Journal of the Korean Society for Heat Treatment*, 10(4), 266-277.
- [102] Ritchie, R. O. (1979). Near-threshold fatigue-crack propagation in Steels. *International Metals Reviews*, 24(1), 205–230.

- [103] Cerny, I., Linhart, V., & Hnilica, F. (1970). Influence of changing of microstructure by the heat treatment on fatigue crack growth properties of the carbon cast steel. *WIT Transactions on Engineering Sciences*, 2.
- [104] Borrego, L. P., Costa, J. M., Antunes, F. V., & Ferreira, J. M. (2010). Fatigue crack growth in heat-treated aluminium alloys. *Engineering Failure Analysis*, 17(1), 11-18.
- [105] Bergner, F., & Zouhar, G. (2000). A new approach to the correlation between the coefficient and the exponent in the power law equation of fatigue crack growth. *International journal of Fatigue*, 22(3), 229-239.
- [106] Kucharski, P., Lesiuk, G., & Szata, M. (2016). Description of fatigue crack growth in steel structural components using energy approach-Influence of the microstructure on the FCGR. In *AIP Conference Proceedings* (Vol. 1780, No. 1, p. 050003). AIP Publishing LLC.
- [107] Lv, Y., Hu, M., Wang, L., Xu, X., Han, Y., & Lu, W. (2015). Influences of heat treatment on fatigue crack growth behavior of NiAl bronze (NAB) alloy. *Journal of Materials Research*, 30(20), 3041-3048.
- [108] Li, S., Kang, Y., & Kuang, S. (2014). Effects of microstructure on fatigue crack growth behavior in cold-rolled dual phase steels. *Materials Science and Engineering: A*, 612, 153-161.
- [109] Sadananda, K., Vasudevan, A. K., Holtz, R. L., & Lee, E. U. (1999). Analysis of overload effects and related phenomena. *International Journal of Fatigue*, 21, S233-S246.
- [110] Carvalho, A. L. M. D., & Martins, J. D. P. (2018). Effect of Interrupted Ageing and Retrogression-Reageing Treatments on Fatigue Crack Growth with a Single Applied Overload in 7050 Aluminum Alloy. *Materials Research*, 21.

- [111] Wicke, M., Brueckner-Foît, A., Kirsten, T., Zimmermann, M., Buelbuel, F., & Christ, H. J. (2018). Understanding the near-threshold crack growth behavior in an aluminum alloy by x-ray tomography. In *MATEC Web of Conferences* (Vol. 165, p. 13007). EDP Sciences.
- [112] Kumar, P., & Ramamurty, U. (2019). Microstructural optimization through heat treatment for enhancing the fracture toughness and fatigue crack growth resistance of selective laser melted Ti6Al4V alloy. *Acta Materialia*, 169, 45-59.
- [113] Xu, X., Lu, C., Li, Y., Ma, X., & Jin, W. (2021). Fatigue Crack Growth Characteristics of 34CrMo4 Steel for Gas Cylinders by Cold Flow Forming after Hot Drawing. *Metals*, 11(1), 133.
- [114] Zheng, X., Lü, B., and Jiang, H. (1995). Determination of probability distribution of fatigue strength and expressions of P-S-N curves. *Engineering Fracture Mechanics*, 50(4), pp. 483-491.
- [115] Lorén, S. (2004). Estimating fatigue limit distributions under inhomogeneous stress conditions. *International Journal of Fatigue*, 26(11), 1197–1205.
- [116] Dejack, Michael & Engler-Pinto Jr, Carlos & Lasecki, John & Frisch, Robert & Allison, John. (2005). *Statistical Approaches Applied to Fatigue Test Data Analysis*. 10.4271/2005-01-0802.
- [117] Wallin, K. R. W. (2011). Statistical uncertainty in the fatigue threshold staircase test method. *International Journal of Fatigue*, 33(3), 354–362.
- [118] Müller, C., Wächter, M., Masendorf, R., & Esderts, A. (2017). Accuracy of fatigue limits estimated by the staircase method using different evaluation techniques. *International Journal of Fatigue*, 100, 296–307.

- [119] Molina, A., Piña-Monarez, M. R., & Barraza-Contreras, J. M. (2020). Weibull S-N fatigue strength curve analysis for A572 GR. 50 steel, based on the true stress—true strain approach. *Applied Sciences*, 10(16), 5725.
- [120] Pollak, R. D., & Palazotto, A. N. (2009). A comparison of maximum likelihood models for fatigue strength characterization in materials exhibiting a fatigue limit. *Probabilistic Engineering Mechanics*, 24(2), 236–241.
- [121] Boylan, G. L., & Cho, B. R. (2011). The normal probability plot as a tool for understanding data: A shape analysis from the perspective of skewness, kurtosis, and variability. *Quality and Reliability Engineering International*, 28(3), 249–264.
- [122] Najim, Abbas & Anwar Taha, Taha. (2015). Comparison Four Methods for Estimating the Fatigue Life Distribution Parameters through Simulation.
- [123] Khameneh, M. J., & Azadi, M. (2018). Evaluation of high-cycle bending fatigue and fracture behaviors in en-GJS700-2 ductile cast iron of crankshafts. *Engineering Failure Analysis*, 85, 189–200.
- [124] Wang, J., Yang, Y., Yu, J., Wang, J., Du, F., & Zhang, Y. (2020). Fatigue life evaluation considering fatigue reliability and fatigue crack for FV520B-I in VHCF regime based on Fracture Mechanics. *Metals*, 10(3), 371.
- [125] Garr, K. R., & Hresko, G. C. (1998). A size effect on the fatigue crack growth rate threshold of alloy 718. *Fatigue Crack Growth Thresholds, Endurance Limits, and Design*.
- [126] Stanzl-Tschegg, S., & Schönbauer, B. (2010). Near-threshold fatigue crack propagation and internal cracks in steel. *Procedia Engineering*, 2(1), 1547–1555.
- [127] Pokorný, P., Náhlík, L., & Hutař, P. (2015). Influence of threshold values on residual fatigue lifetime of railway axles under variable amplitude loading. *Procedia Engineering*, 101, 380–385.

- [128] Hutař, P., Pokorný, P., Poduška, J., Fajkoš, R., & Náhlík, L. (2017). Effect of residual stresses on the fatigue lifetime of railway axle. *Procedia Structural Integrity*, 4, 42-47.
- [129] Yakura, R., Matsuda, M., Sakai, T., & Ueno, A. (2017). Effect of inclusion size on fatigue properties in very high cycle region of low alloy steel used for solid type crankshaft. *Kobelco Technology Review*, 35, 7-13
- [130] Correia, J. A., De Jesus, A. M., Moreira, P. M., & Tavares, P. J. (2016). Crack closure effects on fatigue crack propagation rates: application of a proposed theoretical model. *Advances in Materials Science and Engineering*, 2016.
- [131] Rabbolini, S., Beretta, S., & Foletti, S. (2016). Fatigue crack growth in low cycle fatigue: an analysis of crack closure based on image correlation. *Procedia Structural Integrity*, 1, 158-165.
- [132] Yamada, Y., & Newman Jr, J. C. (2010). Crack closure under high load ratio and K_{max} test conditions. *Procedia Engineering*, 2(1), 71-82.
- [133] Garcia, R., Beserra, A., Pereira-Dias, D., de Assis, K. S., & Mattos, O. R. (2015). Back-face strain compliance relation for SEN (B) specimens for wide range in crack lengths. In *Corrosion 2015*. OnePetro.
- [134] Carboni, M. (2004). Local compliance experiments and crack closure models. In *XVII Convegno Nazionale del Gruppo Italiano Frattura* (pp. 1-8).
- [135] Khor, W. (2018). Crack tip opening displacement (CTOD) in single edge notched bend (SEN (B)) (Doctoral dissertation, Brunel University London).
- [136] Sunder, R. (1995). Studies on fatigue crack growth for airframe structural integrity applications. *Sadhana*, 20(1), 247-285.
- [137] Peel, C. J., & Forsyth, P. J. E. (1980). *The analysis of fatigue failures*.

- [138] Miranda, R. S., Cruz, C., Cheung, N., & Cunha, A. (2021). Fatigue Failure Analysis of a Speed Reduction Shaft. *Metals*, 11(6), 856.
- [139] Laird, Campbell. "The influence of metallurgical structure on the mechanisms of fatigue crack propagation." *Fatigue crack propagation*. ASTM International, 1967.
- [140] Xue, Y., El Kadiri, H., Horstemeyer, M. F., Jordon, J. B., & Weiland, H. (2007). Micromechanisms of multistage fatigue crack growth in a high-strength aluminum alloy. *Acta materialia*, 55(6), 1975-1984.
- [141] K.K. Chawla, M. Meyers, *Mechanical Behavior of Materials*, Prentice Hall, 1999.
- [142] Li, H. F., Zhang, P., & Zhang, Z. F. (2022). A new fatigue crack growth mechanism of high-strength steels. *Materials Science and Engineering: A*, 840, 142969.
- [143] Neumann, P. (1969). Coarse slip model of fatigue. *Acta metallurgica*, 17(9), 1219-1225.
- [144] Gao, Y., Ritchie, R. O., Kumar, M., & Nalla, R. K. (2005). High-cycle fatigue of nickel-based superalloy ME3 at ambient and elevated temperatures: role of grain-boundary engineering. *Metallurgical and Materials Transactions A*, 36(12), 3325-3333.
- [145] Davidson, D. L., & Lankford, J. (1992). Fatigue crack growth in metals and alloys: mechanisms and micromechanics. *International Materials Reviews*, 37(1), 45-76.
- [146] Lynch, S. P., & Moutsos, S. (2006). A brief history of fractography. *Journal of Failure Analysis and Prevention*, 6(6), 54-69.
- [147] Riemelmoser, F. O., Pippan, R., & Stüwe, H. P. (1998). An argument for a cycle-by-cycle propagation of fatigue cracks at small stress intensity ranges. *Acta materialia*, 46(5), 1793-1799.
- [148] Hayes, M., Edwards, D., & Shah, A. (2015). *Fractography in failure analysis of polymers*. William Andrew.

- [149] Parrington, R. J. (2003). Fractographic features in metals and plastics: fractographic features are critical to failure analysis of metals and plastics. *Advanced materials & processes*, 161(8), 37-41.
- [150] Zamanzadeh, M., Larkin, E., & Mirshams, R. (2015). Fatigue failure analysis case studies. *Journal of Failure Analysis and Prevention*, 15(6), 803-809.
- [151] Ranganathan, N., Sedghi, N., Joly, D., Do, T. D., Leroy, R., Chalon, F., & Feraud, P. (2012). A method for quantitative fatigue fracture surface analysis. In 4th International Conference on Crack Path.
- [152] Schijve, J. (1998). The significance of fractography for investigations of fatigue crack growth under variable-amplitude loading. Delft University Press.
- [153] AMS 2759-1D (2007). Heat treatment of carbon and low-alloy steel parts minimum tensile strength below 220 ksi (1517 MPa), SAE International.
- [154] ASTM E466-15 (2015). Standard Practice for Conducting Force Controlled Constant Amplitude Axial Fatigue Tests of Metallic Materials. ASTM International, West Conshohocken, PA.
- [155] ASTM E1012 (2019). Standard Practice for Verification of Testing Frame and Specimen Alignment Under Tensile and Compressive Axial Force Application.
- [156] ISO 7500-1 (2018). Metallic Materials-Verification of Static Uniaxial Testing Machines Tension/Compression Testing Machines-Verification and Calibration of the Force-Measuring Systems.
- [157] Hück, M. (1983). Ein Verbessertes verfahren für die Auswertung von Treppenstufenversuchen. *Materialwissenschaft Und Werkstofftechnik*, 14(12), 406-417.

- [158] Efron, B., & Tibshirani, R. (1986). [Bootstrap methods for standard errors, confidence intervals, and other measures of statistical accuracy]: Rejoinder. *Statistical Science*, 1(1).
- [159] Stüssi, F. (1955). *Tragwerke aus Aluminium*. New York: Springer
- [160] Hazen A. Storage to be provided in the impounding reservoirs for municipal water supply. *Transactions of the American Society of Civil Engineers* 1914; 77:1547–1550. <https://doi.org/10.1061/taceat.0002563>
- [161] Hassan, Azzam. (2018). A new prediction of the fatigue limit based on Brinell hardness and ultimate strength for high strength steels. *International Journal of Energy and Environment*. 9. 77-84.
- [162] Boardman, B. (1990). Fatigue resistance of steels. *Properties and Selection: Irons, Steels, and High-Performance Alloys*, 673–688.
- [163] Clarke GA, Andrews WR, Paris PC, Schmidt DW. Single Specimen Tests for JIc Determination. *Mechanics of Crack Growth*, ASTM STP 590, American Society for Testing and Materials, Philadelphia; 1976;27-42.
- [164] ASTM E1820-11E2, Standard Test Method for Measurement of Fracture Toughness, ASTM International, West Conshohocken, PA, 2011, www.astm.org.
- [165] “NASGRO® Fracture Mechanics and Fatigue Crack Growth Analysis Software,” Version 4.02, NASA-JSC and SwRI, September 2002.
- [166] NASGRO 4.2 manual; 2006.
- [167] El Haddad, M. H., Topper, T. H., & Smith, K. N. (1979). Prediction of non-propagating cracks. *Engineering fracture mechanics*, 11(3), 573-584.
- [168] Kitagawa, H. (1976). Applicability of fracture mechanics to very small cracks or the cracks in the early stage. *Proc. of 2nd ICM*, Cleveland, 1976, 627-631.

[169] Stromeyer, C. E. (1914). The determination of fatigue limits under alternating stress conditions. Proceedings of the Royal Society of London. Series A, Containing Papers of a Mathematical and Physical Character, 90(620), 411-425.

[170] Murakami, Y., & Endo, M. (1986). Effects of hardness and crack geometries on ΔK_{th} of small cracks emanating from small defects. The behaviour of short fatigue cracks, Edited by KJ Miller, ER de los Rios.

[171] Shipilov, S. (2003). Mechanical Testing of Materials: Deliberate Deception or Superficial Knowledge?.

CURRICULUM VITAE

EDUCATION

Degree	Institution	Year of Graduation
MS	METU Metallurgical and Materials Engineering, Ankara	2018
BS	METU Metallurgical and Materials Engineering, Ankara	2015
High School	Nermin Mehmet Çekiç Anatolian High School, Ankara	2009

WORK EXPERIENCE

Year	Place	Enrollment
2016- Present	Turkish Aerospace	Chief Test Engineer

FOREIGN LANGUAGES

English

PUBLICATIONS

Çalışkan, S., & Gürbüz, R. (2021). Determining the endurance limit of AISI 4340 steels in terms of different statistical approaches. *Frattura ed Integrità Strutturale*, 15(58), 344-364.

Çalışkan, S., & Gür, C. H. (2019). Investigating the correlation between magnetic Barkhausen noise emission and the fatigue life of shot-peened AISI 4140 steel. *Insight-Non-Destructive Testing and Condition Monitoring*, 61(12), 701-705.